Kinetics of the Selective Oxidation of o-Xylene to Phthalic Anhydride

Doctoral Thesis
(Dissertation)

to be awarded the degree of

Doctor of Engineering (Dr.-Ing.)

submitted by

Dipl.-Ing. Robert Marx

from Dernbach

approved by the Faculty of

Mathematics/Computer Science and Mechanical Engineering
Clausthal University of Technology

Date of oral examination:
January 27, 2012

Chairperson of the Board of Examiners:

Prof. Dr. rer. nat. Alfred Weber

Chief Reviewer:

Prof. Dr.-Ing. Thomas Turek

Reviewer:

PD Dr. rer. nat. Gerhard Mestl
Süd-Chemie AG

Zusammenfassung

Die Oxidation von o-Xylol zu Phthalsäureanhydrid auf Vanadiumkatalysatoren wird seit einigen Jahrzehnten industriell in Rohrbündelreaktoren betrieben. Moderne Katalysatorsysteme, die in diesen Reaktoren zur Anwendung kommen, bestehen aus mehreren Katalysatorlagen. Obwohl dieser Prozess sowohl industriell, als auch akademisch stark beforscht wurde, gibt es weiterhin eine Reihe offener Fragen. Dies betrifft insbesondere auch das Reaktionsnetzwerk. Die Bildung von Phthalsäureanhydrid verläuft in einem großen Netzwerk mit einigen Intermediaten. Die Hauptreaktionswege sind weitgehend aufgeklärt. Allerdings fehlen im Reaktionsnetzwerk noch einige Zwischenschritte, insbesondere solche, die zu den Nebenprodukten führen.

Da es sich um ein Mehrlagensystem handelt, erfordert die rein empirische Optimierung der Katalysatoren erheblichen experimentellen Aufwand. Die Optimierung auf Basis eines mathematischen Modells der Reaktion bietet hier weitere Möglichkeiten. In der bisherigen Literatur ist die Kinetik dieser Reaktion nur für Laborpräparationen bzw. für vergleichsweise wenig produktive Katalysatoren beschrieben.

In dieser Arbeit wird mit Hilfe eines polytrop betriebenen Zapfstellenreaktors im Pilotmaßstab, dessen Reaktionsrohr die Dimensionen eines industriellen Reaktionsrohrs hat, zum einen das Reaktionsnetzwerk weiter aufgeklärt und zum anderen die Kinetiken der verschiedenen Katalysatoren eines industriellen mehrlagen Katalysatorsystems beschrieben.

Bei Versuchen mit dem beschriebenen Reaktorsystem wurden einige bisher unbekannte Intermediate gefunden. Durch Dosierungsversuche wurden deren Abreaktions- und Bildungspfade untersucht und es konnten dem bisher bekannten Reaktionsnetzwerk einige fehlende Reaktionsschritte, insbesondere die Bildung von Nebenprodukten wie etwa Maleinsäureanhydrid, Benzoesäure, CO oder CO_2 betreffend, hinzugefügt werden.

Bei der Entwicklung der Kinetiken der verschiedenen Katalysatorlagen liegt ein besonderes Augenmerk bei der Berücksichtigung des zuvor entwickelten Reaktionsnetzwerks, sowie in der Auswahl des erforderlichen Reaktormodells zur Beschreibung dieser Reaktion. Es wurde gefunden, dass sich in einer der Katalysatorlagen ein Aktivitätsprofil ausbildet. Darüber hinaus kann die kinetische Beschreibung dieser Reaktion durch Berücksichtigung von Stofftransportlimitierungen deutlich verbessert werden.

Summary

The oxidation of o-xylene to phthalic anhydride on vanadia catalysts has been an industrial process conducted in multitubular reactor for several decades. Modern catalytic systems applied in this reaction consist of multiple catalytic layers. Although this process was researched both industrially and academically, a number of open tasks persist, particularly also considering the reaction scheme. Phthalic anhydride is produced from o-xylene in a large reaction scheme, involving several intermediate reaction steps. The main intermediates are well described. However, particularly in the formation of by-products several links are missing.

In this multilayer system, purely empirical optimization of catalysts involves considerable experimental efforts. Model based optimization offers further perspectives in this point. In literature, the kinetics of this reaction has been described for laboratory preparations or for catalysts with comparatively low productivity for only a small operating range.

In this work, on the one hand the reaction scheme of o-xylene oxidation is further investigated. On the other hand, the reaction kinetics of different layers of an industrial multilayer catalytic system is developed. The experimental set-up applied consists of a single tube pilot reactor with industrial tube dimensions with several axial sampling ports conducted in polytropic regime.

In experiments with said experimental set-up, several previously unknown intermediates of the reaction were found. The production and decomposition routes of these intermediates were investigated by a series of dosage experiments. Thereby several additional reaction paths could be added to the known reaction scheme, particularly considering the formation of by-products such as maleic anhydride, benzoic acid, CO or CO_2.

In the development of reaction kinetics, particular focus was put on the proper representation of the developed reaction scheme as well as the choice of the appropriate reactor model to find the best description of the physical system. It was found that an activity profile develops within one of the catalyst layers. In addition, the kinetic description of this reaction could be significantly improved by taking into account also mass transfer limitations within the catalyst pellet.

Danksagung

Bei der Erstellung dieser Arbeit haben viele Menschen ihren Beitrag gehabt, die an dieser Stelle leider nicht alle einzeln erwähnt werden können, bei denen ich mich aber gerne an dieser Stelle bedanken möchte. Ganz pauschal möchte ich meinen Dank auch an die Süd-Chemie AG richten, in deren Laboren der Großteil der Ergebnisse, die zu dieser Arbeit führten, produziert wurde.

Insbesondere möchte ich Hr. Prof. Dr.-Ing Thomas Turek danken für die Betreuung der Arbeit an der TU Clausthal, für die durchweg gute Zusammenarbeit im Verlaufe der letzten Jahre und für zahlreiche interessante und zielführende Diskussionen.

Darüber hinaus gilt mein Dank Hr. PD Dr. Gerhard Mestl, zum einen natürlich für die Übernahme des Korreferats aber zunächst für die Themenstellung und vor allem für die Begeisterung, mit der er den Verlauf der Arbeit begleitet und bereichert hat.

Besonders bedanken möchte ich mich bei Hr. Dr. Hans-Jörg Wölk, für die täglichen Diskussionen und dafür, dass er mir stets den Rücken frei gehalten hat, damit ich mich auf die vorliegende wissenschaftliche Arbeit konzentrieren konnte.

Bei Hr. Dr. Andreas Reitzmann bedanke ich mich für das Interesse an meiner Arbeit und damit einhergehend viele Anregungen und Diskussionen, häufig zu fortgeschrittener Stunde.

Bei Hr. Bernd Mischke von Chromatographie und Service möchte ich mich für die Durchführung der GC/MS Messungen bedanken.

Meinen Bürokollegen, Fr. Nadine Fromm, Hr. Peter Schinke und Hr. Werner Pitschi möchte ich mich für die gute Arbeitsatmosphäre danken und dafür, dass sie stets zur Stelle waren, wenn zwei Hände einmal nicht ausgereicht haben.

Schließlich möchte ich auch ein Wort des Dankes an meine Familie richten, die mich bei der Erstellung der vorliegenden Arbeit stets unterstützt hat.

Content

1. Introduction

Throughout the last years, the rising awareness that fossil resources will come to an end at some point has led to rising prices for these fossil fuels. The oil price took a stunning development from about 20 US$/barrel in 1999 to currently well above 100 US$/barrel (2011) [1]. Consequently, the optimization of existing chemical processes yields substantial economic impact and also reduces the emission of pollutants.

In a recent publication, it was pointed out that catalytic selective oxidation plays an important role in process intensification and the improved usage of fossil resources [2]. Several processes based on selective oxidation have been important industrially over the last decades. One of these processes is the oxidation of o-xylene to phthalic anhydride. With an annual production of 4.5 million tons in 2005, phthalic anhydride is a significant commodity in chemical industry. Applications are mainly in the manufacture of phthalate plasticizers, phthalocyanine dyes, polyester resins and numerous fine chemicals [3]. Historically, the feedstock for phthalic anhydride production was naphthalene, which has gradually been replaced by o-xylene throughout the past 50 years [4,5]. Considering the quantities produced on an industrial scale, even an increase of 1% in selectivity has a substantial economic effect.

Catalysts applied whether with naphthalene or o-xylene feedstock are vanadia/titania catalysts with different promoters. In the industrial application, multilayer systems find wide distribution [6-10]. The Süd-Chemie PHTHALIMAX^{TM} benchmark consists of four different catalysts in different axial positions. The design and layout of the catalyst filling to the industrial reactor is crucial for the overall performance and product yield obtained in this process.

Despite consistent process optimization, selectivities obtained in the industrial process reach a maximum of around 83 mole% corresponding to a phthalic anhydride yield of around 115 – 117 wt%. In the course of this reaction 12 bonds need to be broken and 12 new bonds are formed [11]. Consequently, the reaction does not comprise only a single step, but passes through a number of intermediates. Typically, o-tolualdehyde (TA) and phthalide (PD) are viewed as the main intermediates in this reaction. In addition, by-products such as maleic anhydride (MA), CO and CO_2 account for the loss in selectivity. However, in spite of the industrial importance of this process and numerous studies [12-22] in this respect, the reaction scheme still lacks a number of linking elements. Especially the formation of non-selective oxidation products is yet not well understood. In this work any oxidation product, which cannot be converted to PA in a subsequent reaction path is considered non-selective.

In order to further optimize catalysts for this reaction, fundamental knowledge about how non-selective by-products are formed is essential. The identification of intermediates in the formation of these components and the development of a more detailed reaction scheme accounting also for the by-product formation is still an open task.

The industrial four layer catalytic system is highly complex and many different parameters influence its performance. Purely empirical research methods to improve this system involve very high experimental efforts. In the light of these limitations, model based description of this process through kinetic and reactor modeling appears to be an interesting approach.

A number of kinetic models and kinetic studies of o-xylene oxidation have been published in literature over the last few decades [13,15,23-31]. In these investigations, different reactor types such as small lab-scale apparatuses as well as bench scale units, pilot reactors or even industrial reactors have been applied. Nevertheless, each of these models has shortcomings in terms of applicability to industrial conditions, range of operating conditions and description of relevant reaction steps.

In this work, the kinetics of the selective oxidation of o-xylene to phthalic anhydride is investigated in an industrial scale sample port pilot reactor. Thanks to this unique experimental set-up, thorough investigation of this industrially important reaction becomes possible, since the quality of measurement is unprecedented due to the possibility of accumulating large data sets at various operating conditions and high analytical sensitivity with sufficiently large sampling quantities.

The aim is to find reaction kinetics describing the chemical comportment of a modern four layer system for a large range of operating conditions and under consideration of the formation of by-products.

2. Industrial Phthalic Anhydride Production

2.1 Production Process

Historically, phthalic anhydride (PA) was produced in slurry phase from naphthalene feedstock from as early as 1872 [32]. The industrial breakthrough as important commodity was made when the production process was modified to oxidize vaporized naphthalene over vanadia catalyst. Since the 1960s o-xylene has replaced naphthalene as feedstock more and more. Several different o-xylene production processes are documented in literature. Although alternative processes such as fluidized bed processes [33] or slurry phase processes [34-36] were developed, still today the fixed bed catalytic process [37] is most common. Figure 1 shows an exemplary flowsheet of such a phthalic anhydride production process from o-xylene.

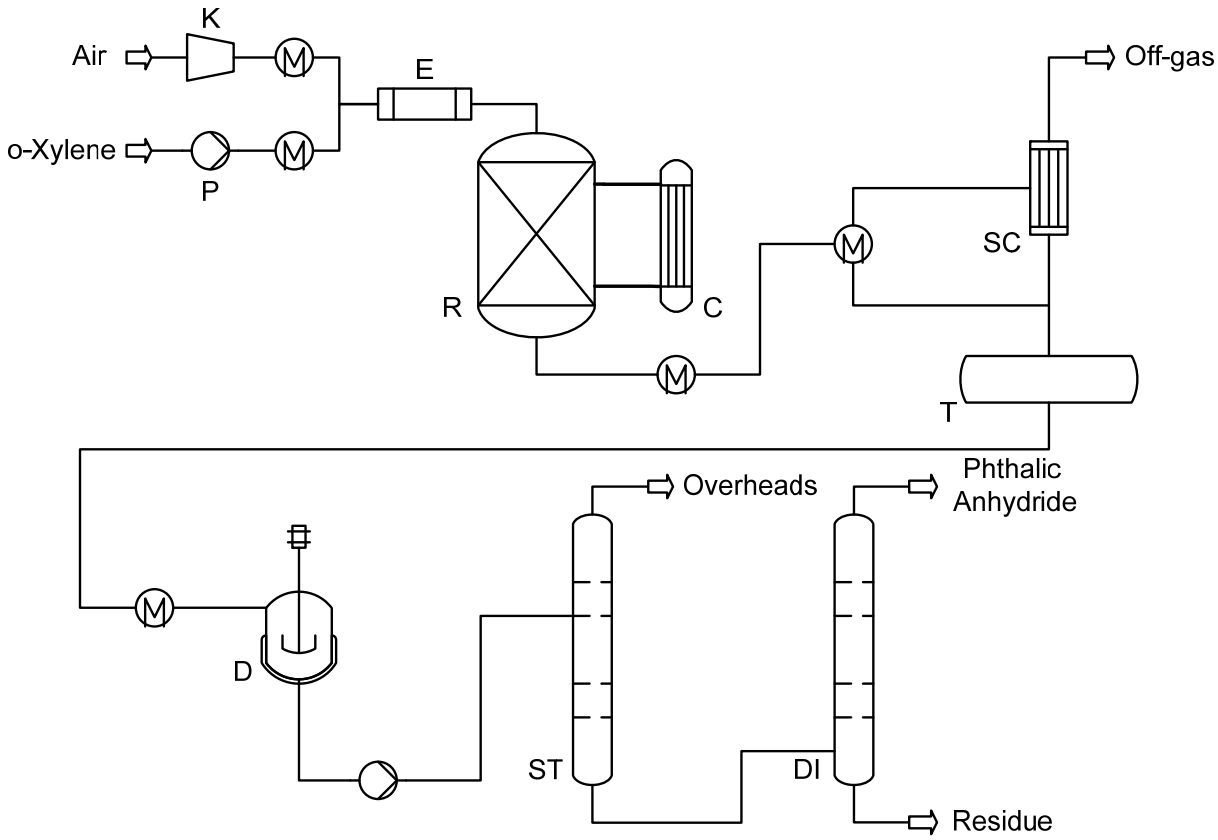

Figure 1: Exemplary flowsheet of an industrial phthalic anhydride production plant, redrawn from [19,32]; air compressor (K), o-xylene pump (P), evaporator (E), reactor (R), salt bath cooler (C), switch condensers (SC), crude phthalic anhydride tank (T), predecomposer (D), stripper column (ST), distillation column (DI)

o-Xylene and air are preheated and mixed and o-xylene is evaporated at temperatures between 100 °C and 150 °C prior to being fed to the catalytic reactor. Industrial reactors are multitubular reactors with up to 30000 tubes. Reaction temperatures range between 330 °C and 480 °C and are adjusted by means of a molten salt bath. Salt is circulated in the shell side of the reactor at nearly isothermal cooling temperatures. The design and layout of the catalyst filling of the reactor tubes is crucial for the overall performance and product yield obtained in this process. Modern catalytic systems such as the PHTHALIMAX™ allow high product yields (up to 115 – 117 g_{PA}/g_{oX}).

Downstream of the reactor, the product gas stream is cooled in several steps and finally directed through switch condensers. The switch condensers are specially equipped heat exchangers constructed as finned tube bundles, which can be heated or cooled. This is the next crucial unit operation in obtaining high overall PA yields since its total sublimation from the product stream is obtained only in optimized systems. The switch condensers are alternately filled with crude PA, which is then melted down and collected in a crude PA tank.

The next larger step of the PA production process involves the purification of crude PA: Several by products, such as benzoic acid, maleic acid or heavy residue are formed in the oxidation of o-xylene. This needs to be separated from in several purification units. Crude PA is first pretreated and homogenized. It is then fed to the stripper column where all light ends are separated from the product stream. In another distillation column, operated at sub-atmospheric pressure pure PA is separated from any high boiling point residue.

The general aim of catalyst development is to raise product yields directly in the catalytic reactor on the one hand and to minimize the concentrations of by-products which need to be removed from the PA product stream in order to also minimize cost and effort in the purification steps.

2.2 Industrial Catalysts

Catalysts most widely applied for the reaction of both naphthalene and o-xylene consist of vanadium and titanium oxides. Historically, vanadium oxide catalysts were applied as bulk catalysts [38,39] and loaded to industrial reactors as extrudates. This resulted in poor conversion rates, low selectivities and limited catalyst lifetimes. In the last decades the development went more and more towards the application of egg-shell catalysts with an inactive carrier, which the active mass is fixed to [40]. The carrier materials most commonly used are nonporous materials such as porcelain, silicon carbide, quartz, steatite or alumina [10,37]. Over the last decades different metals such as potassium, rubidium, silver, cesium and also phosphorous components have been reported of as promoting components [6,10,16,41]

The industrial catalytic systems were gradually modified by adjusting the catalytic behavior dependent on the axial position. Due to the strongly exothermal nature of this reaction, different temperatures appear at different positions. In addition, this reaction is

conducted to reach full conversion. Consequently also the composition of the reaction gas is significantly different at different positions. The single layer system applied until the 1970s [38,39] was then developed to two catalyst layers with different chemical compositions [6,9] and further on to a three layer system in the 1990s [10,37]. Modern catalytic systems for this reaction consist of up to four catalyst layers with optimized activities and selectivities [7,8].

Catalysts applied in phthalic anhydride production vary in composition according to the process conditions applied. Since industrial feed concentrations range from 0.8 vol% in older plants to 2 vol% in modern, high productive production facilities, different catalyst types are optimized for different process conditions.

Catalyst lifetimes range up to four years. During this time a rather lengthy start-up procedure is necessary, until the design feed concentration of o-xylene is reached. Catalysts applied for this reaction have been characterized widely by various methods over the last decades [42-52].

2.3 Typical Performance of an Industrial Reactor

o-Xylene is converted to phthalic anhydride by a number of series and parallel reactions. Tolualdehyde and phthalide are the main intermediates in the selective reaction path. The mentioned phthalic anhydride yield of 115 – 117 wt% or molar selectivities of up to 83% can be obtained with the Süd-Chemie PHTHALIMAX^{TM} benchmark. Main by-products are maleic anhydride CO and CO_2. Benzoic acid and citraconic anhydride are additional components with significant selectivities at the reactor outlet.

Figure 2 shows a typical conversion selectivity plot for the main components. The selectivity of phthalic anhydride rises continuously to reach said 83% selectivity at 100% conversion. The tolualdehyde selectivity profile begins at values around 60% at low o-xylene conversions and continuously drops to zero selectivity at full conversion. The selectivity profile of phthalide begins at zero at low conversions, reaches a maximum around 10% and then gradually decreases to zero again at the reactor outlet. CO and CO_2 selectivity profiles are basically parallel to the conversion axis. The CO_2 selectivity valuing around 9% is slightly higher than the selectivity to CO with about 3 - 4%.

Important performance factors are the phthalic anhydride yield on the one hand, but also the product purity. Unreacted intermediates such as phthalide or tolualdehyde are undesired in the product stream, since they are difficult to separate from phthalic anhydride in the purification units due to very similar boiling points. In addition, this reaction is conducted at full conversion in order to avoid the formation of explosive atmospheres downstream of the catalytic reactor.

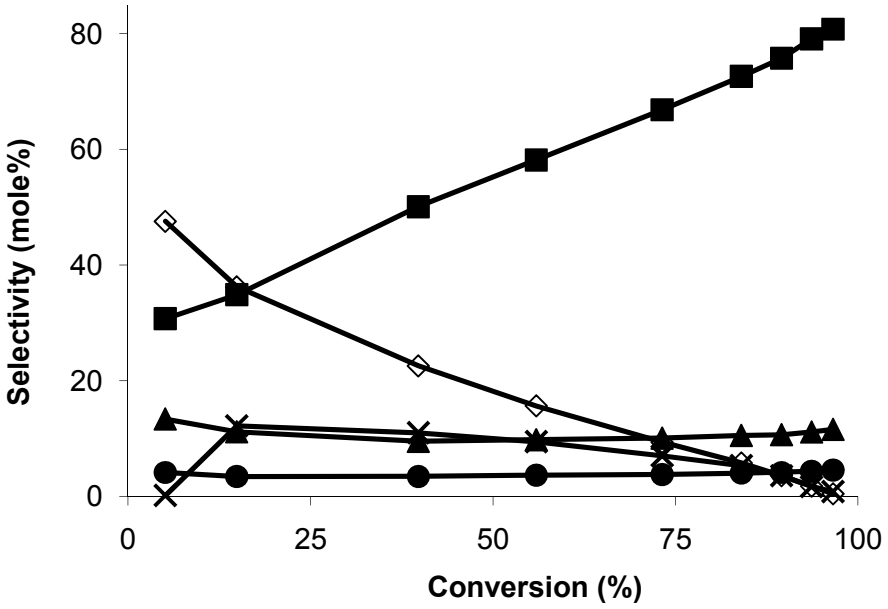

Figure 2: Typical conversion selectivity plot of the main intermediates and products in o-xylene oxidation; TA(◊), PD (x), PA (■), CO(●) and CO_2 (▲)

The oxidation of o-xylene is a strongly exothermic reaction. The adiabatic temperature increase in the formation of phthalic anhydride ranges around 760 K for the selective reaction and 2400 K for the nonselective total oxidation. Although the reactor is cooled by a salt bath in polytropic reaction regime, hot spots of up to 100 K can be observed in this reaction. A typical temperature profile for the four layer system is shown in figure 3. Both temperature and length axis are displayed dimensionless, which is the representation which will be shown throughout this work.

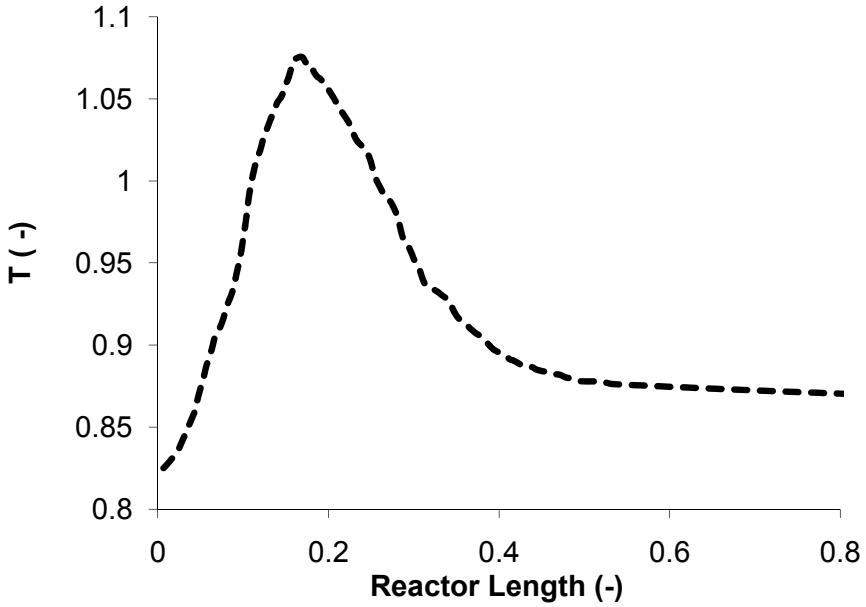

Figure 3: Typical temperature profile of the four layer system

The hot spot forms close to the reactor inlet at up to 130 °C above the salt bath temperature (SBT). Generally, reaction temperatures lay in the range of 330 °C to 480 °C. In the catalyst layers close to the reactor outlet, hot spots are barely visible in an optimized catalytic system.

3. Kinetic and Reactor Modeling

3.1 Reactor Modeling – State of the Art

Chemical reactors are generally described mathematically in application of mass, energy and momentum conservation in the control volume around the reactor [53]. Different types of reactor models vary particularly in the precision of the description of the chemical and physical processes occurring in the reactor. Due to experimental limitations in describing the exact physical system, certain simplifications and assumptions need to be made for each model type in order to reach a set of differential equations which can be solved with the available computing power. Before developing a mathematical model, it must be clear which cause this model is aimed to serve and which effects are aimed to be described. Each simplification decreases the model accuracy to a certain extent. Depending on the aim of the reactor model a trade-off between modeling accuracy and calculation efforts needs to be made. Hofmann [54] defined the following criteria in choice of reactor model:

- The reactor model should be only as detailed as absolutely necessary for the cause of the model.
- The number of parameters should be minimized.
- The parameters of the chosen model should be based on reliable correlations.
- The calculation efforts should be minimized.

The oxidation of o-xylene is conducted in fixed bed tubular reactors with two phases (gas and catalyst). The following overview will therefore be limited to this type of reactor. Due to the commercial importance and the wide distribution of processes conducted in fixed bed reactors, respective models have been discussed extensively in literature [53-60]. The physical comportment of fixed bed catalytic reactors has been described by stochastic-, cell- and continuum models. Most successfully applied and well described are continuum models [58].

The most simple type of model for a catalytic reactor is a one dimensional model assuming that solid and fluid phases can be described by one pseudohomogeneous phase and ideal plug flow regime prevails. In this case only axial temperature and concentration gradients are taken into account. The corresponding model equations are shown in table 1 [53].

Table 1: Model equations of the pseudohomogeneous reactor model as suggested by Froment [53]

overall mass balance	$-\frac{d\,(u_z \cdot C)}{dz} = \rho_s \cdot r_{eff}$	(3.1.1)
heat balance	$u_z \cdot \rho_f \cdot c_p \cdot \frac{d\,(T)}{dz} = -\Delta H_R \cdot \rho_s \cdot r_{eff} - 4 \cdot \frac{U}{d_t} \cdot (T - T_W)$	(3.1.2)
momentum conservation	$-\frac{dP}{dz} = f \cdot \frac{\rho_f \cdot u_z^2}{d_p}$	(3.1.3)
boundary conditions for $z = 0$	$C = C_0, \quad T = T_0, \quad u_z = u_{z,0}$	(3.1.4)

The mass balance comprises the convection term including the axial velocity u_z and the total concentration C as well as the effective reaction rate r_{eff} along with the catalyst density ρ_s. The effective reaction rate in this type of model includes not only the intrinsic reaction rate, but also the influences of all the transport mechanisms taking place at the gas-solid interface and within the catalyst pellet. The heat balance includes the convective term as well as the heat of reaction ΔH_R and the heat transfer term to the reactor wall with U, the overall heat transfer coefficient, the tube diameter d_t and the coolant temperature T_c. The pressure drop in the momentum conservation equation is calculated through the friction factor f, the density of the fluid (gas) phase ρ_f, the axial velocity and the particle diameter d_p of the catalyst particles.

The simple one dimensional homogeneous model can be extended to a one dimensional heterogeneous model by taking into account also the effect of film diffusion and interfacial temperature and concentration gradients. In this case heat and mass balances are solved for both phases independently.

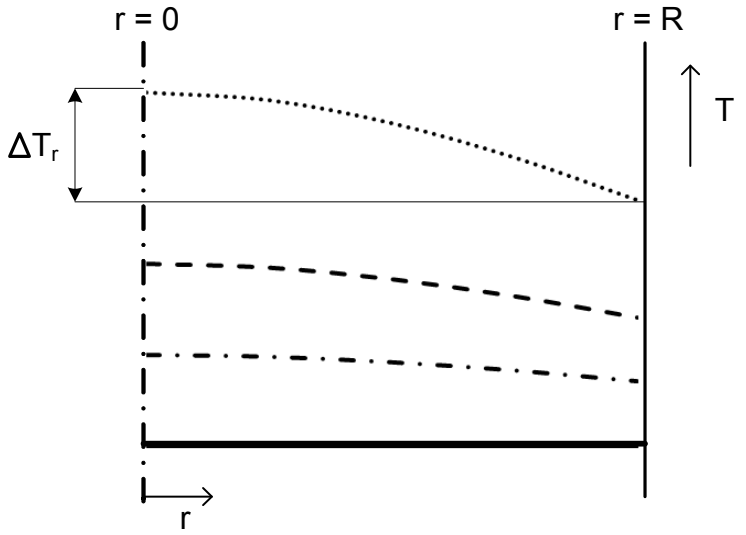

Figure 4: Schematic drawing of radial temperature profiles at different axial positions in a fixed bed reactor with an exothermal reaction; towards the reactor outlet (– · –), before the hot spot (- -), SBT at the reactor inlet (——) and in the hot spot area (···)

In strongly exothermal reactions or in reactors with large diameters in polytropic regime, radial temperature and concentration gradients become significant. This effect is depicted in figure 4. At the reactor inlet and close to the reactor outlet, where also the reaction temperature is close to the SBT, the radial temperature gradient is not extreme. However, around the hot spot area differences between temperature in the reactor center and at its outer perimeter cannot always be neglected. Due to radial temperature gradients, also concentration gradients develop. In such a case, heat and mass transfer in radial direction consequently need to also be represented in the reactor model. Froment and Bischoff [53] document the equations shown in table 2 with the boundary conditions shown in table 3 for such a two dimensional heterogeneous model accounting for one single component.

Table 2: Model equations of the two dimensional heterogeneous reactor model [53]

mass balance fluid phase	$\frac{\partial(u_z \cdot C)}{\partial z} = \varepsilon \cdot D_r \cdot \left(\frac{\partial^2 C}{\partial r^2} + \frac{1}{r}\frac{\partial C}{\partial r}\right) - k_f \cdot a_v \cdot (C - C_s)$	(3.1.5)
heat balance fluid phase	$u_z \cdot \rho_f \cdot c_p \cdot \frac{\partial T_f}{\partial z} = \lambda_{r,f} \cdot \left(\frac{\partial^2 T_f}{\partial r^2} + \frac{1}{r}\frac{\partial T_f}{\partial r}\right) + h_f \cdot a_v \cdot (T_s - T_f)$	(3.1.6)
mass balance solid phase	$k_f \cdot a_v \cdot (C - C_s) = \rho_s \cdot r_{eff}$	(3.1.7)
heat balance solid phase	$h_f \cdot a_v \cdot (T_s - T_f) = -\Delta H_R \cdot \rho_s \cdot r_{eff} + \lambda_{r,s} \cdot \left(\frac{\partial^2 T_s}{\partial r^2} + \frac{1}{r}\frac{\partial T_s}{\partial r}\right)$	(3.1.8)

The mass balance of the gas phase comprises the convection term along with the radial dispersion term and the mass transfer term to the solid phase. D_r represents the radial dispersion, ε the bed porosity, k_f the gas solid mass transfer coefficient and a_v the interfacial area. In a similar fashion, the axial convection, radial heat conduction within the fluid phase and a heat transfer term to the solid phase make up the heat balance of the gas phase. $\lambda_{r,f}$ is the radial heat transfer coefficient in the fluid phase, while h_f is the gas-solid heat transfer coefficient.

The mass balance of the solid shows, that the reaction rate on the catalyst surface is equivalent to the transfer rate to from the gas phase. The heat of reaction is released or consumed at the catalyst surface. In steady state, this heat energy is transferred to or from the gas phase. Froment additionally suggests radial heat conductivity within the solid phase, where $\lambda_{r,s}$ is the radial heat transfer coefficient in the solid phase.

Table 3: Boundary conditions of the two dimensional heterogeneous reactor model [53]

for *z = 0*	$C = C_0, \quad T = T_0, \quad \frac{\partial C}{\partial r} = 0$	(3.1.9)
for *r = 0*	$\frac{\partial T_f}{\partial r} = \frac{\partial T_f}{\partial r} = 0, \quad \frac{\partial C}{\partial r} = 0$	(3.1.10)
for *r = R*	$\alpha_{W,s} \cdot (T_W - T_s) = \lambda_{r,s} \cdot \frac{\partial T_s}{\partial r}$	(3.1.11)
	$\alpha_{W,f} \cdot (T_W - T_f) = \lambda_{r,f} \cdot \frac{\partial T_f}{\partial r}$	(3.1.12)

The separate heat transfer mechanisms in solid and fluid phases are also represented in the boundary conditions at the outer perimeter of the reactor, where $\alpha_{W,f}$ and $\alpha_{W,s}$ are the wall heat transfer coefficients of the fluid and solid phases.

The influence of intraparticular mass transfer limitations on conversion can be evaluated through the Thiele modulus concept [61]. Apparent reaction rates at the catalyst surface (e.g. r_{eff} in eq. (3.1.7)) are then compared to intrinsic reaction rates, taking into account also diffusion of the reactants within the pore structure of the catalyst, which leads to lower actual reactant concentrations. As a result, an efficiency factor η can be evaluated for each reaction, which depends only on diffusion coefficients and reaction rates. The intrinsic reaction rate, which is discussed in more detail in chap. 3.2, multiplied by the efficiency factor results in the effective reaction rate as shown in eq. (3.1.13).

$$r_{eff} = \eta \cdot r_{\text{intrinsic}} \tag{3.1.13}$$

Figure 5 shows a typical concentration distribution within the catalyst pellet at a bed position close to the reactor inlet. The gas phase concentration of the reactant is higher within gas phase than at the catalyst surface. Due to mass transfer resistance, the concentration reduces towards the inner perimeter of the catalyst pellet. A constant efficiency factor in this case is smaller than unity. In such a setting, the concentration of a product or intermediate shows the opposite run. The concentration has a maximum in the center of the pellet and decreases towards the outer perimeter. In the gas phase it is even lower. A constant efficiency factor would be larger than unity.

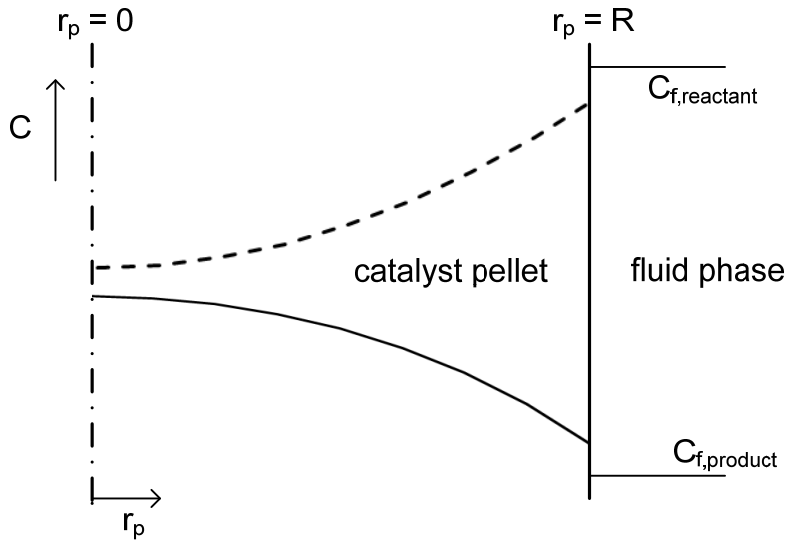

Figure 5: Qualitative concentration gradients of a reactant (- -) and an intermediate or product (—) within a cylindrical catalyst pellet

Nevertheless, in complex reaction systems certain effects may find an ill representation applying a constant efficiency factor which makes it necessary to solve also said balances within the catalyst pellet [59].

Under certain operating conditions, the assumption of ideal plug flow cannot be maintained. In these cases the residence time distribution or backmixing is described through axial dispersion terms in both mass and heat balances [60,62].

The difficulty in considering all possible effects lays in the fact that numerous transport parameters are applied [60]. Quite often it is tedious or sometimes impossible to find reliable correlations to predict such transport parameters accurately. In addition, the existing correlations have a broad error range, so the improvement in description through further detail in the reactor model is overridden by inaccuracies in the prediction of transport parameters.

3.2 Kinetic Modeling

In two-phase chemical reactions, such as the oxidation of o-xylene, the reactants are fed to the reactor in fluid, i.e. gas, phase while the reaction takes place at an active center on the surface of a solid catalyst. In the most general mechanistic idea of the intrinsic reaction, the gaseous reactants first adsorb on the surface, then the surface reaction takes place and finally the reaction products desorb again.

The intrinsic reaction rate is described mathematically through a power law formulation with the surface coverage of the reactant(s) as driving force. In a bimolecular, non-reversible reaction, such as the oxidation of o-xylene and each of its reaction intermediates and by-products, the generalized reaction rate r is expressed through the surface coverage of each reactant θ_1 and θ_2 and the rate constant of the reaction on the solid k_s as shown in eq. (3.2.1).

$$r = k_s \cdot \theta_1 \cdot \theta_2 \tag{3.2.1}$$

One way of describing adsorption and desorption is to consider an equilibrium according to a Langmuir-type isotherm [63]. The surface coverage of a reactant θ_j for the adsorption of multiple, competing components, can therefore be written as shown in eq. (3.2.2).

$$\theta_j = \frac{K_j \cdot p_j}{1 + \sum_n K_n \cdot p_n} \tag{3.2.2}$$

where *K* represents the Langmuir adsorption rate coefficient and *p* the gas phase partial pressure of the reactants. The complete general reaction rate formulation then results in the so-called Langmuir-Hinshelwood type rate expression for a simple reaction (eq. (3.2.3)).

$$r = \frac{k \cdot p_1 \cdot p_2}{(1 + \sum_n K_n \cdot p_n)^2} \tag{3.2.3}$$

with

$$k = k_s \cdot K_1 \cdot K_2 \tag{3.2.4}$$

If one of the reactants does not adsorb, but reacts directly from the gas-phase, a so-called Eley-Rideal [64] kinetic formulation is applied (eq. (3.2.5)).

$$r = \frac{k \cdot p_1 \cdot p_2}{1 + \sum_n K_n \cdot p_n} \tag{3.2.5}$$

For selective oxidation reactions on metal oxide catalysts, Mars and van Krevelen [65] have developed a reaction rate formulation for the intrinsic reaction kinetics, which is based on a more mechanistic approach. In this model, the oxidation of the hydrocarbon is assumed to be carried out by lattice oxygen of the solid catalyst. The catalyst itself is then later re-oxidized by surrounding gas-phase oxygen. The reaction rate is therefore expressed through the rate constant, the surface coverage of oxygen and the partial pressure of the hydrocarbon (eq. (3.2.6)).

$$r_{org} = k \cdot p_{org} \cdot \theta_{O_2} \tag{3.2.6}$$

The surface coverage of oxygen itself is dependent on the oxidation rate of the catalyst *r* on the one hand and on the rate of re-oxidation r_{O2} on the other hand.

$$r_{O_2} = \beta \cdot r_{org} = k_{Ox} \cdot {p_{O_2}}^m \cdot (1 - \theta_{O_2}) \tag{3.2.7}$$

where β is the stochiometric coefficient of lattice oxygen consumption and *m* the exponent to the oxygen partial pressure. Solving eq. (3.2.7) for the oxygen surface coverage θ_{O2}, the overall intrinsic reaction rate for a simple heterogeneous reaction results in the following expression.

$$r = \frac{k \cdot k_{Ox} \cdot p_{org} \cdot {p_{O_2}}^m}{k_{Ox} \cdot {p_{O_2}}^m + \beta \cdot k \cdot p_{org}} \tag{3.2.8}$$

Calderbank et al.[41] extended this Mars-van-Krevelen type reaction rate expression for complex reactions, involving several parallel and consecutive reactions, where different reactions consume the lattice oxygen (eq. (3.2.9))

$$r_j = \frac{k_j \cdot k_{Ox} \cdot p_{org,i} \cdot {p_{O_2}}^m}{k_{Ox} \cdot {p_{O_2}}^m + \sum_n \beta_n \cdot k_n \cdot p_n} \tag{3.2.9}$$

The temperature dependency in the depicted reaction rates is expressed through the Arrhenius correlation between the rate constant and the reaction temperature, with the activation energy E_A, the reaction temperature T, the gas constant R and the frequency factor of the reaction k_0.

$$k_j = k_{0,j} \cdot exp\left(-\frac{E_{A,j}}{R \cdot T}\right) \tag{3.2.10}$$

Langmuir-Hinshelwood rate expressions, as well as Eley-Rideal and Mars-van-Krevelen rate expressions count amongst the generalized Hougen-Watson [66] type rate expressions.

$$r = \frac{kinetic\ term\ \cdot potential}{inhibition\ term} \tag{3.2.11}$$

The kinetic term in each of the rate expressions is equivalent to the rate constant, while the potential term is represented by the partial pressures of the reactants. In both Eley-Rideal and Langmuir-Hinshelwood type rate expressions, the inhibition term is characterized by the adsorption of reactants and products, while in the Mars-van-Krevelen rate expression, the inhibition is represented by the re-oxidation of the catalyst and the consumption of lattice oxygen.

However, industrial catalysts are in most cases porous materials, where the active centers are situated within the pores of the catalyst. Consequently, the process of a chemical reaction on a solid catalyst involves also several mass transfer and transport mechanisms [55]. The reactants diffuse first within the bulk fluid phase until they reach the interface of the

solid catalyst and the fluid. The reactants are further transferred in a film diffusion mechanism at the solid-fluid interface, to reach the solid.

Depending on the pore sizes, different diffusion mechanisms prevail in the mass transport within the porous solid to the active center. If the pore diameter is larger than the mean free path of the reactant molecule, molecular diffusion can be considered the primary diffusion mechanism. At pore diameters smaller than the mean free path of the reactant molecule, the Knudsen diffusion regime becomes more significant. Knudsen diffusion also takes in account interaction of the gaseous particle with the walls of the pore. At pore diameters in the range of 0.3 to 1 nm, configural diffusion becomes the prevailing diffusion regime [55].

The described diffusion within the catalyst particle can strongly influence observed reaction kinetics and can therefore influence the validity of evaluated kinetic parameters. Depending on the necessary precision of the kinetic model, such effects need to be kept in mind when evaluating kinetic parameters.

4. Experimental

4.1 Reactor

Experiments for both the identification of the reaction scheme and subsequent kinetic experiments were carried out in a continuous, pilot scale, single tube fixed bed sample port reactor, supplied by MAN/DWE. The reactor consists of a 4 m cylindrical tube with an inner tube diameter of 25 m, which is filled with catalyst pellets. Reactor dimensions are equivalent to industrial conditions. The cooling temperature is adjusted by means of a molten salt bath, which is stirred to ensure isothermicity and mixing.

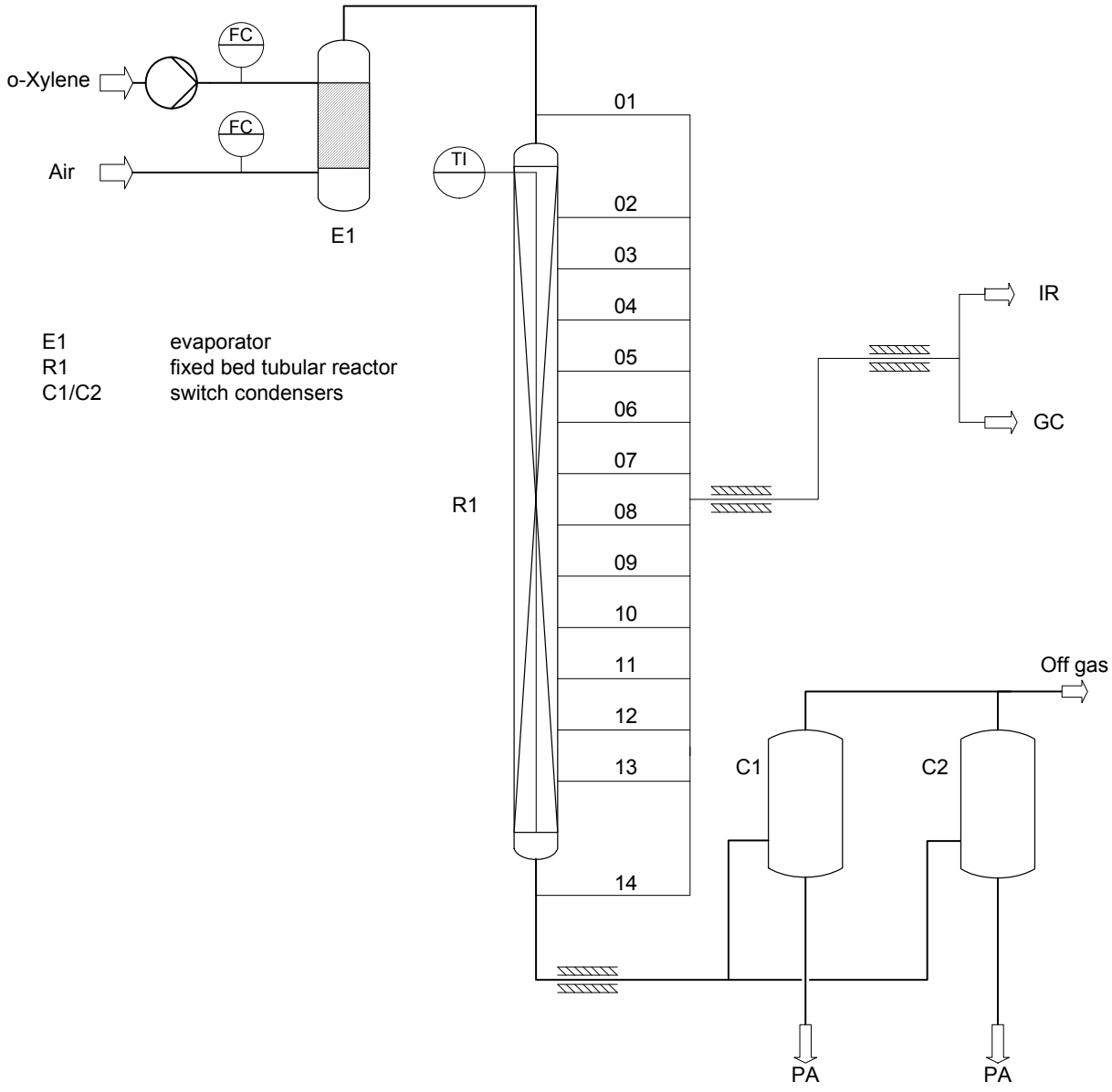

Figure 6: Simplified flowsheet of the sample port reactor

The air flowrate is measured by a mass flow controller with thermal measurement principle (Brooks), while the organic feed stream is controlled by a Coriolis-type mass flow controller (Brooks). Flow measurement of the liquid stream is therefore independent of its composition. The organic reaction feed is vaporized by a preheated hot air flow in a separate self-constructed evaporator at temperatures ranging from 100 °C to 140 °C. Mixing of the feed gas stream is ensured by an inert bed prior to the catalyst bed. In analogy to the industrial process, the reaction product, crude PA is collected in switch condensers, which are operated in parallel with typical cycle times of 48 h (figure 6). Cooling agent is water during operation at 50 °C, while the condensers can be heated with steam at 160 °C in order to melt and recover the product. The remaining gas stream is conducted over a catalytic air purification unit before being released to the atmosphere. The process control of the reactor is automated through a Siemens programmable control system, to ensure non-stop operation. Industrial safety standards are applicable in both process control and design of each of the unit operations.

The o-xylene (BHM Chemikalien) is provided by the central o-xylene supply at a pressure of 2.5 bar, which also supplies a number of other reactors, not subject of this work. O-xylene purity generally ranges around 99%, with p-xylene, m-xylene and cumene being the major impurities. Also nonane can be detected in traces.

The air at 7 bar used for the oxidation reaction is generated by the compressor of the central low pressure air system and subsequently dried. In order to conduct experiments with varying entry concentrations, an additional feed system is provided. It consists of a 15 L tank and a micro annular gear pump (HNP Mikrosysteme mzr 2905). During the operation of dosage experiments, the liquid (an intermediate or by-product solved in o-xylene) is circulated to reach the required pressure of 2.5 bar which is adjusted manually through an ordinary adjustable pressure relief valve (figure 7).

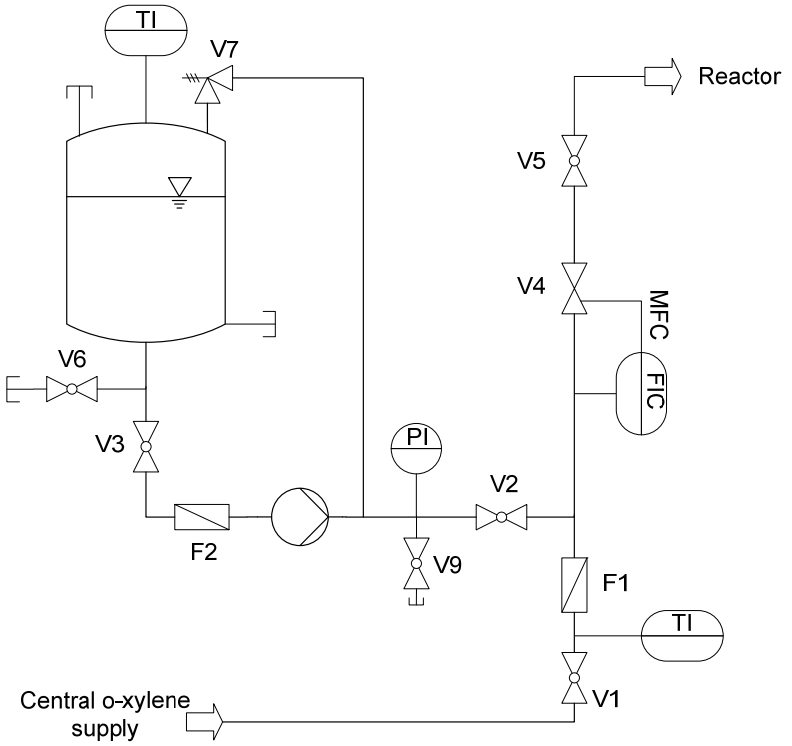

Figure 7: Simplified flowsheet of the supplementary o-xylene supply system for the dosage of intermediates and by-products in solution with o-xylene

Reaction temperatures are measured by means of a multiposition thermocouple positioned in a 3 mm thermo-well in the center of the reactor tube.

The 14 sampling points (including reactor inlet and outlet) are connected to an analysis station where both the organic compounds and the remaining gas phase compositions are analyzed online. The transfer lines to the analysis station are heated by a heat exchanger using oil as heating medium.

The quantitative analysis of organic compounds is conducted by a standard gas chromatograph (Agilent 6820N) using a capillary column (Zebron ZB-5, 60 m). Concentrations of total oxidation products (CO and CO_2) as well as oxygen in the remaining gas phase are analyzed in an infrared analyzer (Emerson NGA2000) with a paramagnetic channel for oxygen.

Within the analysis station, a 16 port multiposition valve (VICI) joins all sampling points to one single analysis line, which is then directed through a 6-port, two position sampling valve (VICI). After the sample loop for the gas chromatograph, the sample stream is passed through a series of condensers in which the temperature is reduced from 250 °C to the ambient temperature. The sample stream is thereby cleaned from any heavy components. The remaining gas stream is dried and filtered in a gas cooler and then conducted to the infrared analyzer. In the analysis station, concentrations of each sampling point are

measured consecutively. The cycle time is 25 minutes due to necessary flushing times to obtain a constant IR signal. The analysis station is controlled by a Labview™ control system, which also records the concentration measurement data. The carbon balance was regularly closed with a deviation of 1 - 2%.

In addition to the online analysis, offline analysis ports are provided at the reactor outlet and several intermediate sampling lines. A small portion of the product or intermediate stream is directed through acetone in a cooling trap, cooled to -70 °C by means of an isopropanol and dry ice cooling bath. All organic components within the gas stream are thereby condensed and solved in acetone directly. This procedure is applied to control the quality of the online analysis through manual injection in the above mentioned GC, on the one hand, but also to analyze gas samples qualitatively to identify unknown intermediates.

The identification of unknown components within the intermediate gas stream is conducted by a standard GC (5890II, Hewlett Packard) equipped with a mass spectrometer (5971A, Hewlett Packard). Mass spectrum identification was carried out applying corresponding data supplied in the NIST database [67].

4.2 Catalyst

The catalyst applied in this investigation is the industrial PHTHALIMAX™ S4 catalyst supplied by Süd-Chemie [7,8,40,69], which can be considered the most selective of catalysts currently available on the market. It is optimized for an o-xylene feed of up to 1.75 vol%, which corresponds to an o-xylene load of 80g per Nm³ of air in the reactor feed.

The catalyst consists of V_2O_5 supported on TiO_2 as an eggshell catalyst on a steatite inert carrier. The catalytic system consists of four different catalyst layers, with each different functions. Layer zero, the first catalyst layer, can be considered an initial layer while the majority of the reaction takes place in layer one, the second catalyst layer. In the industrial application, with catalyst lifetimes of up to four years, the function of layer two, the third catalyst layer, is to ensure that performance is still reached when layers zero and one are aged after long operation time. Finally, layer three, the fourth layer, cleans the reaction product from any undesired by-products. The lengths of the catalyst bed and of each layer are varied depending on the aim of the experiment. However, the total bed length ranges between 200 and 400 cm. The catalyst bed is not diluted with inert material.

Calcination and formation of the catalyst were conducted according to procedures described in literature [69,70].

5. Reaction Scheme

5.1 Literature Overview

Despite some theoretical investigations by Ivanovskaya [71], who suggest phthalane and isocoumarone as intermediates, it is commonly accepted that tolualdehyde (TA) and phthalide (PD) are the main intermediates in the selective o-xylene (oX) oxidation to phthalic anhydride (PA) [17,19].

Bernardini and Ramacci [12,72,73] succeeded in directly oxidizing all intermediates and by-products previously identified in the o-xylene oxidation in presence of a vanadium oxide catalyst. Selective oxidation products include PA, PD, toluic acid (TAc), TA and methylbenzylalcohol (MBA). Also non-selective oxidation to CO, CO_2 and MA is observed. On the same vanadia catalyst, TAc oxidation yields MA, citraconic anhydride (CA) and benzoic acid (BAc), which are commonly known impurities in crude PA. While Bernardini has theoretically developed a much more detailed reaction scheme, the experimentally confirmed reaction scheme is depicted in figure 8.

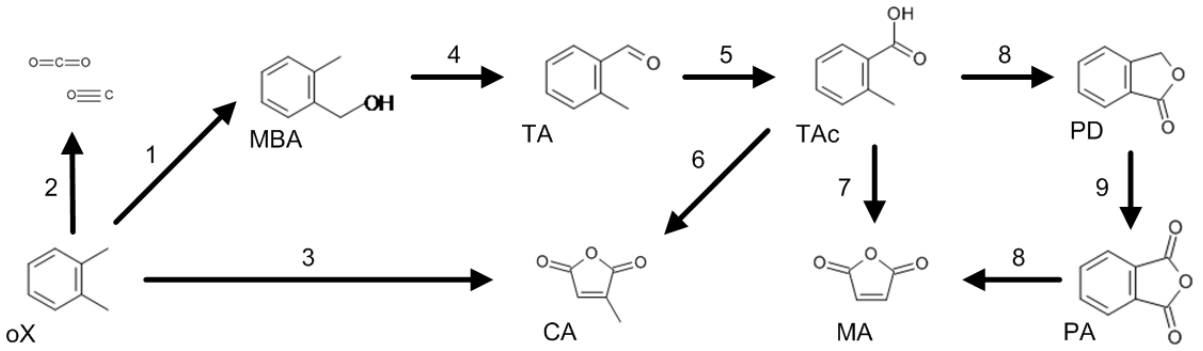

Figure 8: Experimentally confirmed reaction scheme evaluated by Bernardini and Ramacci [12]

Blanchard and Vanhove [74] have studied the reaction mechanism by radioactive tracing of methyl groups of o-xylene. Apart from intermediates and by-products mentioned above, dimethyl-maleic anhydride (DMMA) was identified. Due to lacking radioactivity of MA, they concluded that MA formation, no matter from which source, occurs by oxidative attack of the aromatic ring. A theoretical MA formation path via quinones (benzoquinone (BQ), toluquinone (TQ) and 2,3-dimethyl-p-benzoquinone (DMBQ)) is postulated in analogy to benzene [75-77] and toluene oxidation [76,78] paths observed on vanadia catalyst.

Recently, Ballarini et al. [16] reported benzoic acid, phthalic acid (PAc) and phthalaldehyde (PAld) as intermediates or by-products in o-xylene oxidation. While PAld has already been identified in older publications [20,79], its involvement in the reaction scheme of o-xylene oxidation had not been clearly identified. Ballarini investigated this experimentally

by feeding PAld dissolved in toluene comparing the product spectrum to that of toluene oxidation. The resulting reaction scheme is depicted in figure 9.

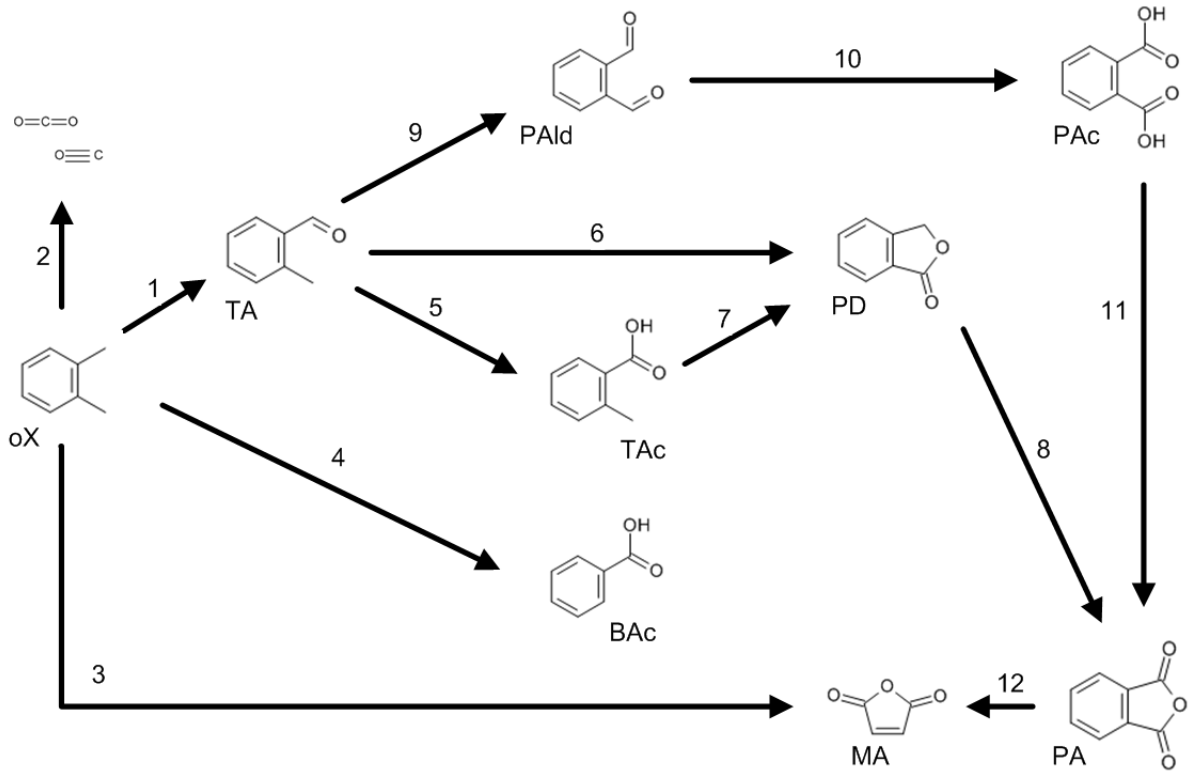

Figure 9: Reaction scheme suggested by Ballarini et al. [16], based on experimental data

While the focus of Bond [11] lay on the investigation of the reaction mechanism on the catalyst surface, the reaction scheme suggested consists of a rake mechanism with the main intermediates detectible in the gas phase along with surface species thereof.

Saleh and Wachs [15] have conducted a study of the reaction scheme based on conversion selectivity profiles obtained by controlling different reaction temperatures. According to these experimental results, MA is formed mainly by oxidation of PA. Possible intermediates in this path are not indicated.

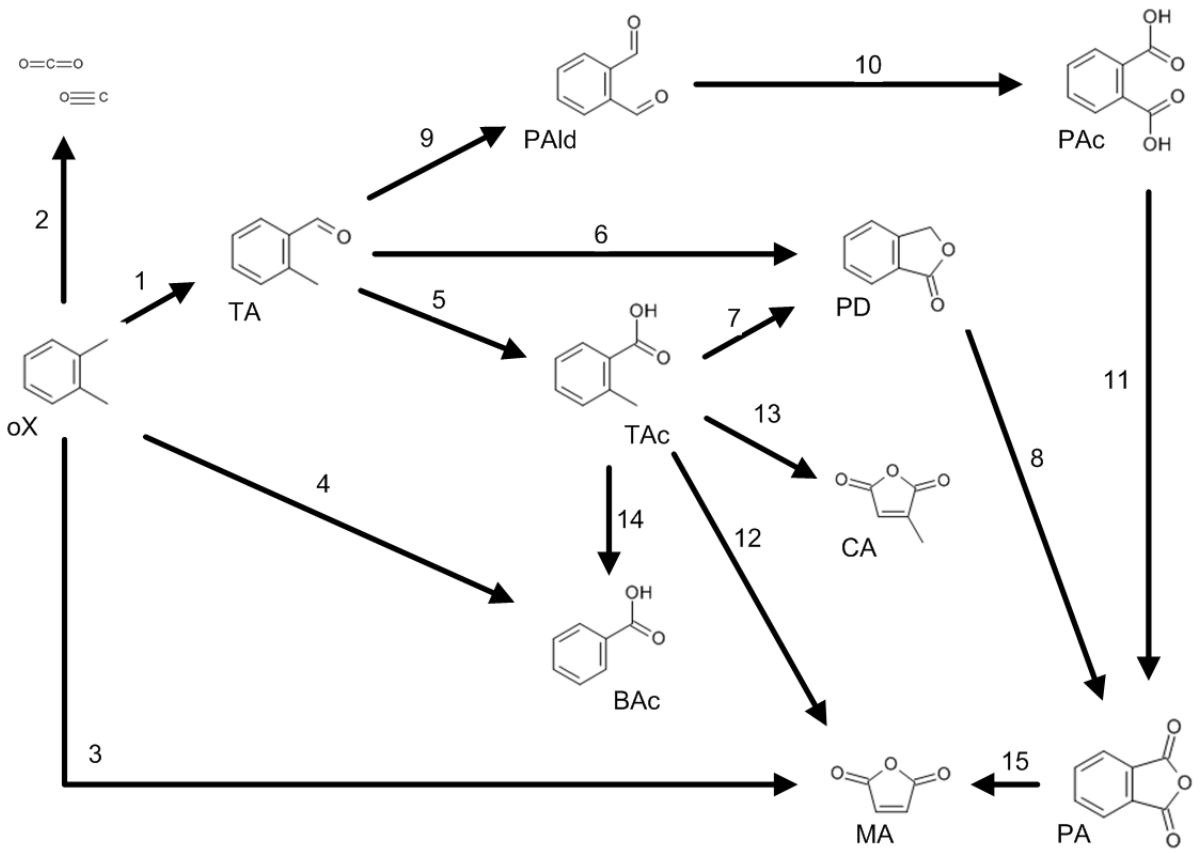

Figure 10: Reaction scheme as excerpted from literature [11,12,15,16,74]

Figure 10 shows the resulting reaction scheme as described in literature [11,12,15,16,74]. The phthalic anhydride formation path in o-xylene oxidation is quite well described and experimentally backed. In contrast, the formation paths of by-products such as benzoic acid, maleic anhydride, CO and CO_2 and especially their sources are widely unknown.

5.2 Selectivity Profiles

The reaction scheme of o-xylene oxidation and in particular the formation of by-products was studied through the analysis of conversion selectivity plots. In irreversible reactions, at isothermal conditions, a component with constantly rising selectivity profile can be considered a final product of a consecutive reaction. In contrast, a parallel reaction yields a constant selectivity profile over the complete conversion range. Intermediates are generally characterized through decreasing selectivity profiles. While the selectivity of a primary intermediate decreases over the complete range of conversion, a selectivity profile of a secondary or higher intermediate bears a clear maximum.

Extrapolating the selectivity profiles of intermediates to zero conversion gives an indication in which order a consecutive reaction takes place. If a non-zero value is obtained, it can be considered a primary intermediate, if the profile takes the value of zero with a slope larger than zero, it is a secondary intermediate, if the slope is also zero it can be considered a higher intermediate [80]. At non-isothermal conditions, this general strategy can also be pursued. However, certain small deviations must be taken in account.

In the four layer system applied in this study, the different catalysts lead also to different selectivities at different positions, making certain reactions more or less significant. However, the general reaction scheme is assumed to be identical. A typical conversion selectivity plot of the main components recorded in o-xylene oxidation is depicted in figure 11. The PA selectivity rises with conversion to reach a value above 80% at 95% conversion. TA has a high selectivity at low conversions which then decreases to zero at nearly full conversion. The shape of the PD selectivity profile, showing a distinct maximum, can be attributed to the fact that it is a secondary intermediate. Both CO and CO_2 selectivities remain nearly constant throughout the course of the reaction. However, they slightly rise to reach a lumped value of about 15 mole% at high conversions, indicating that they are produced mainly in a parallel reaction. The decrease of CO_2 selectivity at low conversions can be attributed to temperature effects on the one hand and the total oxidation of impurities within o-xylene on the other hand. Consequently, selectivity profiles measured in the sampling port reactor represent very well the generalized and simplified reaction scheme as published in literature (compare to figure 10).

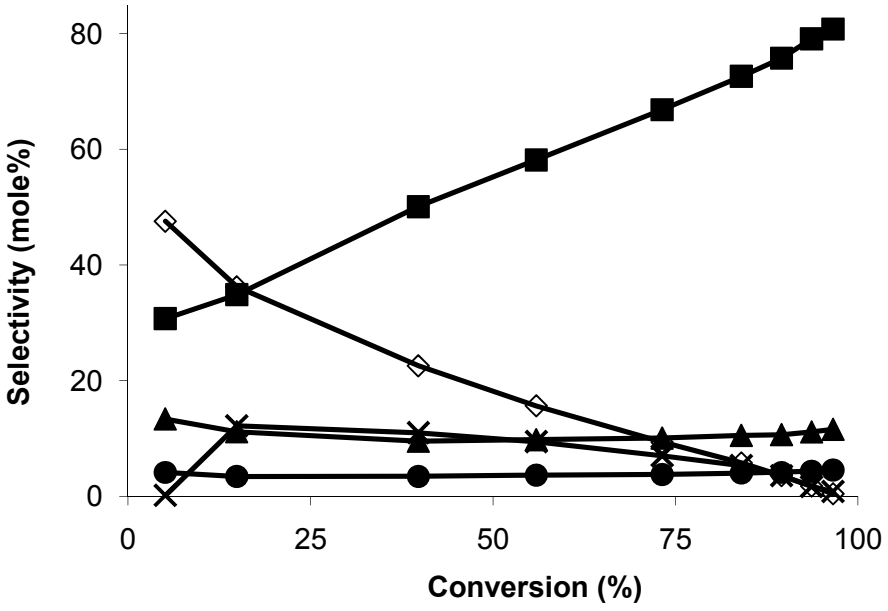

Figure 11: Typical conversion selectivity plot of the main intermediates and products in o-xylene oxidation; TA (◊), PD (x), PA (■), CO (●) and CO_2 (▲)

Selectivities of components with lower concentrations are shown in figure 12. The most important component in this respect is MA, a final product. Its selectivity rises with o-xylene conversion to reach a value of 2.3% at nearly full conversion, leading to the conclusion that it is a final product, which is produced in a consecutive reaction. According to its selectivity profile with a maximum at about 20% conversion TAc is also a secondary intermediate.

BAc selectivity shows a very interesting selectivity profile. It reaches a maximum at lower conversions to subsequently decrease. However, at conversions above 60%, BAc selectivity begins again to rise. This leads to the conclusion, that BAc is produced via multiple reaction paths.

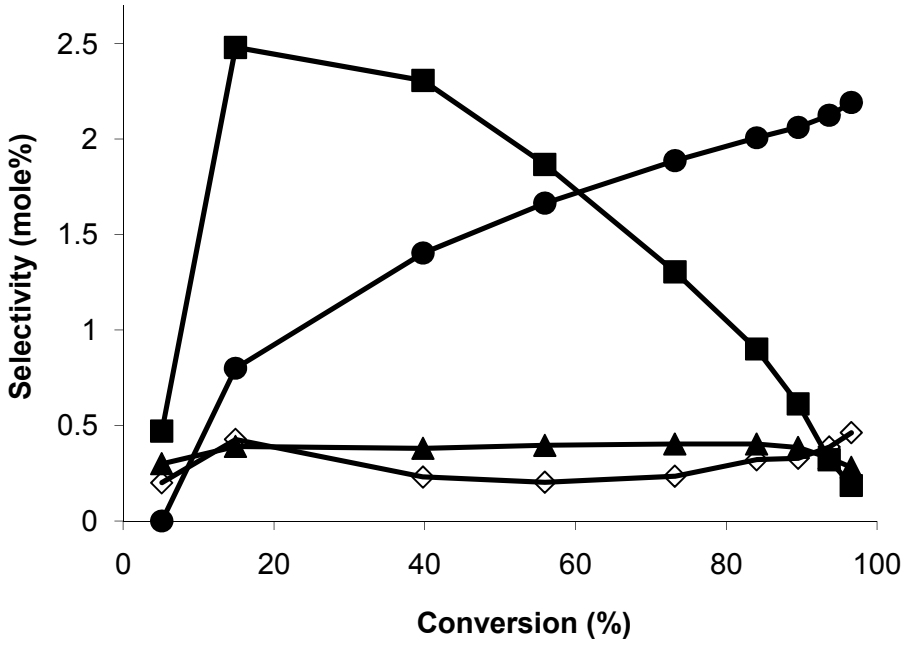

Figure 12: Conversion selectivity plot of the components with low concentrations; TAc (■), CA (▲), MA (●) BAc (◊)

The selectivity profile of CA shows a broad maximum where it remains nearly constant at conversions between 20% and 80%. However, at high conversions, the CA selectivity decreases to reach a value close to zero at full conversion.

Apart from the components depicted in figures 11 and 12, phthalaldehyde (PAld), dimethyl-maleic anhydride (DMMA) and benzoquinone (BQ) are identified in traces.

5.3 Identification of Intermediates

In experiments with the sampling port reactor a number of additional components appeared in the GC measurements at intermediate positions within the catalyst bed. These

are not only certain high boiling point components, in very small quantities, but also a number of low boiling point compounds which could complete reaction paths to undesired by-products.

In order to identify these components, samples were taken at several intermediate reactor positions by means of a cold trap, cooled by a cooling mixture of isopropanol and dry ice. This method corresponds to the industrially applied sampling method. The reaction gas sample is dissolved directly in acetone. These samples were then analyzed by GC/MS. The resulting mass spectra were analyzed according to the methods described by Hesse, Zeeh et al. [81] and compared to the data published in the NIST database [67]. The aim of this analysis is not to fully describe and reproduce the complete decomposition in the mass spectrometer, but to identify components by their footprint.

5.3.1 Toluene

Toluene is an impurity within o-xylene at very low concentrations. However, it appears to also be one of the previously unknown components, which reach a maximum concentration at intermediate bed positions. Although it is mentioned as a theoretically possible intermediate in o-xylene oxidation on vanadia catalyst by Bernardini and Ramacci [12], Andersson [78] as well as in the patent literature [82,83], it has never been experimentally confirmed. The mass spectrum as measured in several reaction gas samples is depicted in figure 13.

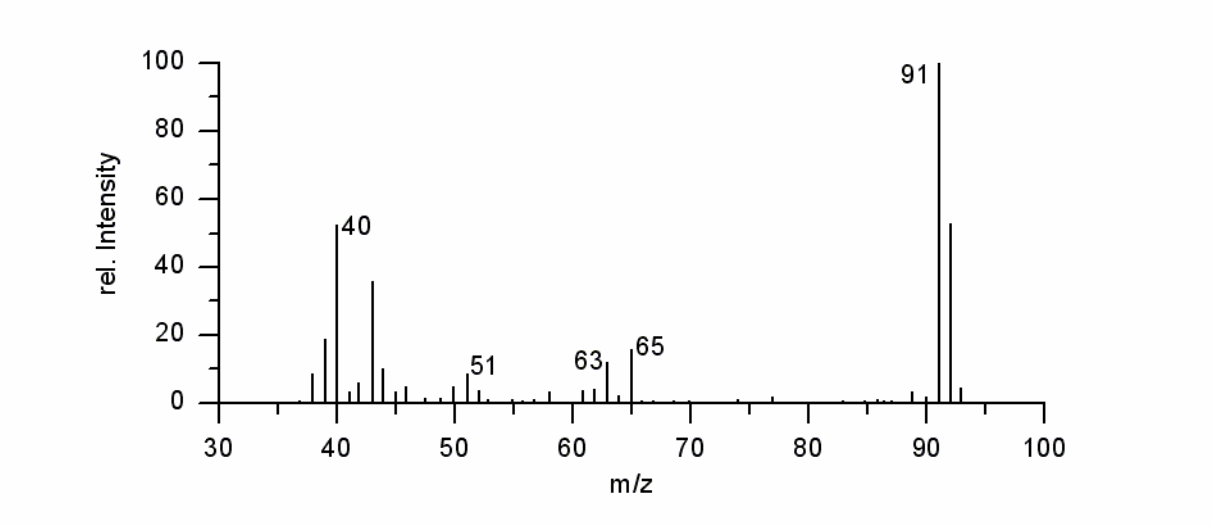

Figure 13: Mass spectrum of toluene in a reaction gas sample

In order to confirm the finding, pure toluene was analyzed and gave the following mass spectrum (figure 14).

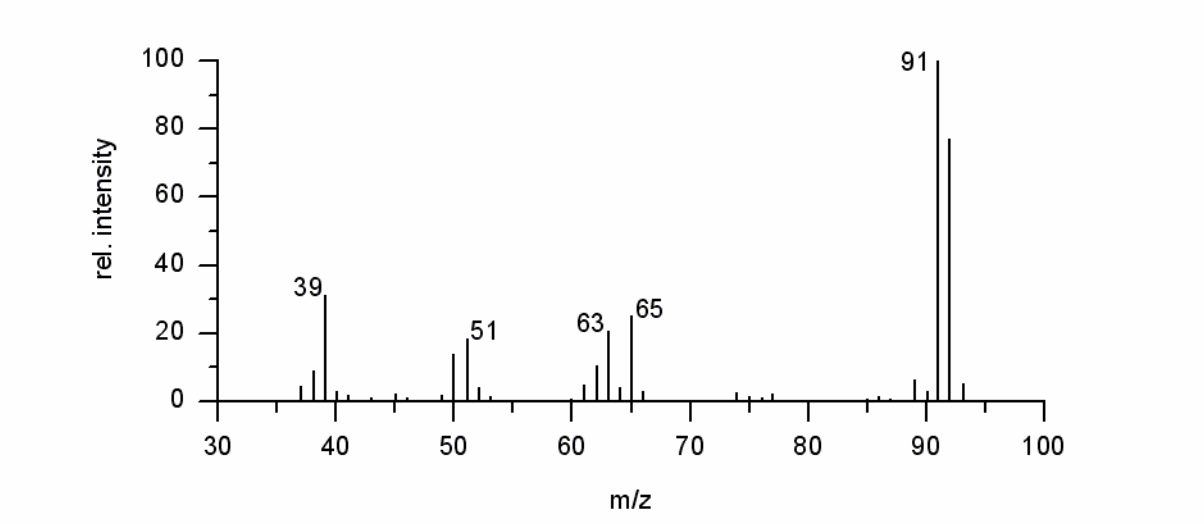

Figure 14: Mass spectrum of pure toluene

The peak at a weight of 91, which is characteristic for toluene is observed in both the analysis of pure toluene and component within the reaction gas sample. In addition, the main masses (i.e. 39, 51, 63, 65) are recorded in both the reference and the measurement samples. In conclusion the component can be undoubtedly identified as toluene.

5.3.2 Toluquinone

Another unknown component with significant intermediate concentrations yields a mass spectrum as shown in figure 15.

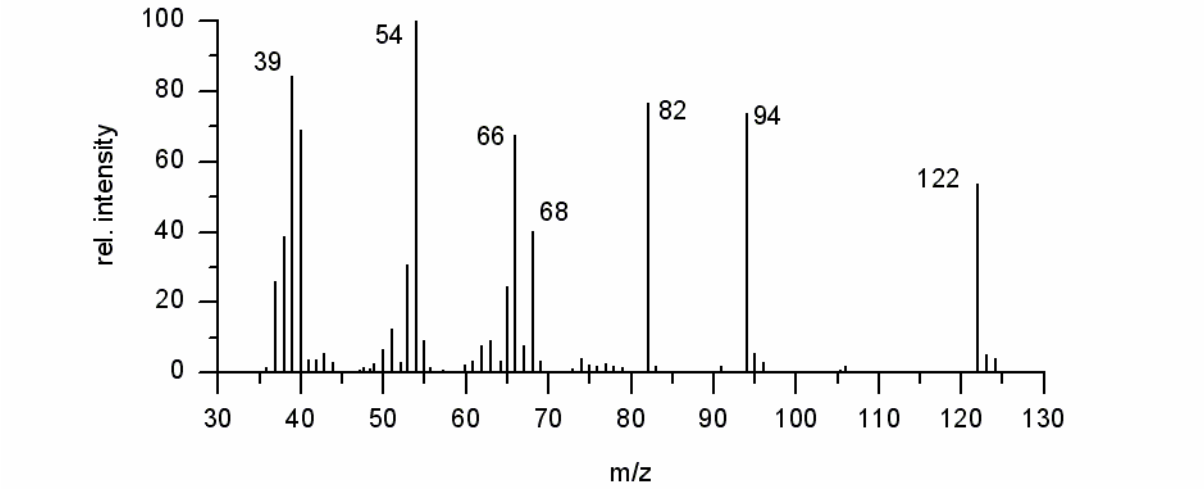

Figure 15: Mass spectrum of toluquinone in a reaction gas sample

The parent peak has a mass of 122. The mass of 54 often appears on spectra of cyclohexene and its derivatives, while masses of 82 and 94 imply cyclic ketones [81]. Quinones in general comply with all these criteria. The parent mass of 122 leads to the assumption this component may be toluquinone.

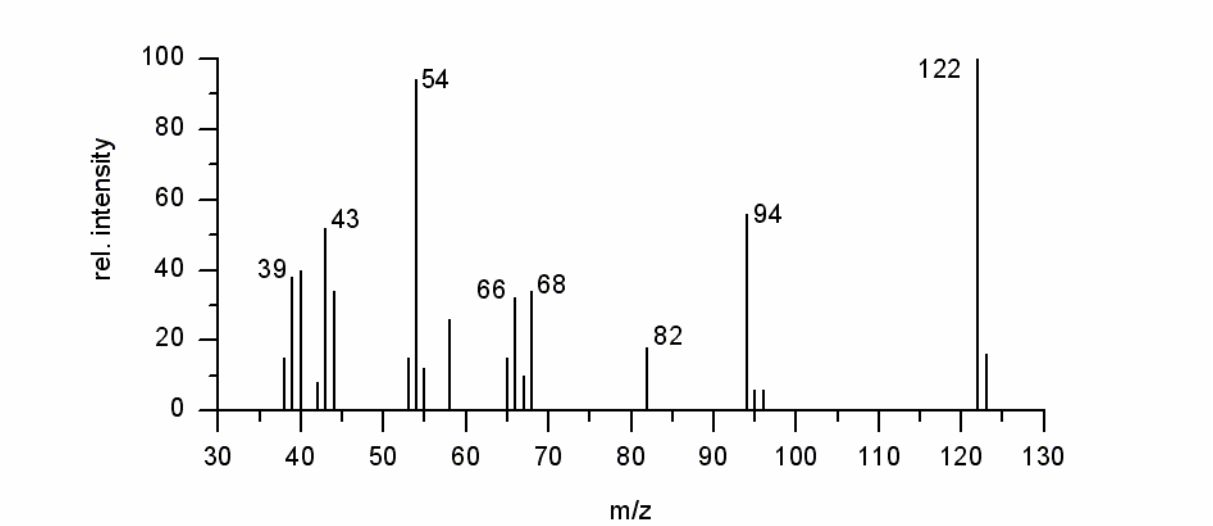

Figure 16: Toluquinone mass spectrum according to Bowie et al. [84,85]

Comparing the measured spectrum to mass spectra of different quinones published by Bowie et al. [84,85], as shown in figure 16, it can be concluded that the component in question is toluquinone. The occurrence and proportions of parent and side peaks correspond very well with the literature spectrum.

5.3.3 2,3-Dimethyl-p-benzoquinone

figure 17 depicts the mass spectrum of another component with significant concentrations, particularly at low conversions.

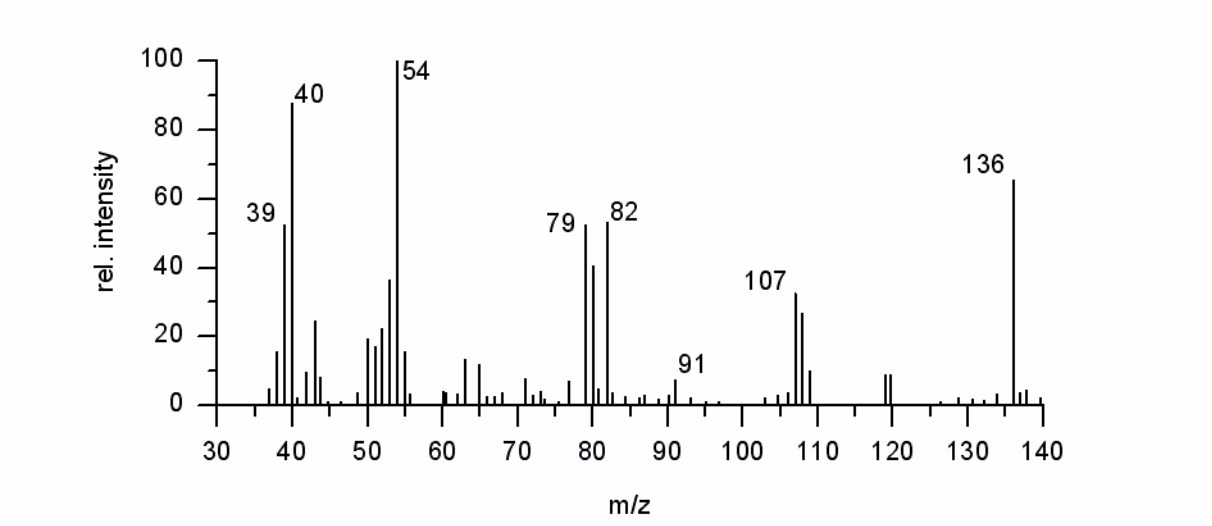

Figure 17: Mass spectrum of 2,3 Dimethyl-p-benzoquinone measured in a reaction gas sample

The parent mass of this component is 136. The masses 39, 54 and 82 appear again supporting a cyclic ketone. The mass of 136 proposes a dimethyl-p-benzoquinone. There are three possible configurations of this compound: 2,6 dimethyl-p-benzoquinone, 1,5 dimethyl-p-benzoquinone and 2,3 dimethyl-p-benzoquinone.

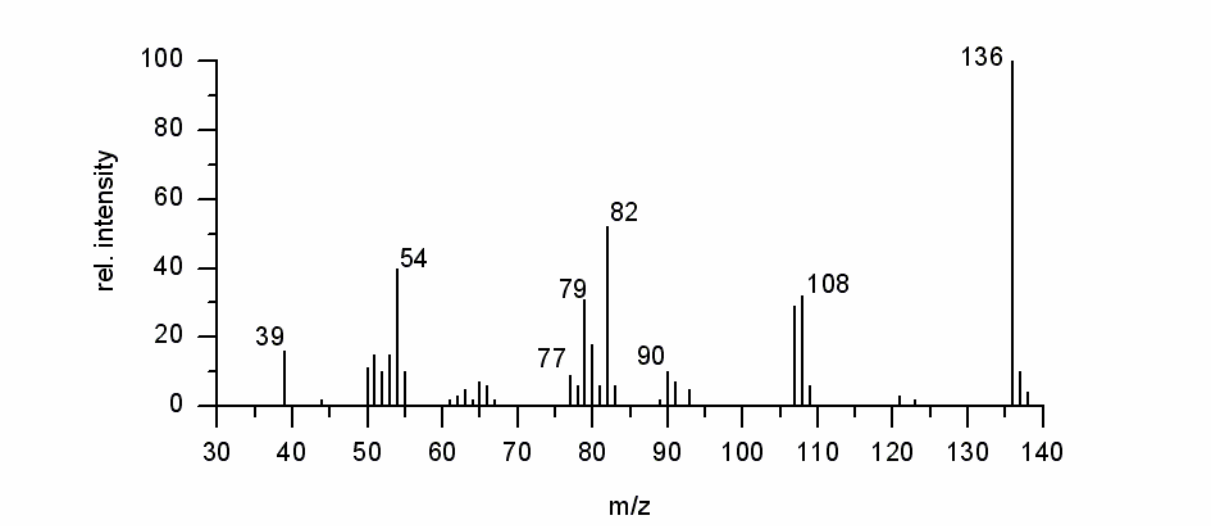

Figure 18: Mass spectrum of 2,3 dimethyl-p-benzoquinone according to Bowie et al. [84,85]

The spectra of each of these configurations have been published by Bowie et al. [84,85]. In particular the signal at a mass of 54 is unique to 2,3 dimethyl-p-benzoquinone. The corresponding mass spectrum is presented in figure 18. Generally, the proportions of the side peaks within both spectra correspond very well.

5.3.4 Compounds Detected in Traces

In online analysis of the intermediate reaction gas stream, two peaks appear at retention times that yield the solvent, acetone when analyzed offline. In order to identify these components, a number of samples were dissolved in pentanone, which elutes at a significantly later retention time. The two peaks were analyzed to acetic acid and acetone.

5.4 Theoretical Aspects

The quinones identified, as well as benzoquinone do not appear in reaction schemes of o-xylene oxidation. However, they are frequently mentioned in oxidation reactions of other aromatic compounds on vanadia catalysts.

Particularly toluene appears to play a key role in the formation of by-products like maleic anhydride and benzoic acid in o-xylene oxidation. The oxidation of toluene on vanadia catalyst has been studied repeatedly. Germain and Laugier [76] identified the formation of benzoic acid as the main route of toluene oxidation. However, also toluquinone, one of the previously identified intermediates, as well as maleic anhydride and citraconic anhydride are reported as oxidation products. Also benzene was identified in traces. These results have later been confirmed by several researchers [78,86-93].

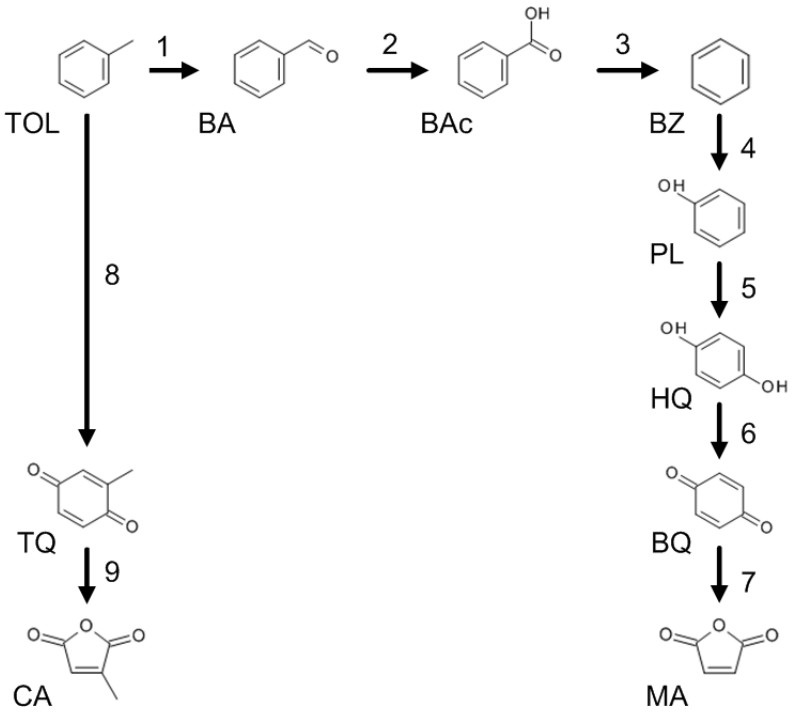

Figure 19: Reaction scheme of the main toluene oxidation paths on vanadia catalyst according to Andersson [78]

Figure 19 shows the reaction scheme finally developed by Andersson [78]. Two different oxidation paths are identified. On the one hand it is oxidized to benzaldehyde (BA),

benzoic acid (BAc) to benzene (BZ) through a nucleophilic attack of the methyl group. On the other hand, it is oxidized to toluquinone (TQ) and subsequently citraconic anhydride through an electrophilic attack of the aromatic ring. Once the methyl group is completely consumed, benzene can also be further oxidized to maleic anhydride with phenol (PL), hydroquinone (HQ) and benzoquinone (BQ) as intermediates. The main selectivities in this reaction are with benzaldehyde and benzoic acid. Both Andersson and Germain suggest also a third path, in which two toluene molecules are coupled to form naphtoquinone, which decomposes to phthalic anhydride. According to the reported experimental data, the desalkylation of citraconic anhydride to maleic anhydride does not occur.

The oxidation of benzene to maleic anhydride has been an industrial process conducted on V_2O_5/MoO_3 catalysts for many decades. Bielanski et al. [77] as well as Dolgov [75] have concluded a reaction scheme based on the attack of the aromatic ring to form phenol which is further converted to hydroquinone, benzoquinone and finally MA (figure 20). Krylova et al. [94] detected precisely these compounds in mass spectroscopic analysis of the reaction product.

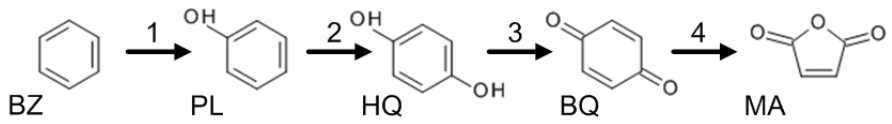

Figure 20: Benzene oxidation path on V_2O_5/MoO_3 reported in literature [75,77,94]

According to Dolgov [75], the oxidation of citraconic anhydride yields acetic acid as intermediate to later be further oxidized to CO and CO_2. The selectivity profile of DMBQ recorded in o-xylene oxidation, as shown in figure 21 shows clearly that it is a primary intermediate, while the runs of both TQ and toluene profiles indicate they are secondary or tertiary intermediates.

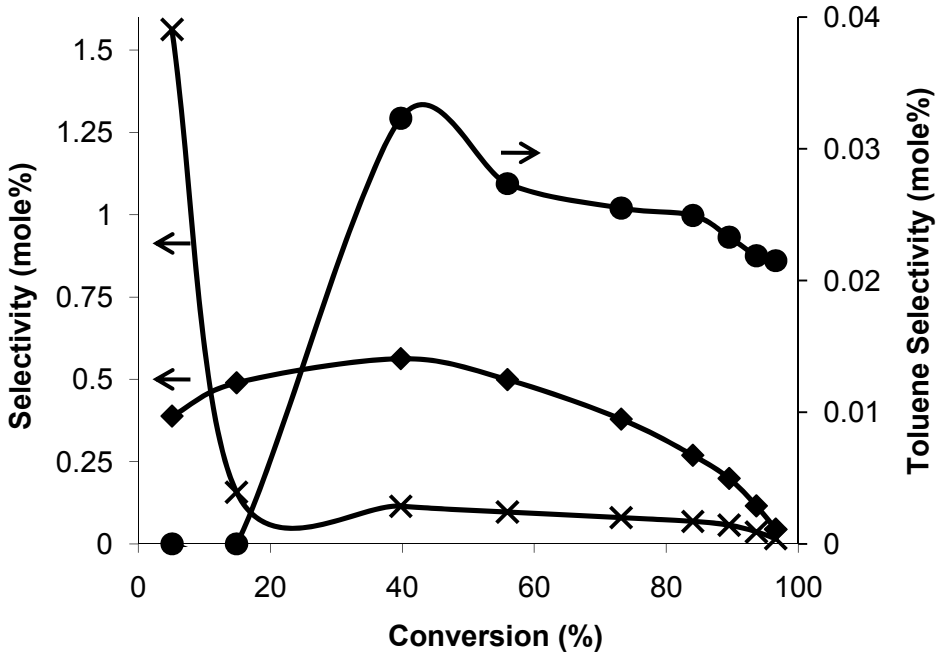

Figure 21: Conversion selectivity plot of the identified intermediates TQ (♦), DMBQ (x) and toluene (●)

Taking in account the literature findings of the oxidation of o-xylene and the identified intermediates, as well as the recorded conversion selectivity profiles, the following reaction scheme can be postulated, considering only the components actually measured in the pilot reactor (figure 22).

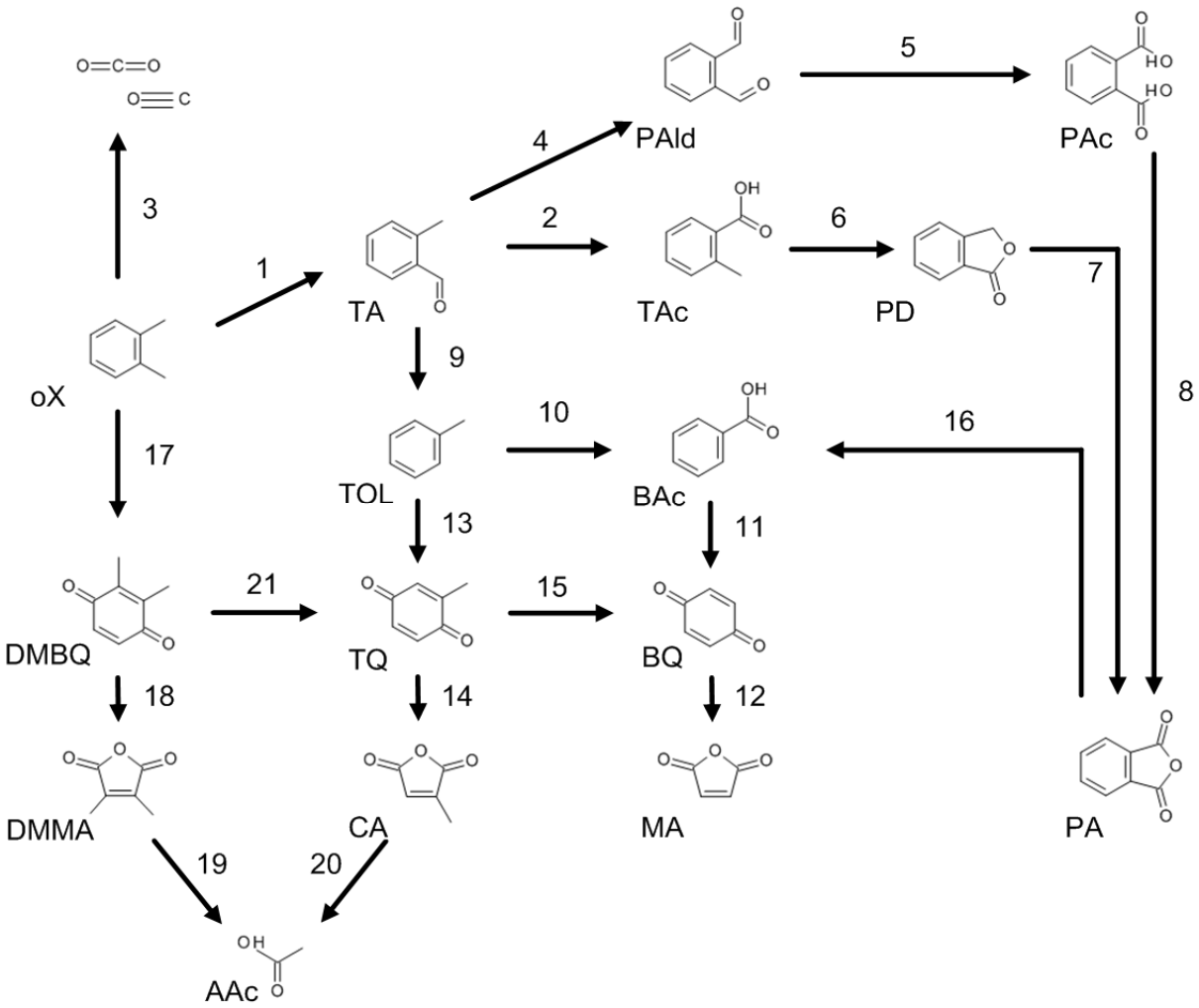

Figure 22: Reaction scheme of o-xylene oxidation taking into account literature data and o-xylene oxidation data

Reaction paths 1, 2, 6 and 7 in figure 22 represent the main PA formation paths as commonly cited in literature. Paths 4, 5 and 8 have been identified by Ballarini et al. [16]. Reaction paths 10 through 15 represent the reaction scheme of toluene oxidation on vanadia/titania catalyst. As shown in figure 21, DMBQ is a primary intermediate. Consequently, the attack of the aromatic ring is supposed in analogy to the formation of toluquinone from toluene.

Although considered a very stable component, Volfson et al. [95] have studied the oxidation comportment of phthalic anhydride on vanadia catalyst in naphthalene oxidation and has concluded that it can be oxidized to maleic anhydride and CO_2. In addition, Plisov et al. [96] report that benzoic acid is formed by decarboxylation of phthalic anhydride on metal oxides. A direct, one step oxidation of PA to MA seems improbable, a decomposition route via benzoic acid seems more likely and is therefore postulated.

The formation path of toluene is not clear. It is a secondary or higher intermediate. Therefore, the direct formation from o-xylene is improbable. Theoretically, the abstraction of the aldehyde group from TA or the acid group from TAc seem more likely.

5.5 Experimental Confirmation

In order to identify oxidation paths of the different reaction intermediates, a series of dosage experiments was conducted. The aim of each dosage experiment is to identify the conversion selectivity plot a particular compound. Intermediates are dosed by adding up to 10mole%, or their maximum solubility concentration in o-xylene to the feed. Consequently, each dosage experiment requires a reference of pure o-xylene feed in order to clearly distinguish between selectivities of o-xylene and of the compound in question. The formation of toluene and the confirmation of reaction paths reported in literature in selective benzene and toluene oxidation with the vanadia/titania catalyst optimized for highly selective o-xylene oxidation are of particular interest.

The catalyst applied for this investigation, was completely activated according to literature methods [69,70] and has gone through several weeks of steady state operation at the design inlet concentration of 1.5% o-xylene in air.

These experiments were conducted in the sample port reactor, which operates at non-isothermal conditions. The inlet concentrations of the intermediates were deliberately kept low, in order not to change the temperature profile significantly and to keep operating conditions and gas phase concentrations as close to industrial conditions as possible. The optimal inlet concentration to meet both requirements of sufficient measurement accuracy and comparability was identified in the range of 3 – 10 mole%.

In cases where a clear conversion selectivity plot could not be identified due to low inlet concentrations, which is the case for compounds with low solubility level in o-xylene, the stream tables were compared.

5.5.1 Toluene Dosage

The oxidation of toluene added to the feed over the applied catalyst yields results which are in good accordance with the presented literature data. The main final selectivities (figure 23) of toluene are MA, CO and CO_2.

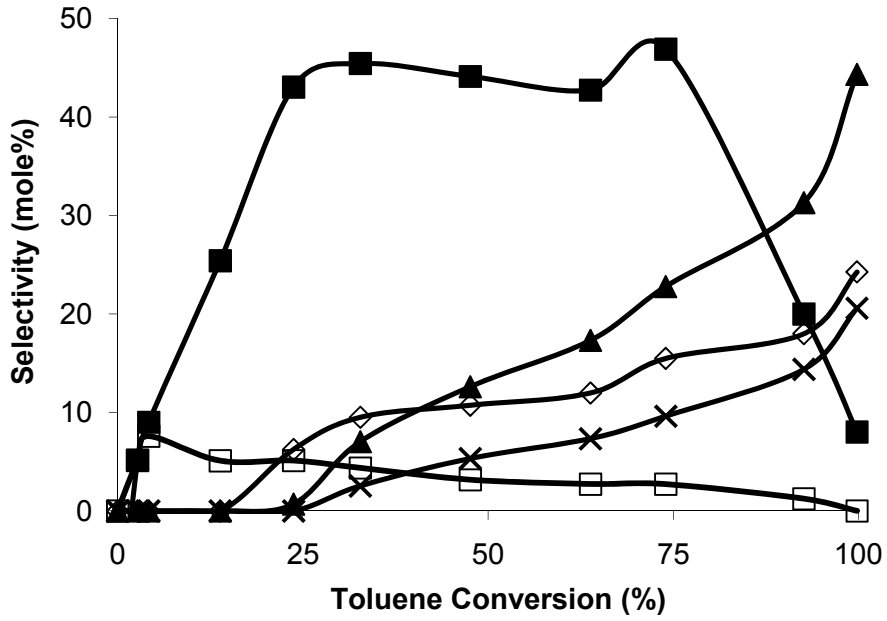

Figure 23: Conversion selectivity plot of toluene oxidation, with BAc (■) showing intermediate selectivity and MA (◊), CO (x), and CO_2 (▲) showing selectivities profiles of final products

Components with high intermediate selectivities in toluene oxidation are especially BAc, but also BQ. Both components have a profile of a secondary or higher intermediate. Benzaldehyde (BA), which is identified in GC/MS analysis of a condensed reaction gas sample, but is not quantified in the online analysis, appears to be the primary intermediate.

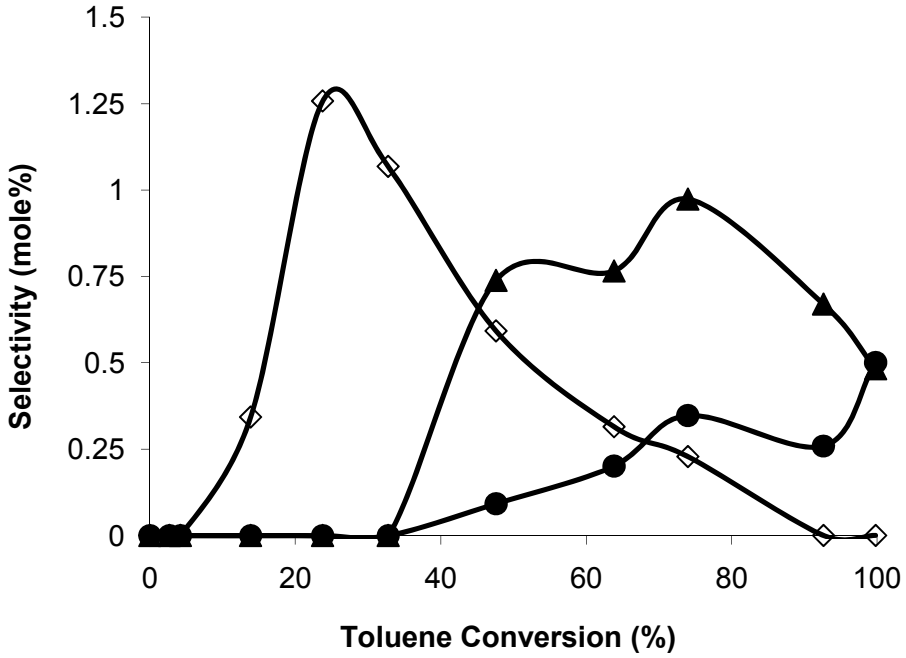

Figure 24: Conversion selectivity plot of toluene; low selectivities; TQ (◊) is a secondary intermediate, CA (▲) a higher intermediate and AAc a final product (●)

AAc can clearly be determined as final product (figure 24), while TQ and CA show minor intermediate selectivities. Additional components detected in traces by GC/MS analysis are benzene (Bz) and phenol (PL), which just as BA are not quantified.

5.5.2 Toluquinone Dosage

TQ dosage proved particularly difficult due its oligomerization in solution with o-xylene. However, a data set of TQ dosage was successfully acquired. Due to the difficulties in the experiment, the conversion selectivity shows the tendencies, but the measurement error in the quantification needs to be kept in mind.

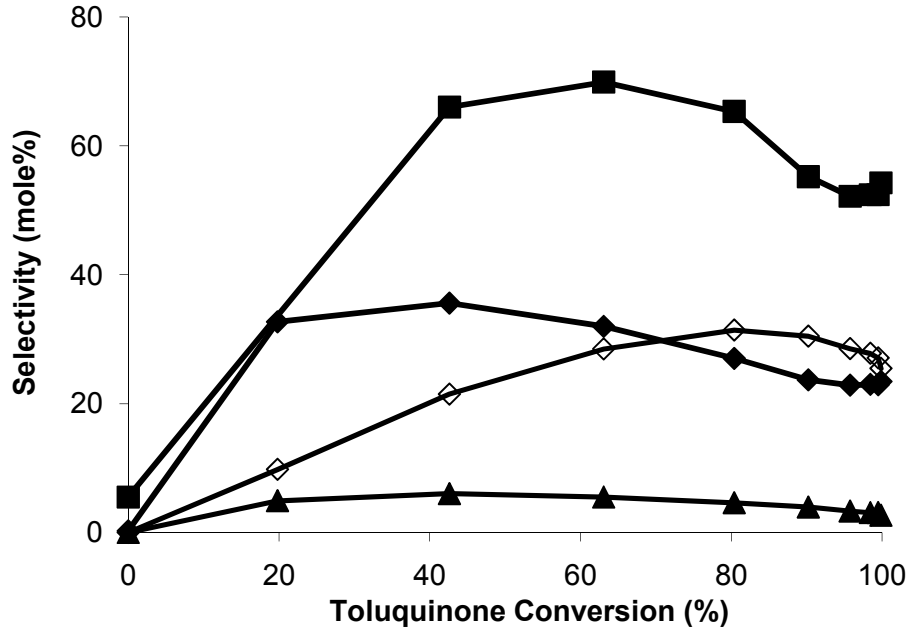

Figure 25: Conversion selectivity plot of the main products of TQ oxidation; MA (◊), CO_2 (■) CA and CO (♦)

TQ oxidation products comprise CO, CO_2, MA and CA, with CA showing the selectivity profile of an intermediate (figure 25). In addition, AAc shows increasing selectivities at nearly complete TQ conversion. Selectivities towards BQ could not be observed. Also GC/MS analysis of the gas sample did not yield any unexpected components.

5.5.3 Benzoic Acid Dosage

Due to its relatively high boiling point, the evaporation of benzoic acid in the same evaporator with o-xylene required substantial optimization efforts. In addition, the solubility of around 5 mole% is relatively low. Therefore the stream tables are compared for this component.

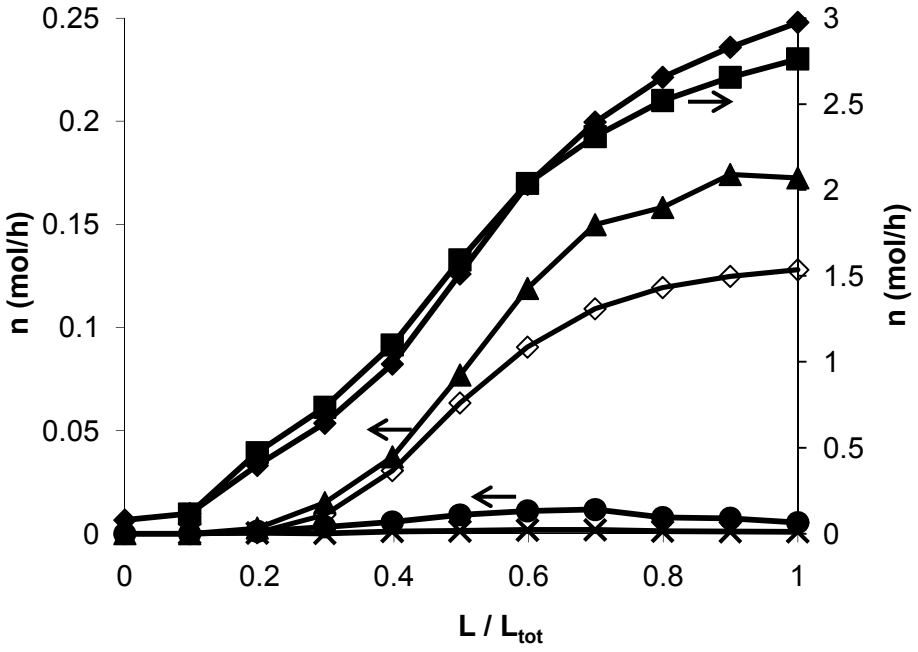

Figure 26: Comparison of molar flowrates in the BAc dosage experiment; MA reference (◊), MA dosage (▲), BQ reference (x), BQ dosage (●), CO_2 reference (■), CO_2 dosage (♦)

The main products of BAc oxidation on said catalytic system are MA and CO_2 while BQ appears to be an intermediate (figure 26). Each of these components shows significantly higher flow rates in the dosage experiment than in the reference, although the total organic feed rate remains constant. Additional compounds identified in traces comprise hydroquinone, phenol and benzene.

5.5.4 Benzoquinone Dosage

In BQ dosage, similar difficulties were encountered as in TQ dosage. Therefore the stream tables give a more clear and coherent picture.

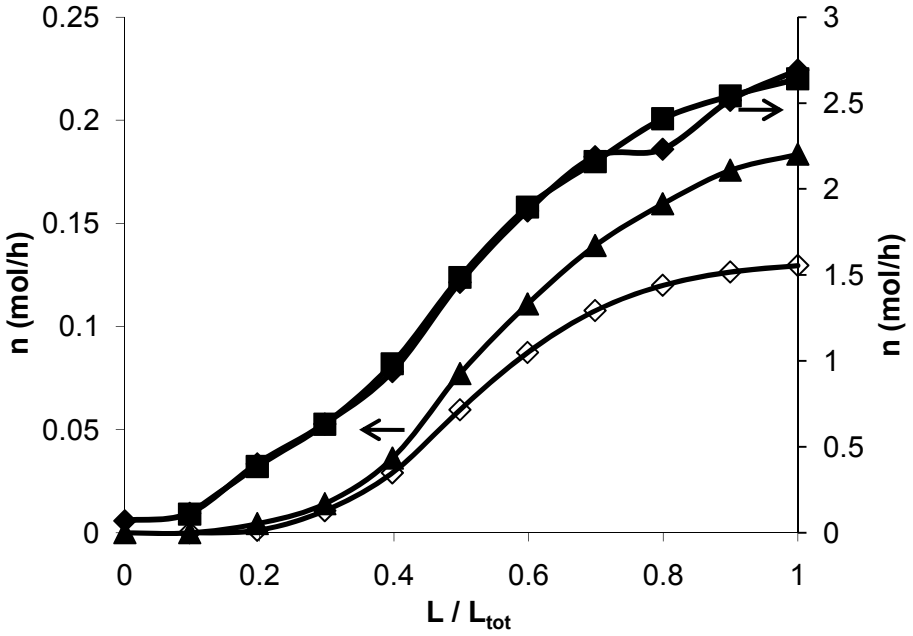

Figure 27: Stream table of the BQ dosage experiment MA reference (◊), MA dosage (▲), CO_2 reference (■), CO_2 dosage (♦)

The main product of BQ oxidation is MA. The molar flow rate in the dosage experiment is significantly higher than in the reference run (figure 27). CO_2 is also formed in very little, almost negligible quantity. Intermediates could not be established. BQ consequently appears to be a very selective intermediate in the MA formation path. GC/MS analysis of reaction products also did not yield any unexpected components specific to BQ oxidation.

5.5.5 Citraconic Anhydride Dosage

CA appears to be comparably stable and is oxidized only in minor amounts. The main oxidation products of CA are CO_2 and CO. AAc shows very small selectivities. On the applied catalyst, MA is not formed from CA oxidation. In consequence, the decarboxylation of CA to MA apparently is not an actual reaction path.

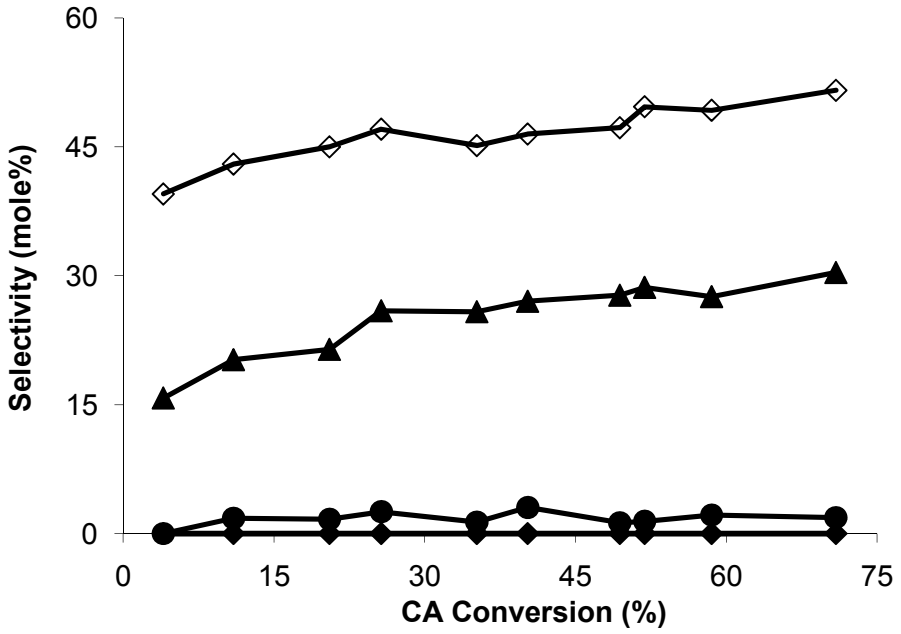

Figure 28: Conversion selecitivity plot of CA oxidation CO_2 (◊), CO (▲), AAc (■), MA (♦)

In correspondence with reaction gas samples from regular o-xylene oxidation, where CA in some cases occurs as an impurity with very small quantities, the CA fed to the reactor is also not completely consumed.

5.5.6 Toluene Formation

Two possible paths of toluene formation were theoretically identified. On the one hand it can be formed directly from tolualdehyde, on the other hand, the preferred path could go via TAc. Both of these components were added to the reactor feed was dosed.

Bernardini et al. [73] reported on MA selectivities in TAc oxidation. Also, it seems likely that the acid group of TAc is abstracted to give toluene. However, the dosage experiment of TAc unambiguously revealed that main products are PA and PD. While selectivities to other components such as CO_x or MA could not clearly be identified, measured toluene concentrations in the dosage experiment are significantly higher than in the reference experiment.

At the reactor outlet TA oxidation yields a final selectivity to PA of around 90%. However, at full tolualdehyde conversion, MA exhibits a selectivity of about 1.6%. Combined CO and CO_2 selectivities range around the same value. Intermediates with high maximum selectivities are TAc and PD, which account for the selective path to PA.

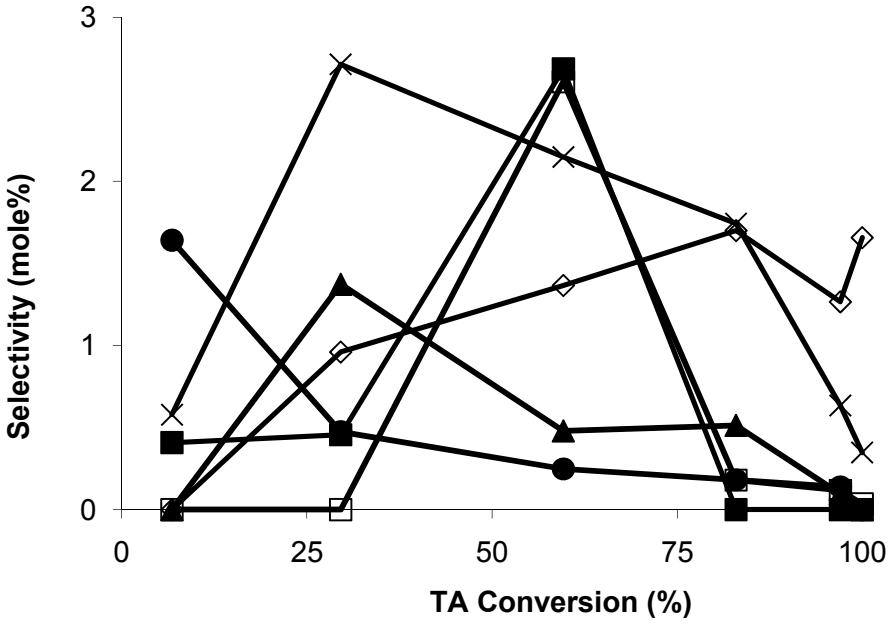

Figure 29: Selectivity conversion plot of the low selectivities in o-tolualdehyde oxidation; MA (◊), CO (x), BAc (■), TOL (●), TQ (▲), BQ (□)

The selectivity profile of toluene (figure 29) clearly shows the run of a primary intermediate. The oxidation products of toluene, BQ, TQ and BAc, too show significant intermediate selectivities while traces of benzene, phenol and benzaldehyde can be identified by GC/MS analysis of intermediate gas samples. Consequently, it can be concluded that both TAc and TA can be sources of toluene. Its main source however appears to be TA.

5.6 Novel Reaction Scheme

The presented spectrum of by-products and intermediates can be divided into two different reaction schemes. The first describes the oxidation of o-xylene with a selective reaction path to PA together with the non-selective paths to MA via DMBQ and to CO and CO_2. The selective oxidation of TA occurs via TAc and PD or PAld and PAc as intermediates. TA is converted to PA with relatively high selectivity. However, both TA and TAc have non-selective paths to toluene (figure 30).

The second reaction scheme consists of the toluene oxidation paths. A large number of intermediates lead to the formation of CO_x, MA and CA.

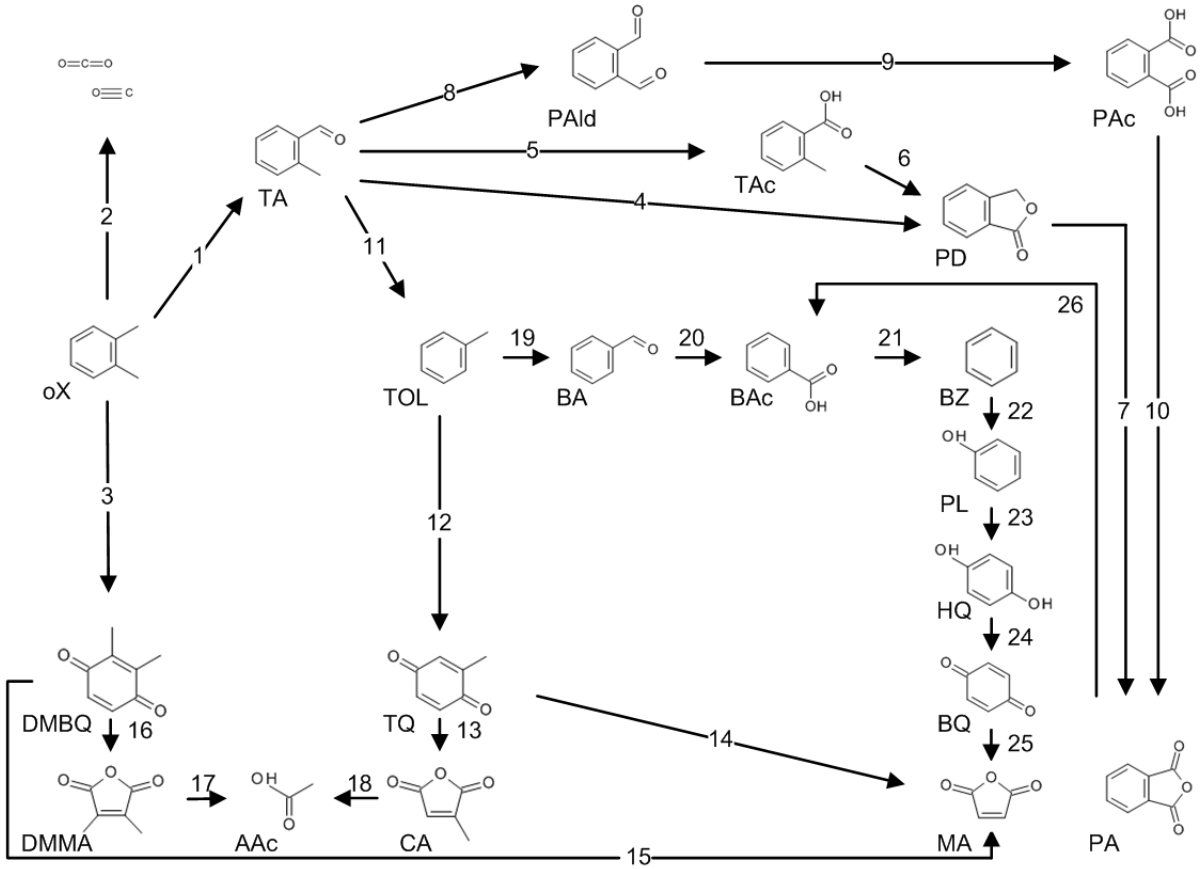

Figure 30: Novel reaction scheme of o-xylene oxidation

At certain operating conditions, the PA selectivity profile shows a clear maximum, while the BAc selectivity reveals a second maximum, and the selectivities to MA, CO and CO_2 increase. Consequently, PA is considered to be oxidized to MA in a path via BAc and its intermediates (path 26 in figure 30).

In general, two main mechanisms can be observed. The first is the nucleophilic oxidative attack of the methyl group, the other the electrophilic attack of the aromatic ring. Once the side chain is oxidized, the attack of the aromatic ring is prevented, unless one side chain is completely consumed. In a similar way, once the aromatic structure of the ring is cracked, the oxidation of the side chains becomes less likely. The attack of the aromatic ring can occur for any aromatic compound with no or only alkyl side groups.

In analogy to the formation of MA from TQ, it is assumed that DMBQ is an intermediate to MA formation directly from o-xylene. Dimethyl-maleic anhydride (DMMA), which only occurs in minor concentrations, is a rather stable product. In analogy to CA oxidation it is assumed, this compound may be oxidized to AAc, but not to MA.

The investigation of the reaction scheme could confirm the reaction paths previously published (paths 1, 2 and 4 – 10). In addition, paths 3 and 11 – 26 were additionally found and experimentally confirmed for the first time in this work [97].

6. Kinetic Modeling and Simulation

6.1 o-Xylene Oxidation Kinetics in Literature

Next to the identification of the reaction scheme of o-xylene oxidation, the kinetic description of this process, particularly taking into account the information gained from the previous experiments is another aim of this work. The kinetic model developed shall describe the general reactor comportment as well as the formation of by-products for the different catalyst layers applied in the industrial application. The kinetics of this reaction has been studied widely in literature, which will be presented briefly in the following passage.

While early studies [65,95,98-100] of kinetics in phthalic anhydride production were devoted to the oxidation of naphthalene, the oxidation kinetics of o-xylene on vanadia catalyst has been studied in detail since the 1960s. As early as 1968, Herten and Froment [13] published a first study of the o-xylene oxidation kinetics. The aim of this study was to evaluate the kinetics of the main overall reaction steps, the formation of PA, its subsequent total oxidation as well the parallel reaction of o-xylene to CO and CO_2. Kinetic measurements were conducted at quasi-isothermal conditions in a bench-scale tubular reactor with diluted, low productive industrial catalyst. The kinetics was described by a simple power law rate equation and was developed mainly to be able to describe the disappearance rate of o-xylene.

Downie et al. [99,101-103] studied the kinetics of the oxidation of several aromatic hydrocarbons (benzene, toluene, naphthalene and o-xylene) on vanadia catalysts in a series of investigations. The aim of the kinetic investigations of o-xylene oxidation was to discriminate different kinetic models, particularly the Eley-Rideal, Langmuir-Hinshelwood and several Mars-van-Krevelen type redox models, which take into consideration different reaction orders for oxygen on the one hand and oxygen desorption on the other hand. Experiments were carried out in a lab-scale differential bed reactor and selectivities were determined only at conversions inferior to 10%. Downie concluded that the reaction rate equation as described by Mars and van Krevelen most suitably describes o-xylene oxidation.

Lyubarskii et al. [104-106] have conducted a series of kinetic studies studying the oxidation of o-xylene and its intermediates and by-products in the PA formation path. The experimental set-up applied comprises a fixed bed reactor with circulating reactant flow. In order to evaluate the oxidation reaction kinetics, each intermediate and organic product, i.e. MA, PA, TA and o-xylene, is oxidized separately and the reaction rates of the resulting reaction steps are evaluated. This way, the reaction kinetics evaluated includes a very detailed reaction scheme. The numerous kinetic parameter values of a Langmuir-Hinshelwood type rate expression were numerically fitted. At the chosen operating conditions an influence of oxygen or CO_2 concentrations on the reaction kinetics could not be identified.

In a publication on parameter estimation strategies in heterogeneous catalysis, Froment [107] referenced an unpublished kinetic study of o-xylene oxidation in an integral

reactor in which Langmuir-Hinshelwood type reaction rate equations were applied. In this study, kinetics of intermediate reaction paths was determined. Unfortunately, parameter values are not indicated.

Vanhove and Blanchard [108] conducted a kinetic study of this reaction as a part of a series of studies on the oxidation of o-xylene on vanadia catalyst. Kinetic experiments were carried out at low o-xylene and tolualdehyde conversions in order to study the type of reaction rate equation by analyzing differential reaction rates. The reactor applied was a tubular differential reactor. Vanhove concluded that the dependence of initial reaction rates on the o-xylene concentrations is reduced and non-proportional at inlet concentrations above 0.5 mole%. Therefore the description with a simple power law rate equation yields inaccurate model predictions above this concentration. The determination whether a Langmuir-Hinshelwood or Mars-van-Krevelen type rate expression are more favorable in the description of this reaction was reduced to the question which intrinsic reaction step is rate limiting. The oxidation rate of tolualdehyde was evaluated to be far quicker than the oxidation rate of o-xylene. Overall, Vanhove concluded that according to the kinetic measurements it appears that the adsorption of o-xylene is not rate limiting, and therefore the Langmuir-Hinshelwood approach was considered more accurate in describing the o-xylene oxidation. In addition, he concluded that the reaction order of oxygen is zero.

Hoffmann [109] applied o-xylene oxidation kinetics in order to study different reactor models describing fixed bed reactors. Generally, a large amount of reaction steps were described, including the formation and decomposition of maleic anhydride. TA was considered the only intermediate in the oxidation to PA. However, a direct formation path was also included. Selective oxidation steps are considered to follow Eley-Rideal type rate laws as shown in eq. (6.1.1) while the total combustion steps follow power law rate equations.

$$r_j = \frac{k_j \cdot C_i}{1 + a_i \cdot C_{oX} + b_i \cdot (C_{TA} + C_{PA} + C_{MA})} \tag{6.1.1}$$

The inhibition parameters as well as the frequency factors of each reaction step have a temperature dependency according to the Arrhenius equation. Additionally, the inhibition constants were different for each reaction step. Together with the large amount of reactions considered, this led to 40 kinetic parameters. In the combustion reactions, the relation of CO and CO_2 formation was assumed 1:3. Calculations were conducted for spherical catalysts with 6 mm diameter.

Calderbank et al. [41] developed a frequently cited kinetic model including several intermediate reaction steps. This investigation was carried out in a spinning catalyst basket reactor with relatively small amounts of a commercial catalyst. The results were then confirmed with a pilot reactor. The resulting parameter estimates from the lab-scale apparatus needed to be tuned in order to fit the data obtained from the pilot reactor [110].

With the catalyst applied, a first order reaction with respect to oxygen concentration was observed at high temperatures, while at low temperatures, the reaction rates showed first order dependency on the o-xylene concentration. Consequently, the rate equation applied is of Mars-van-Krevelen type. The reaction scheme accounted for in this kinetic model allows PA formation by ways of the sequential reaction from o-xylene via TA and PD as well as the direct formation of the PA from o-xylene. The Calderbank model has repeatedly been successfully applied in modeling industrial o-xylene oxidation reactors.

Wainwright and Hoffmann [25] conducted another study of o-xylene oxidation kinetics in the same time period. This study however was directed towards the deactivation dynamics of the applied industrial catalyst and the kinetic mechanism at the catalyst surface. Therefore, the reaction was carried out with and without oxygen feed, thus studying the redox comportment of the catalyst. In fact, for a limited amount of time, the catalyst continued to oxidize o-xylene, at first more selectively to PA and after several minutes preferably to CO_2. Consequently, a Mars van Krevelen type rate expression was suggested. Kinetic parameters were not evaluated.

Lopez-Isunza [30], Kershenbaum [111-116], Mongkhonsi [31] and co-workers have applied the Calderbank kinetics to model an industrial pilot reactor. Their studies were aimed more towards describing the dynamics of the reaction. However with slight modifications of the Calderbank kinetics, they managed to describe the general characteristics of the pilot reactor with decent accuracy. The activity of the catalyst was found to vary considerably according to its axial position. The introduction of activity profiles allowed an improved representation of experimental data. In continuation of this work, Lopez-Isunza et al. [117] recently published a new study, in which resulting activity profiles were traced to the oxidation state of the catalyst, which was introduced to the kinetic model. Along with irreversible deactivation, oxidized and reduced active sites were described. The balance of oxidized sites is then (eq. (6.1.2))

$$N_s \cdot \frac{\partial \theta_o}{\partial t} = k_o \cdot \theta_r - \left(k_r + \sum_i \beta_i \cdot k_i \cdot p_{org,i} \right) \cdot \theta_o \tag{6.1.2}$$

where N_s represents the number of active sites, θ_r the surface coverage of reduced sites, θ_o the surface coverage of oxidized sites and k_r and k_o are the rate constants of reduction and oxidation of active sites. In case of steady state operation, this surface coverage corresponds to an additional inhibition term.

$$\theta_o = \frac{k_o}{1 + k_r + \sum_i \beta_i \cdot k_i \cdot p_{org,i}} \tag{6.1.3}$$

Basically, this description of oxidized sites reiterates the Mars-van-Krevelen model of consumption of lattice oxygen. In the cited communication, this surface coverage is linked with the Calderbank kinetic model, which already takes into account the consumption of oxygen on the catalyst surface. Unfortunately, parameter values for the oxidation and reduction rate constants are not indicated.

Skrzypek et al. [24,118] described the kinetic data acquired in a pilot plant reactor. The catalyst applied was an industrial catalyst, which was tested undiluted in a differential bed at low conversions in order to maintain isothermicity. Kinetic measurements indicated a strong o-xylene inhibition at inlet concentrations above 1%, where reaction rates decrease significantly. This effect could not be described accurately by a Mars-van-Krevelen type rate expression, since in this model structure, the reaction rate always either rises or remains constant with rising o-xylene concentrations. Consequently, a Langmuir-Hinshelwood rate expression was applied. Contrary to most other kinetic models, the Skrzypek model not only describes intermediate reaction steps, but also the formation of MA.

Li [26] conducted a kinetic study of o-xylene oxidation to PA for use in reactor optimization. In this study, a bench-scale sample port reactor was applied with diluted, lab-prepared catalyst. Experiments were conducted at isothermal conditions. In the description of reaction kinetics, a Langmuir-Hinshelwood type rate expression was applied. In order to reduce the number of parameters, TA and PD were lumped as intermediates in the kinetic description. In addition, the kinetic parameters were estimated for different isothermal conditions independently, so activation energies are not indicated.

Papageorgiou et al. [23,119] compared different model formulations in order to investigate the reaction mechanism on the catalyst surface. The experiments were conducted in a bench-scale reactor with diluted industrial catalyst at isothermal conditions. In the kinetic model, the surface coverage of oxygen was described by a redox model, which is more detailed than the model proposed by Mars and van Krevelen. Oxidized and reduced catalyst sites were quantified explicitly. The range of operating conditions in terms of concentrations was chosen quite broad, particularly considering the oxygen concentration. Comparing low to intermediate oxygen partial pressures (4 kPa and 20 kPa), a significant difference in the selectivity profiles could be observed, at higher partial pressures this is not the case.

The different kinetic models compare the rate limiting step of the oxidation reaction. This is considered to either be the re-oxidation of reduced catalytic sites or the oxidation of the hydrocarbon. Papageorgiou concluded that the oxidation of the hydrocarbon is rate limiting. Unfortunately, the effect of possible mass transfer limitations of the catalyst pellet was not taken into account.

Yabrov et al. [21,120-122] conducted several studies on the oxidation of o-xylene in the last decades. The reaction kinetics were investigated in order to compare different reactors, a fluidized bed and a fixed bed reactor, with the aim of determining the possibility of obtaining higher yields in a fluidized bed [120]. The kinetics was described in a simple triangular reaction scheme with a selective path to PA as well as a parallel total oxidation and a

consecutive over-oxidation path. A simple Langmuir-Hinshelwood type rate expression was applied considering the adsorption only of o-xylene.

Anastasov et al. [27,28,123-128] repeatedly studied kinetics and the influence of operating conditions on the performance of o-xylene oxidation on industrial catalysts. The data was acquired in an industrial fixed bed reactor with several thousand reactor tubes, as well as in a plot plant reactor. It was found that the Calderbank kinetic model describes the comportment of an industrial reactor with low productive catalyst reasonably well [28]. In the most recent investigation on reaction kinetics, the parameters this model were adjusted in order to fit data from an industrial reactor charged with an improved catalyst [27]. In this publication, a second catalyst layer was mentioned and the resulting temperature profiles were fit through adjustment of the layer activity.

Gimeno et al. [29] investigated the kinetics of o-xylene oxidation on a lab-prepared catalyst in a fluidized bed reactor more recently. Different types of redox models were compared. In one case, the hydrocarbon was considered to react directly from the gas-phase, as suggested by Mars and van Krevelen. In another model, the hydrocarbon adsorption was also taken in account in the kinetic model. Gimeno concluded that the classical redox model describes the kinetics sufficiently well. The catalyst applied reached PA selectivities of maximum 50%, which is far from any industrial value. In addition, the evaluated activation energies were in the range of 1 – 30 kJ/mol, which is particularly low and indicates mass transfer limitations [61].

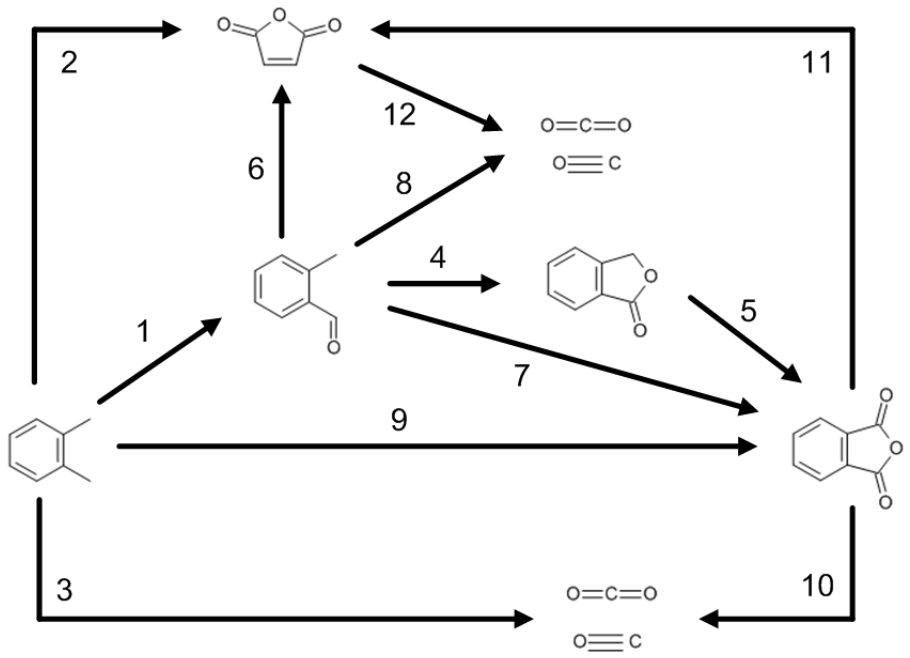

Figure 31: Generalized and simplified reaction scheme of o-xylene oxidation

Table 4 summarizes the reaction paths, which kinetic parameters were evaluated for in different literature publications (compare numbering with figure 31). The most detailed reaction schemes are suggested by Lyubarskii, Skrzypek and Hoffmann, which all include the formation of maleic anhydride. In terms of rate equations, several different kinetic models in particular power law, Mars-van Krevelen, Langmuir-Hinshelwood and Eley-Rideal rate equations were successfully applied to describe the reaction kinetics.

Table 4: Summary of all reaction paths which kinetic parameters were established for; reaction paths are numbered according to figure 31

Author	1	2	3	4	5	6	7	8	9	10	11	12
Froment (1968) [13]			x						x	x		
Lyubarskii (1973) [104,105]	x	x	x			x	x	x	x	x	x	x
Froment (1975) [107]	x		x	x	x		x					
Vanhove (1976) [108]	x		x	x	x		x			x		
Calderbank (1977) [41]	x		x	x	x				x	x		
Hoffmann (1977) [109]	x	x	x			x	x	x	x	x	x	x
Skrzypek (1985) [24]	x	x	x	x	x		x		x	x		
Li (1991) [26]	x		x				x		x	x		
Papageorgiou (1994) [23]	x		x	x	x		x					
Yabrov (1997) [120]			x						x	x		
Anastasov (2003) [27]	x		x	x	x				x			
Gimeno (2008) [29]	x		x	x	x				x	x		
Lopez-Isunza (2010) [117]	x		x	x	x				x	x		

In order to evaluate the applicability of these literature models on modern high productive industrial catalysts, several models were selected and the resulting data was compared to measured selectivity and temperature profiles. Froment (1968), Li, Yabrov and Vanhove only describe a limited number of reaction steps. In the models of Froment (1975) and Lopez-Isunza (2010) important parameters are not indicated. The parameters, particularly activation energies evaluated by Gimeno are outside the expected range. Since the Calderbank model was successfully applied to describe the general comportment of industrial or pilot reactors [28,111,113,114,124] and this model was extended by Anastasov in order to describe a more modern catalyst these kinetic models were taken into account in the evaluation.

The aim of this work is not only to describe the reaction kinetics of the main components but also to describe significant by-products, particularly MA. Models describing also the formation of MA were published by Lyubarskii, Hoffmann and Skrzypek. Due to the large amount of kinetic parameters in the Lyubarskii and Hoffmann models, the Skrzypek model is additionally chosen in the evaluation of literature kinetic models.

6.2 Reactor Model

Hoffmann [109] has shown that the application of a two dimensional model to describe the oxidation of o-xylene yields substantially different results compared to a conventional one-dimensional model as described in chap. 3.1, particularly in the hot spot region. In this area, the temperature difference between the reactor center and the cooling medium ranges up to 100 °C which suggests strong radial temperature gradients. The kinetic models which will be considered [24,27,41] were evaluated when catalyst and gas phases are modeled separately. Consequently, a two-dimensional heterogeneous reactor model is chosen to evaluate different literature kinetic models. The concentrations and temperatures in the catalyst pellet are assumed constant, which for the egg-shell type catalysts for o-xylene oxidation seems applicable for maximum diffusion lengths of about 250 µm [129].

The model equations applied are depicted in table 5. Due to practical limitations several modifications have been made in the applied reactor model when comparing to the standard heterogeneous model presented in chap. 3.1. This includes the fact that numerous components are present in the reactive system of o-xylene oxidation. Depending on the kinetic model, this can amount to a total of ten different compounds. Consequently, mass-balances of fluid and solid phases need to be formulated for each component separately (eqs. (6.2.1) and (6.2.4)). The overall mass balance is shown in eq. (6.2.2).

Another difficulty in the practical implementation of the heterogeneous reactor model is the treatment of heat transfer. In the heterogeneous reactor model presented in chap. 3.1, separate sets of heat transfer coefficients ($\alpha_{W,f}$, $\lambda_{r,f}$ and $\alpha_{W,s}$, $\lambda_{r,s}$) are postulated for fluid and solid phases. However, correlations for parameter values for each of these transport mechanisms separately have only been studied scarcely. Following the practical modeling approaches of several researchers [27,28,127,129-131], only one set of lumped heat transfer coefficients for both mechanisms was taken into account. According to Tsotsas [60], in terms of heat transfer description, two types of heterogeneous models can be applied. On the one hand, the solid phase can be considered as a continuous phase with radial heat conductivity. On the other hand, in a discontinuous solid phase, heat transport in radial direction is considered only in the fluid phase, while heat transfer from the solid is only through the fluid phase.

According to Hofmann [54] or Froment [57], the temperature difference between solid and fluid phases ranges around a maximum of 5 K. The application of the second type of heat transfer model suggested by Tsotsas leads to far larger differences. Therefore, the

model with continuous solid phase is applied and radial heat conductivity is accounted for within the solid phase.

Table 5: Model equations of the applied reactor model

mass balance of component *i* in the fluid phase	$\frac{\partial \dot{N}_z^i}{\partial z} = \varepsilon \cdot D_r \cdot \left(\frac{\partial^2 C_f^i}{\partial r^2} + \frac{1}{r}\frac{\partial C_f^i}{\partial r}\right) - k_f \cdot a_v \cdot \left(C_s^i - C_f^i\right)$	(6.2.1)
overall mass balance fluid	$\dot{M}_{z,tot} = \sum_i \dot{N}_z^i \cdot M_W^i = \rho_f \cdot u_z$	(6.2.2)
heat balance fluid phase	$u_z \cdot \rho_g \cdot c_p \cdot \frac{\partial T_f}{\partial z} = \frac{1}{r} \cdot \frac{\partial}{\partial r} \cdot r \sum_i D_r \cdot \frac{\partial C_f^i}{\partial r} \cdot c_p^i \cdot M_W^i \cdot T_f + h_f \cdot a_v \cdot \left(T_s - T_f\right)$	(6.2.3)
mass balance of component *i* solid phase	$k_f \cdot a_v \cdot \left(C_s^i - C_f^i\right) = \sum_j \left(\nu_{ij} \cdot r_j \cdot \rho_{cat} \cdot (1-\epsilon)\right)$	(6.2.4)
heat balance solid phase	$h_f \cdot a_v \cdot \left(T_s - T_f\right) = -\sum_i \sum_j \Delta H_R^j \cdot \nu_{ij} \cdot r_j \cdot \rho_{cat} \cdot (1-\epsilon) - \frac{1}{r} \cdot \frac{\partial}{\partial r} \cdot r \cdot \lambda_r \cdot \frac{\partial T_s}{\partial r}$	(6.2.5)
Momentum conservation	$\frac{\partial P}{\partial z} = -150 \cdot \frac{\eta_f \cdot u_z}{d_p^2} \cdot \frac{(1-\epsilon)^2}{\epsilon^3} - 1.36 \cdot 1.75 \cdot \frac{\rho_f \cdot u_z^2}{d_p} \cdot \frac{(1-\epsilon)}{\epsilon^3}$	(6.2.6)

However, the catalyst filling causes a certain radial dispersion of the fluid. Consequently, also certain heat dispersion linked to radial mass transfer is considered in this reactor model. This measure further extends the model formulation Froment and Bischoff [53] suggest. The radial conduction term in the fluid phase as shown in eq. (3.1.6) is replaced by a dispersion term. Following the suggestion of Froment and Bischoff [53], the corresponding radial dispersion coefficient D_r is evaluated by estimating the Péclet number for radial mass dispersion to 10 (eq. (6.2.7)).

$$D_r \cdot 10 = \frac{u_z}{\epsilon \cdot d_p} \tag{6.2.7}$$

Mass and heat balances for the solid phase (eqs. (6.2.4) and (6.2.5)) correspond in general to the representation shown in chap. 3.1. However, the amount of catalyst in the reactor tube, which is characterized by the density of the catalyst ρ_{cat} and the porosity of the catalyst bed ε, is included in the model formulation.

Momentum conservation (eq. (6.2.6)) is represented by the Ergun equation [133,134] with an adjusted factor for the quadratic term. Due to Bodenstein numbers ranging from 2000 to 4000, dependent on the fluid temperature, ideal plug flow can be assumed. In accordance with literature [132], an axial dispersion term is therefore not taken into account in neither heat and nor mass balance.

The boundary conditions for this model are shown in table 6. For the evaluation of kinetic models, as well as the evaluation of reaction kinetics from experimental data from the pilot reactor, constant wall temperature is assumed over the complete reactor length.

Table 6: Boundary conditions for the applied reactor model

for *z = 0*	$T_f = T_s = T_0, \quad C_f^i = C_{f,0}^i, \quad \frac{\partial C}{\partial r} = 0,$ $u_z = \frac{\dot{M}_{z,tot,0}}{\rho_f}, \quad \dot{M}_{z,tot} = \dot{M}_{z,tot,0}$	(6.2.8)
for *r = 0*	$\frac{\partial u_z}{\partial r} = \frac{\partial \dot{M}_z^i}{\partial r} = \frac{\partial T_f}{\partial r} = \frac{\partial T_s}{\partial r} = 0$	(6.2.9)
for *r = R*	$\alpha_W \cdot (T_W - T_s) = \lambda_r \cdot \frac{\partial T_s}{\partial r}, \quad \frac{\partial T_W}{\partial r} = 0, \quad \frac{\partial C_f^i}{\partial r} = 0$	(6.2.10)

Heat- and mass-transfer coefficients between solid and fluid (h_f and k_f) are estimated according to standard j-correlations documented by Baerns et al. [55]. Heat transfer coefficients in eq. (6.2.10) are estimated according to the α_W-model suggested in the VDI Wärmeatlas [135]. For the estimation of mass-transfer coefficients, it becomes necessary to evaluate also binary diffusion coefficients. Satterfield [159] and Perry [136] suggest various models to estimate the binary diffusion coefficient. It was found that out of Wilke-Lee, Chapman-Enskog or Fuller type equations to estimate binary diffusion coefficients, the Fuller estimate allows the numerically most stable description. It is further assumed that all components diffuse in pure nitrogen.

The resulting system of differential equations was solved in gPROMS® [137], in application of the corresponding model libraries. Due to near atmospheric operating pressures, ideal gas comportment was assumed and the material data was derived from the DIPPR database. The values for formation enthalpies were compared also with other sources in literature [67,138].

Within gPROMS® the implemented partial differential equations are broken down to a system of differential algebraic equations. The discretization method as well as the distribution of grid points is chosen by the user. The system of equations is then decomposed in several blocks which are solved equation oriented, allowing rapid calculation.

6.3 Comparison of Kinetic Models in Literature to Reactor Data

Recently, Orozco et al. [139] published a simulation study, comparing different literature kinetic models for o-xylene oxidation. The kinetic models were discriminated in application of a one-dimensional reactor model, mainly by comparing the formation of hot spots. The reactor performance in terms of selectivity was not studied closely. In addition, the characteristics of the catalyst bed which are applied in terms of particle sizes or porosities vary considerably from those found in modern catalyst set-ups.

In this study, the kinetic models published by Anastasov, Skrzypek and Calderbank are evaluated in order to identify their potential to describe the industrial reactor. These models were compared at an o-xylene load of 80 g/Nm³, an air flow rate of 4 Nm³/h and a salt bath temperature of 355 °C. The reaction is considered to take place in a reactor tube of 25mm diameter and a length of 3 m.

The extended Mars-van-Krevelen type approach applied in the kinetic model of Calderbank includes a total of six reaction steps. The total oxidation of PA was found kinetically insignificant, reducing the model to five steps. The mathematical description of this reaction kinetics (eq. (6.3.1)) includes the consumption of lattice oxygen, which is represented in the inhibition term.

$$r_j = \frac{k_j \cdot p_i \cdot k_c \cdot p_{O_2}}{k_c \cdot p_{O_2} + p_{oX} \cdot (k_1 + 6.5 \cdot k_3 + 3 \cdot k_9) + k_4 \cdot p_{TA} + k_5 \cdot p_{PD}} \tag{6.3.1}$$

The rate constants are considered to have the following Arrhenius type temperature dependency.

$$k_j = k_{j,0} \cdot exp\left(-\frac{E_{A,j}}{R \cdot T}\right) \tag{6.3.2}$$

Furthermore, the oxygen dependency was evaluated to be constant, so the factor $k_c p_{O2}$ gives the value 0.772 x 10^{-5} mol g^{-1} s^{-1}. The kinetic parameters of the Calderbank model are shown in table 7.

Table 7: Kinetic parameters of the Calderbank kinetic model; reaction paths are enumerated according to the paths in figure 31

Path Nr.	$k_{0,j}$ (mol g^{-1} s^{-1} atm^{-1})	$E_{A,j}$ (kJ mol^{-1})
1	3.828	61
3	0.358	51
4	1.295	55
5	0.556	47
9	3.19	58

The conversion selectivity plot obtained with this kinetic model is shown in figure 32. At low conversions, the PA selectivity shows values around 40% and then gradually rises to reach around 55% at the reactor outlet. At this point an o-xylene conversion of 93% is obtained. The selectivity of PD increases gradually to reach a maximum at around 90% conversion. At the reactor outlet, the selectivity to PD still values around 15%.

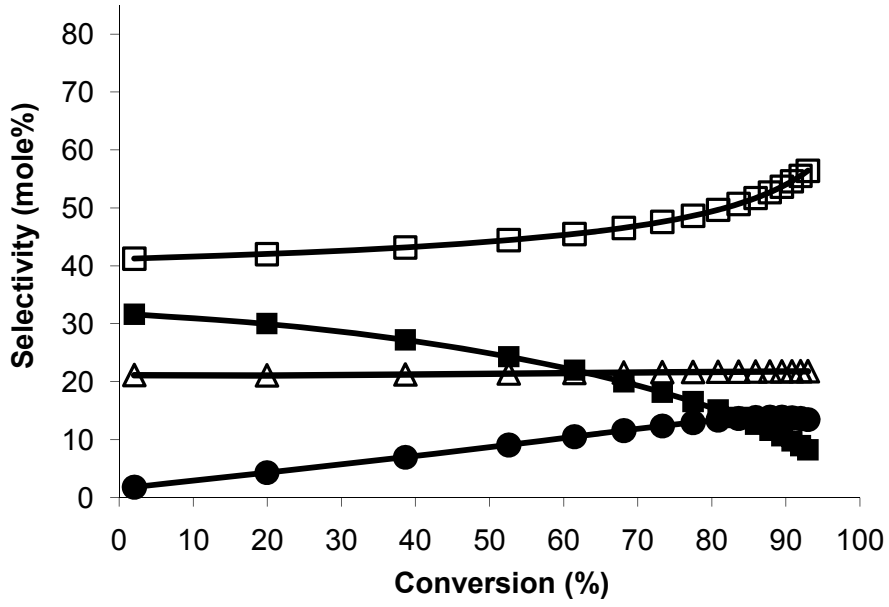

Figure 32: Conversion selectivity plot simulated with the Calderbank kinetic model with the selectivities to PA (□), TA (■), PD (●) and CO (Δ)

TA selectivity values range around 30% at low conversions to then decrease gradually until around 10% are reached at the reactor outlet. In this model, the total oxidation is considered to yield only CO. Its selectivity profile is constant at around 20% for all conversions. Comparing the obtained data to experimental conversion selectivity plots (chap.

2.3), the general comportment is represented quite well. However, particularly at low conversions, strong deviations in the selective oxidation products are observed.

Table 8: Kinetic parameters of the Anastasov kinetic model; reaction paths are enumerated according to the paths in figure 31

Path Nr.	$k_{0,j}$ (kmol kg^{-1} s^{-1} Pa^{-1})	$E_{A,j}$ (J mol^{-1})
1	1.5090 x 10^{-5}	69417
3	2.2690 x 10^{-6}	46473
4	1.4010 x 10^{-6}	54512
5	5.1610 x 10^{-6}	52586
9	1.2632 x 10^{-5}	38419

The conversion selectivity plot in figure 33 shows the corresponding data obtained when simulating the PA reactor with the Anastasov kinetics. This kinetic model extended the Calderbank model in order to fit the temperature profiles obtained with more modern catalysts. The mathematical formulation is equivalent to the model equation shown in eq. (6.3.1). The updated parameter values are given in table 8.

The conversion obtained at the reactor outlet is merely 50%. The run of the PA selectivity profile is slightly rising, but nearly parallel to the conversion axis. Particularly the high selectivity at low conversion suggests that in this kinetic model, the parallel PA production path is predominant. The TA selectivity profile decreases gradually, but not as severely as it can be observed in measured selectivity profiles (chap. 2.3). At low conversions, the TA selectivity is only around 10%, which is substantially lower than in measurements. While the frequency factors of the reaction path to TA and the direct PA formation path are of the same order of magnitude, the activation energy for the direct path is substantially lower than that of the TA formation. This explains somewhat the obtained selectivity profiles.

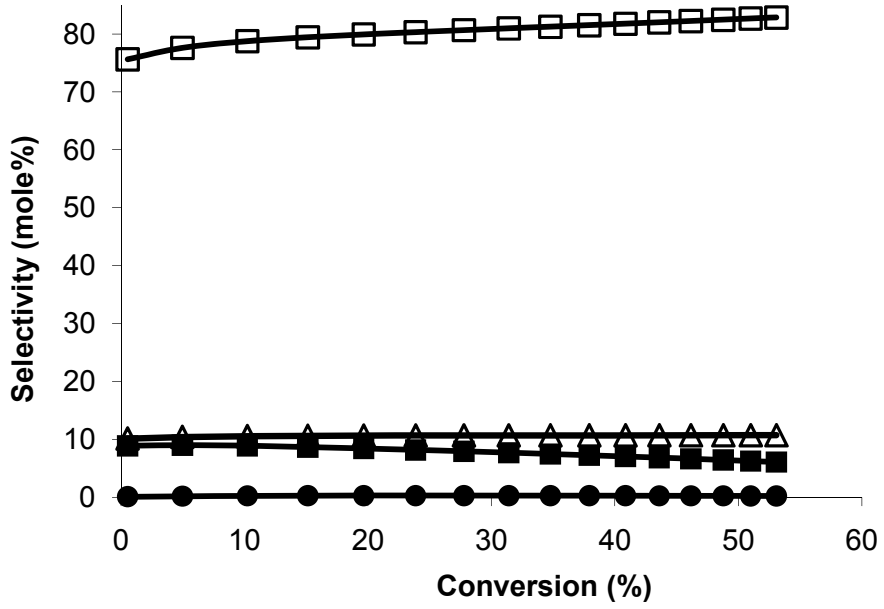

Figure 33: Conversion selectivity plot simulated with the Anastasov kinetic model with the selectivities to PA (□), TA (■), PD (●) and CO (Δ)

Only very low values are simulated for the PD selectivity. In fact, at similar activation energies, the consumption of PD is five times its production. In experimental selectivity profiles, PD shows a clear maximum at around 10% selectivity. This is not at all represented by this kinetic model. The combustion reaction is again considered to be only to CO, which shows a constant selectivity profile at 10% with advancing conversion. CO_2 is not taken into account, which significantly influences the reaction enthalpy and thereby the formation of temperature profiles.

Skrzypek has applied a Langmuir-Hinshelwood type rate expression to describe the reaction kinetics the applied catalyst. This kinetic model involves only a limited amount of parameters, but nevertheless it describes the formation of MA as well as it includes CO_2 in the reaction scheme. The relation of CO and CO_2 is reported to be 1:3, which is accounted for in the kinetic model.

$$r_j = \frac{k_j \cdot p_i \cdot p_{O_2}}{\left(1 + K_{O_2} \cdot p_{O_2} + K_{oX} \cdot p_{oX} + K_{TA} \cdot p_{TA} + K_{PD} \cdot p_{PD} + K_{PA} \cdot p_{PA} + K_{MA} \cdot p_{MA}\right)^2} \quad (6.3.3)$$

The rate constants again have the Arrhenius type temperature dependency shown in eq. (6.3.2). Additionally, all adsorption constants are considered temperature dependent as follows.

$$K_i = K_{i,0} \cdot exp\left(+\frac{\Delta H_{Ads,i}}{R \cdot T}\right) \tag{6.3.4}$$

The kinetic parameters evaluated are shown in table 9 while the parameters of the adsorption are depicted in table 10.

Table 9: Kinetic parameters of the Skrzypek kinetic model; reaction paths are enumerated according to the paths in figure 31

Path Nr.	$k_{0,j}$ (mol dm^{-3} s^{-1} atm^{-2})	$E_{A,j}$ (J mol^{-1})
1	0.13 x 10^{13}	108 443
2	0.17 x 10^{11}	96 720
3	0.70 x 10^{10}	85 415
4	0.38 x 10^{11}	85 415
5	0.18 x 10^{12}	93 789
7	0.28 x 10^{12}	108 862
9	0.84 x 10^{12}	96 301

Table 10: Adsorption parameters of the Skrzypek kinetic model

Component	$K_{0,i}$ (atm^{-1})	$\Delta H_{Ads,i}$ (J mol^{-1})
oX	1.00	27 718
TA	1.93	30 984
PD	5.80	24 285
PA	3.81	16 748
MA	3.87	24 326
O_2	0.202	0

Applying exactly these kinetic parameters, a conversion of only 20% is achieved at the reactor outlet. However, the initial runs of the selectivity profiles, particularly of PA, PD and TA are promising when compared to experimental data. Apparently the catalyst applied by Skrzypek has substantially lower activity than the high productive industrial catalyst applied in this investigation. Hence, the activity level was raised gradually to a value of several times the initial activity. The resulting conversion selectivity plot is depicted in figure 34.

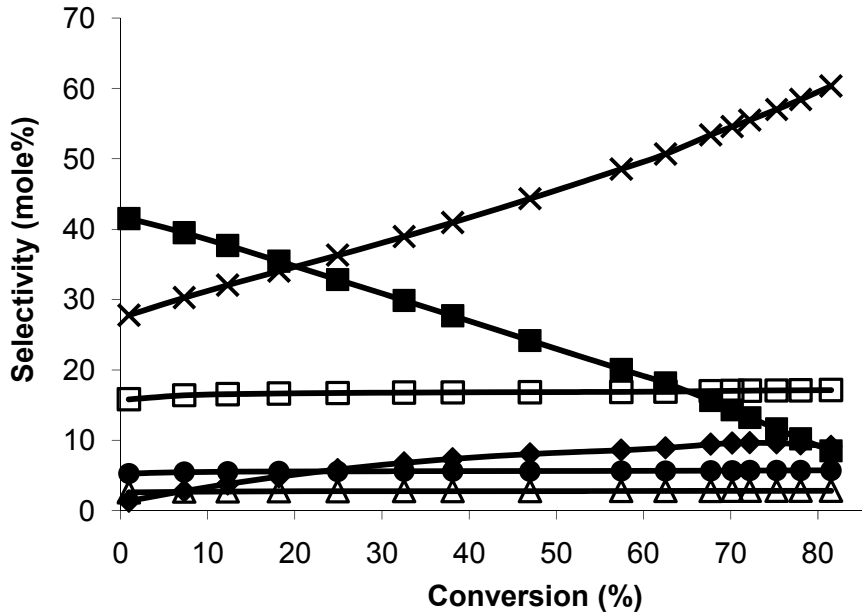

Figure 34: Conversion selectivity plot simulated with the Skrzypek kinetic model where the activity was considered several times the original activity; PA (x), TA (■), PD (♦), CO (●), CO_2 (□) and MA (Δ)

The PA selectivity profile as modeled with the modified Skrzypek kinetic model begins at a value around 30% at low o-xylene conversions then rises gradually to reach around 60%

at 80% conversion. Like the experimental data, the TA selectivity profile decreases with advancing conversion. Contrary to the Anastasov and Calderbank models, the initial selectivity value reaches more realistic 40% and then decreases more strongly than in the other kinetic models. CO and CO_2 selectivity profiles are both parallel to the conversion axis at values of around 5% and 15% respectively. In addition, the MA selectivity also runs parallel to the conversion axis at selectivities of around 2.5%, which corresponds to final values obtained in experiments.

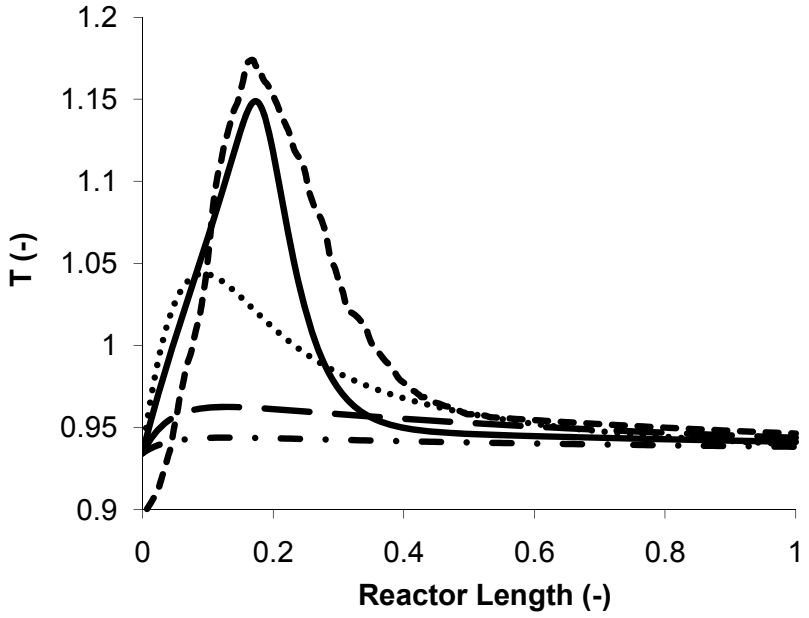

Figure 35: Comparison of temperature profiles simulated with different literature models at operating conditions of 4 Nm³/h airflow, 80 g/Nm³ o-xylene load; Skrzypek (– · –), Skrzypek modified (——), measured (- -), Anastasov (– –), Calderbank (···)

In comparison to a temperature profile measured with the four layer system, the temperature profiles obtained with the different kinetic models, applying the characteristics of the industrial catalyst bed, show significantly lower hot spots than are measured. The original Skrzypek model shows a temperature profile which remains nearly constant at the salt bath temperature. This can explain the low conversions obtained.

The Anastasov model not only yields selectivity profiles which do not correspond at all to any measured data, but also the hotspot temperature is significantly lower than measured values. The temperature profile obtained with the Calderbank model nearly reaches realistic conditions, but still is significantly lower than a measured profile at similar conditions.

Applying higher activity to the Skrzypek model, a hot spot profile similar to a measured profile can be simulated, while the selectivity profiles also correspond in general tendency to measured data. Unfortunately, in this case the Skrzypek kinetic model becomes very

sensitive to temperature and concentration changes and is only applicable for a very limited range of operating conditions.

6.4 Shortcomings of Literature Kinetic Models

The presented literature reaction kinetic models for the oxidation of o-xylene all describe a single catalyst. While Li [26] actually performs kinetic measurements for different catalyst compositions, Anastasov et al. [27] as only literature source on kinetic models mention the existence of multiple catalyst layers in an industrial reactor. Concentration data measured consists of only input and output data. Thus, the kinetic description is also limited to one single catalyst layer. Modern catalytic systems consist of up to four catalyst layers, which were not accounted for in any literature model.

As shown in the previous paragraph, simple models, which are frequently cited in literature, fail to describe both temperature and selectivity profiles of high productive catalyst systems. Both the qualitative nature of temperature and concentration profiles and their quantitative magnitudes are represented very poorly.

Out of the nearly 15 literature kinetic models, only those published by Lyubarskii, Hoffmann and Skrzypek describe the formation of MA, which is the most significant organic by-product. The Lyubarskii and Hoffmann models both comprise a very large number of reaction paths and corresponding kinetic parameters. All other published reaction kinetics only consider CO and in very few cases also CO_2 as by-products.

Only very few researchers have systematically reduced the number of kinetic parameters necessary to describe the reaction. The significance of oxygen has been widely studied. However, the inhibiting effect of organic components was not systematically studied.

In addition, all of the kinetic models evaluated in more detail require a direct formation path of phthalic anhydride from o-xylene, which chemically involves numerous microkinetic steps. The direct formation is therefore highly unlikely. The investigation of the reaction scheme has shown that such a direct reaction path cannot be backed by experimental data.

Thus, published literature kinetic models each have their merits in terms of effects that can be described. However, each of the presented models also has a number of flaws, which limits its applicability to modern industrial catalytic systems.

One aim of this work is to develop reaction kinetics describing the oxidation of o-xylene, which use a minimal number of parameters, which each is significant in the estimation. This kinetic model is aimed to describe a high productive four layer industrial catalytic system as it is applied large scale reactors nowadays. Furthermore, an aim is to apply the information gained on the reaction scheme and on different reaction pathways in order to be able to properly predict the formation of by-products. This is essential for the model based optimization of the catalytic system.

7. Kinetic Experiments

7.1 Preliminary Experiments and Experiment Design

The aim of this investigation is to evaluate the reaction kinetics of the industrial catalyst system through experiments conducted in the previously described pilot reactor. Kinetic parameters are evaluated through non-linear regression of the experimental data in application of an adequate mathematical model, describing the physical and chemical comportment of the fixed bed reactor using gPROMS^{TM} software.

The operation of the pilot reactor involves substantial financial efforts. In order to establish the reaction kinetics in an efficient manner, considerable efforts were put into experiment design. The aims were primarily to minimize the experimental time while acquiring a sufficiently large set of high quality data for later kinetic parameter estimation. The general suggestions in policy of Mason [140] were followed in this effort.

The industrial PHTHALIMAX^{TM} catalyst system consists of four catalyst layers (layers 0 – 3). All catalyst layers are significantly different in activity and chemical composition. Due to intellectual property issues particularly of layer zero catalyst, the kinetics of layers 1, 2 and 3 are evaluated and discussed in detail.

Normal operation of a PA production plant consists of the ramp-up time after which an industrial reactor is conducted at a constant or only minimally changing set of operating conditions. During the acquisition of kinetic data, the operating conditions need to be varied considerably in a rather short stretch of time. Experience in this point is not available from industrial or pilot plant data. Consequently, a number of preliminary experiments become necessary both in order to identify the constraints in kinetic testing and to define a realistic and sufficiently accurate set of experiments. Amongst these factors are:

- definition of influencing variables,
- determination of process ranges,
- maximum times for kinetic data acquisition after ramp-up, before considerable deactivation is observed,
- definition and optimization of measurement time,
- determination of operation times after the change of operating conditions until a new steady state is reached,
- determination of cycle times and total test time,
- reproducibility of ramp up and catalyst formation procedures.

The adjustable variables influencing temperature, conversion and selectivity profiles are reactor pressure, total gas flow rate, salt bath temperature (SBT) and the inlet concentration of o-xylene. In the industrial application, steady state operating conditions of the S4 type catalyst in terms of air flow rate range from 3.5 to 4 Nm³/h and in terms of o-xylene load they range from 70 g/Nm³ to 85 g/Nm³. Considering the total bed length this results in gas hourly space velocities (GHSV) of 1000 – 3500 1/h.

The cooling temperature is strongly dependent on the other operating conditions and cannot be adjusted completely independently, particularly since it strongly influences position and magnitude of the hot spot. At the design load of around 80 g/Nm³, the SBT is reduced to 350 °C. With gradual deactivation of the catalyst during its four year life span, the SBT is slowly raised to eventually reach a maximum of 360 – 365 °C.

The operating pressure of an industrial reactor, which is nearly atmospheric pressure, is limited by the pressure drop of the catalyst bed on the one hand and by the pressure drop of any unit operations or installations downstream of the reactor on the other hand. Usually, the inlet pressure is controlled to a value of 1.4 bar total pressure. However, this pressure can vary between 1.35 and 1.5 bar, depending on layout and state of an industrial production plant.

Cooling temperatures influence mainly the energy balance of the system, while the total flow rate influences both impulse balance and mass balance, through varying residence times. The inlet concentration has an impact only the mass balance of the reactor. The operating pressure influences both impulse and mass balances.

Through variation of the inlet pressure, both the total concentration of the gas stream and the residence time on the catalyst are modified. The dependence of the reaction kinetics on the residence time and the feed concentrations, particularly of o-xylene can be investigated through variation of air flow rates and o-xylene load. In an effort to minimize the experimental efforts, the variation of inlet pressures is therefore dropped from the experimental plan. During all kinetic experiments, the inlet pressure remains at the constant value of 1.4 bar.

In order to obtain the necessary data on experimental constraints, such as ramp-up times, equilibration times and measurement times, a standard four layer catalyst system was filled to the pilot reactor. With this setup the open critical questions were evaluated with a reduced experimental plan which corresponds to a simple factorial plan on three levels considering the air flow rate and four levels considering the o-xylene inlet concentration. In addition, in the middle and at the end of the plan, the reference operating condition is repeated to monitor any catalyst deactivation. The SBT is adjusted according to the magnitude of the hot spot. This results in a total of twelve sets of operating conditions.

In comparison to a number other pilot experiments with S4 type catalyst, this experiment showed, that the ramp-up time of this catalyst takes several weeks, until the design load of 80 g/Nm³ at an air flowrate of 4 Nm³/h is reached. When the design load is obtained catalyst formation continues at constant operating conditions for a few days. At this point a steady-state is observed during which catalyst deactivation can be neglected. This catalyst formation procedure yields reproducible results in terms of steady-state activity and selectivity.

When the operating conditions are not changed radically, this steady-state remains for a very long stretch of time. Due to heavily changing operating conditions during acquisition of kinetic data, catalyst deactivation is observed far earlier, about five weeks after the beginning

of kinetic data acquisition. Taking in account also turnaround times of the reactor, this results in cycle times of about three months in total.

In order to record the maximum possible amount of data within the limited time stretch, analysis methods and procedures were optimized to allow the acquisition of one concentration profile per day.

As a result of these preliminary tests, it was established, that the change in operating conditions, as long as they are comparatively minimal, leads to the formation of new steady state quite rapidly. Modifying the inlet o-xylene concentration or air flow rate leads to the formation of a new steady state within about 30 minutes. Due to the inertia of the pilot reactor and the salt bath, changing the SBT has significantly longer response times, ranging around two hours until a complete steady state is reached again when changing the temperature by 2 °C.

Consequently, if the operating conditions are adjusted in small steps, i.e. within a range of 5 g/Nm³ daily, a maximum difference of 0.2 Nm³/h in air flow rate and a maximum of 3 °C shift in SBT, concentration and temperature profiles can be recorded daily for one set of operating conditions. In total this results in a maximum 25 operating conditions that can be recorded per run.

In order to monitor possible deactivation, a measurement of the reference operating conditions needs to be carried out at the beginning and at the end as well as at least once during the acquisition of kinetic data.

In the development of a kinetic model describing the oxidation of o-xylene, Papageorgiou et al. [23] applied 180 combinations of GHSV, temperature and inlet concentration. In the tap point reactor, each set of operating conditions yields results for 11 such combinations, since every sampling point is equivalent to a different GHSV. In analogy, around 15 sets of operating conditions within the relevant parameter space can be seen as sufficient for the development of the kinetic model. This implies the addition of five operating conditions to the reduced experimental plan. The remaining eight operating conditions are variable between the kinetic run, depending on which effect is studied in more detail.

In total, the kinetics of three different catalysts are aimed to be evaluated, first, second and third layer. In a first experiment, only first layer catalyst is filled. Completely filling the reactor with second layer catalyst does not appear advantageous, since in the industrial set-up, the feed to second layer catalyst is never pure o-xylene in air, but a mixture of intermediates at different concentrations. Consequently, the filling of first layer catalyst at a length to some extent and the reactor length with second layer catalyst seems favorable.

Table 11: Final experimental plan

o-Xylene Flowrate (g/h)	Air Flowrate (Nm³/h)	Load (g/Nm³)
320	4	80
304	3.8	80
340	4	85
306	3.6	85
342	3.8	90
360	4	90
328	4	82
320	4	80
280	3.5	80
300	4	75
266	3.8	70
245	3.5	70
260	4	65
234	3.6	65
280	4	70
262.5	3.5	75
320	4	80

In a similar way, the kinetics of third layer catalyst are evaluated by filling first and second layers and the remaining reactor length is filled with third layer catalyst. In all of these three runs, data for first layer catalyst is acquired, while second layer data is gathered in two of the three runs. On the one hand, this directly reproduces results from previous fillings in cases where the same SBT is chosen, on the other hand by deliberately choosing slightly modified SBTs, additional information is gained for kinetic parameter estimation.

Table 11 shows the final experimental plan. Operating conditions with o-xylene loads of up to 90 g/Nm³ and down to 65 g/Nm³ were added. The SBTs are adjusted according to the o-xylene load and range between 345 °C and 370 °C.

7.2 Single Layer Data

The components of particular interest for kinetic modeling are the main components and their reaction paths. Many of the components identified and integrated in the detailed reaction scheme have selectivities inferior to one percent. In the development of reaction kinetics, the components with larger concentrations and selectivities play a more important role. Consequently, these components (oX, PA, PD, TA, CO, CO_2 and MA) are more in focus when discussing the results of kinetic experiments.

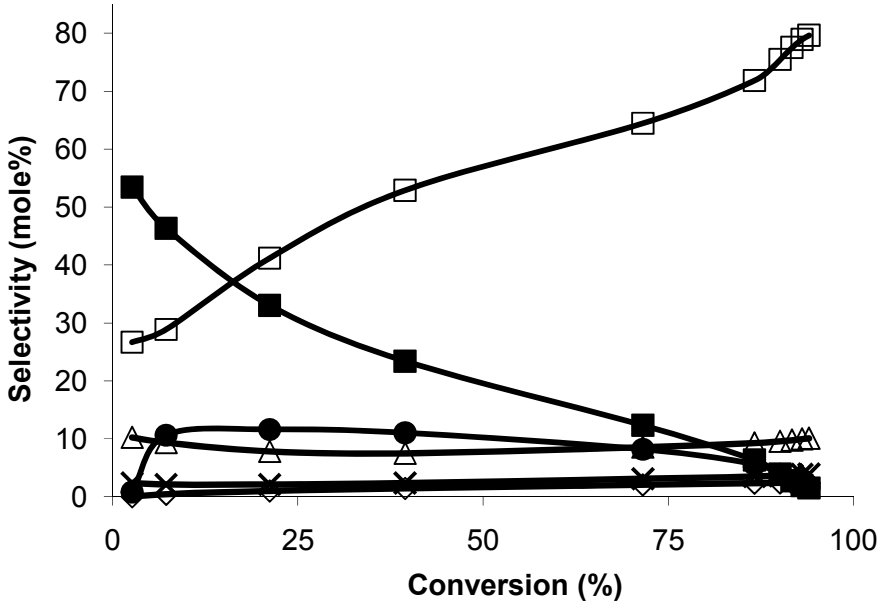

Figure 36: Conversion selectivity plot of L1 catalyst at a high SBT; MA (◊), CO(x), TA (■), PD (●), PA (□)

A conversion selectivity plot of first layer catalyst at a relatively high SBT is depicted in figure 36. Complete conversion is not reached when the reactor is filled completely with first layer catalyst. Generally, the PA selectivity rises continuously to reach a value of around 80% selectivity at a conversion of 95%. Extrapolating the selectivity to zero gives a non-zero value, around 20%. The gradient of the PA selectivity profile is comparatively large at low conversions and is reduced at intermediate conversions. At high conversions when TA and PD are consumed preferably, the gradient rises again.

The TA selectivity profile decreases gradually with advancing conversion to reach nearly zero at the reactor outlet. The extrapolation to zero conversion yields values around 60%.

The PD selectivity profile shows a clear maximum at a conversion around 20%, but remains nearly constant at intermediate conversions. At high conversions this selectivity also decreases to zero.

CO and CO_2 selectivity profiles show an unexpected effect at low o-xylene conversions. Theoretically, at isothermal conditions, the selectivity profile of CO_2 cannot decrease since it is not consumed in this reaction. This effect can be attributed to the lack of isothermicity on the one hand and to impurities within o-xylene, that are directly oxidized to CO_2 on the other hand. The reaction paths leading to CO and CO_2 appear to be parallel reactions to the selective reaction to tolualdehyde. However, the non-selective reactions appear to be favored by lower temperatures. At high conversion, also CO and CO_2 selectivities rise again, suggesting additional consecutive formation paths.

The MA selectivity profile begins at zero selectivity and continuously rises to a final selectivity of around 2.5% at the reactor outlet.

Comparing the data described above to a conversion selectivity profile at a lower SBT, the general run of each of the components changes only minimally (figure 37). However, at low o-xylene conversions, some differences become visible. These operating conditions allow the acquisition of several data points at conversions below 5%. The effect of increased CO_2 formation at these process conditions is further enforced, supporting the theory of a temperature effect.

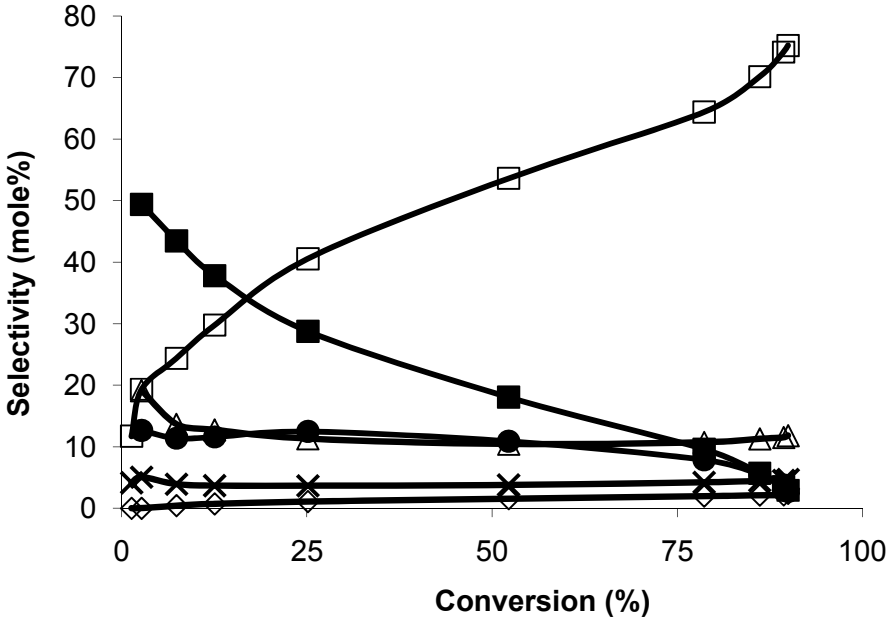

Figure 37: Conversion selectivity plot of L1 catalyst at a low SBT; MA (◊), CO(x), CO_2 (Δ), TA (■), PD (●), PA (□)

The decrease of CO_2 and also of CO selectivity is more pronounced. In addition, the PA selectivity profile shows a very clear drop at extremely low conversions, which could be extrapolated to zero. In kinetic modeling, a component with non-zero selectivity at zero conversion needs to be modeled through a direct formation path, which in case of PA is

chemically inconsistent as previously discussed. The low SBT measurements show, that such a direct formation path may not be necessary in kinetic modeling.

Contrary to the selectivity profiles, which at intermediate conversions are not significantly different with changing operating conditions, the temperature profiles show very strong sensitivity to the both SBT and the variation of inlet concentrations and flow rates. Consequently also the conversion profiles significantly change with varying operating conditions.

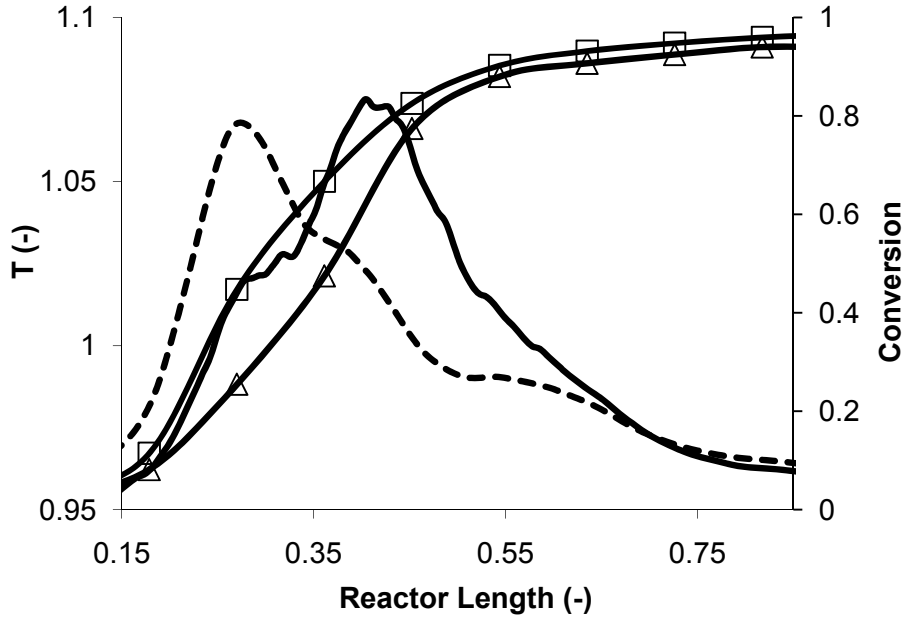

Figure 38: Temperature profiles (T_1 (- -), T_2 (-)) and corresponding conversion profiles ($X_{oX,\,T1}$ (□), $X_{oX,\,T2}$ (Δ)) at different operating conditions;

Compared to the four layer filling (compare chap. 2.3), the hot spot temperature is significantly lower while its position is deeper within the catalyst bed. In terms of kinetic data acquisition, this has the advantage that the o-xylene conversion is spread more over the reactor and a larger number of significant concentration gradients can be recorded in the sample port reactor.

The temperature profiles shown in figure 38 show a clear difference in operating conditions. The hot spot of the profile with higher SBT has a bed position closer to the reactor inlet. Since this profile was recorded after the profile with deeper bed position this shift of the hot spot cannot be explained by deactivation. Both profiles show a sort of inflection point, at different bed positions, after which the gradient of the temperature profile increases and the formation of the hot spot begins.

7.3 Two Layer Data

Apart from the general experimental plan, the influence of the SBT was studied in detail in the two layer experiment. Generally, both the start-up procedure and the steady state operation were very reproducible with respect to the comportment of the first layer catalyst and hot spot development. The selectivity profiles of both single and two layer experiments are compared in figure 39.

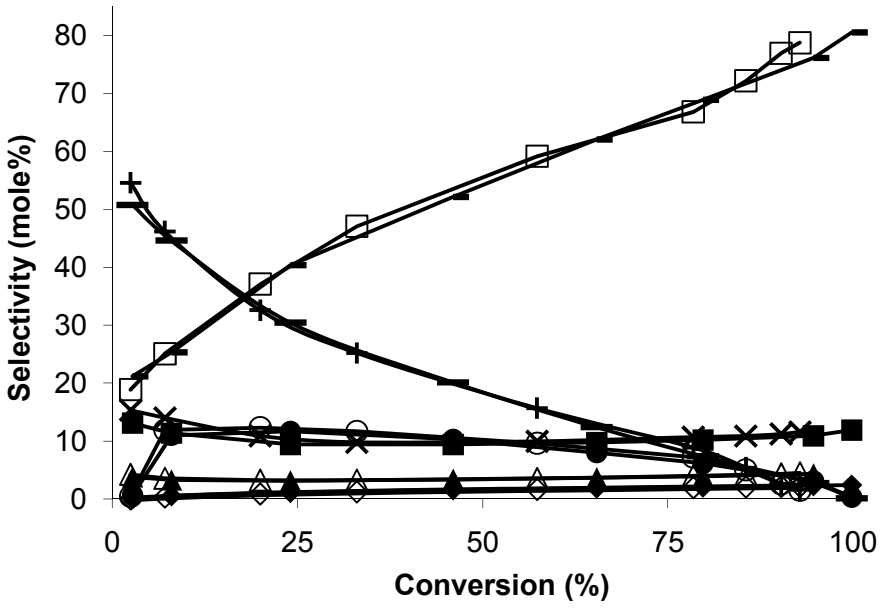

Figure 39: Comparison of selectivity profiles in single layer and two layer kinetic runs, where TA (+), MA (◊), CO_2 (x), PA (□), CO (Δ), and PD (○) are results of the single layer experiment and TA (−), CO_2 (■), PA (-), PD (●), CO(▲), and MA (♦) are results of the two layer experiment; the vertical line indicates which conversion is reached in the two layer experiment when the reaction gas contacts second layer catalyst

The variation of operating conditions allowed recording data for process conditions, where the o-xylene conversions at the barrier between first and second layer range between 65% and 90%. Until a conversion of about 80%, the selectivity profiles of all products and intermediates are reproduced in very good accuracy between the two experiments. While the maximum conversion in the first layer experiment is only around 95%, full conversion is reached with second layer catalyst.

At high conversions, when in the two layer experiment the second layer catalyst is reached a difference especially of the PA selectivity profile is observed. The final selectivies of PA in both experiments range around 80%. However, compared to the two layer experiment, this selectivity is reached at far lower conversions in the single layer experiment.

Also PD and TA selectivities profiles are different in the second layer compared to the first layer at the same conversion. With second layer catalyst, both selectivities drop to zero at full conversion, while a significant slip of intermediates is observed for only the first layer. The MA selectivity profile rises continuously in both experiments and no significant difference in selectivity can be observed between the two experiments. Also the CO and CO_2 selectivity profiles overlay very well until about 95% conversion. In the two layer experiment, they both show a clearly visible rise at nearly 100% conversion.

In this experiment, the influence of the SBT was studied more closely by running a sequence of operating conditions, where the o-xylene load and air flow rate both remain constant, while the SBT is gradually raised. The resulting temperature profiles of these experiments are shown in figures 40 and 41. At lower SBTs a hot spot forms at deeper bed positions than at higher SBTs. The effect, that hot spots at lower SBTs are higher in magnitude however is somewhat unexpected when theoretically studying the kinetics and reactor behavior of selective oxidation reactions [53,129,132].

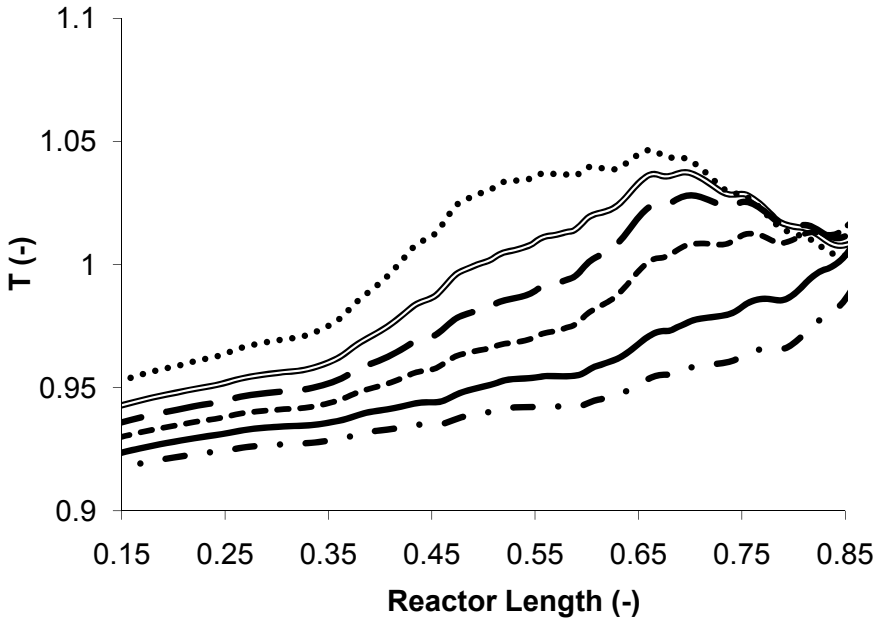

Figure 40: Comparison of layer 1 temperature profiles at different SBTs and a constant entry condition of 3.8 Nm³/h air flowrate and 80 g/Nm³ o-xylene load; the corresponding SBTs are T_1 (– · –), T_2 (——), T_3 (- -), T_4 (– –), T_5 (—),T_6 (···) where $T_1 < T_2 < T_3 < T_4 < T_5 < T_6$

In a series of kinetic studies and investigations of reactor dynamics, Kershenbaum et al. [111-116] reported of similarly shaped temperature profiles in the oxidation of o-xylene using a pilot reactor. In a dynamic experiment, the evolution of the hot spot profile with changing coolant temperatures was studied and yielded similar effects as presented in figures 40 and 41. At relatively low coolant temperatures, a high hot spot is recorded at a relatively deep bed position. With rising SBT, the hot spot first decreases, then moves more

towards the reactor inlet, to increase again at a bed position closer to the reactor inlet. Kershenbaum also reports of completely deactivated catalyst at the reactor inlet, which cannot be observed in these experiments.

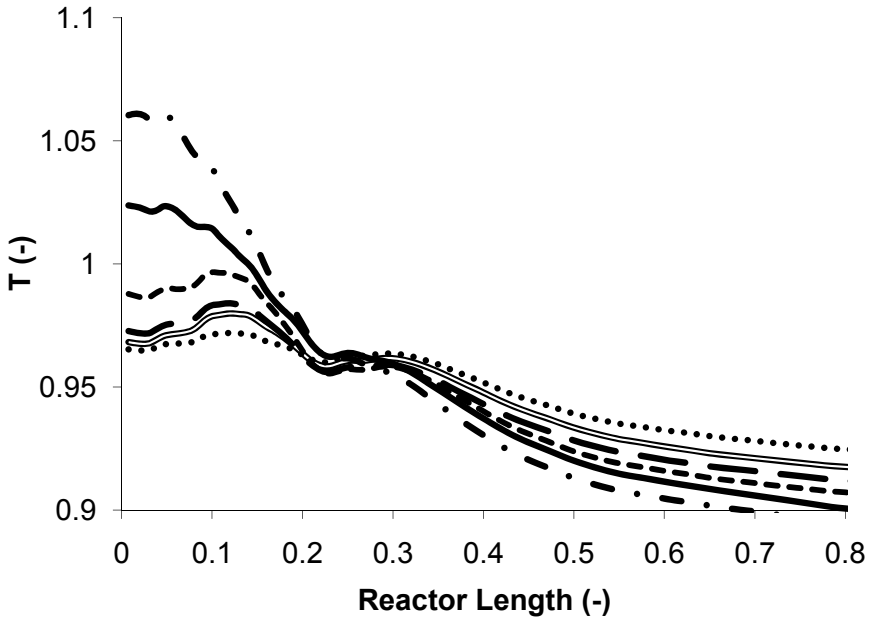

Figure 41: Comparison of layer 2 temperature profiles at different SBTs and a constant entry condition of 3.8 Nm³/h air flowrate and 80 g/Nm³ o-xylene load; the corresponding SBTs are T_1 (– · –), T_2 (——), T_3 (- -), T_4 (– –), T_5 (——), T_6 (···) where $T_1 < T_2 < T_3 < T_4 < T_5 < T_6$

The description of exothermal reactions usually yields temperature profiles which correspond in shape more to the profile recorded in the four layer experiment (figure 3). This unexpected effect is one of the major challenges in kinetic description of the oxidation process of o-xylene.

7.4 Three Layer Data

The comparison of the conversion selectivity plots of two layer and three layer experiments is shown in figure 42 for the complete reactor. The runs of the selectivity profiles in layers 1 and 2 are reproduced very accurately for all components.

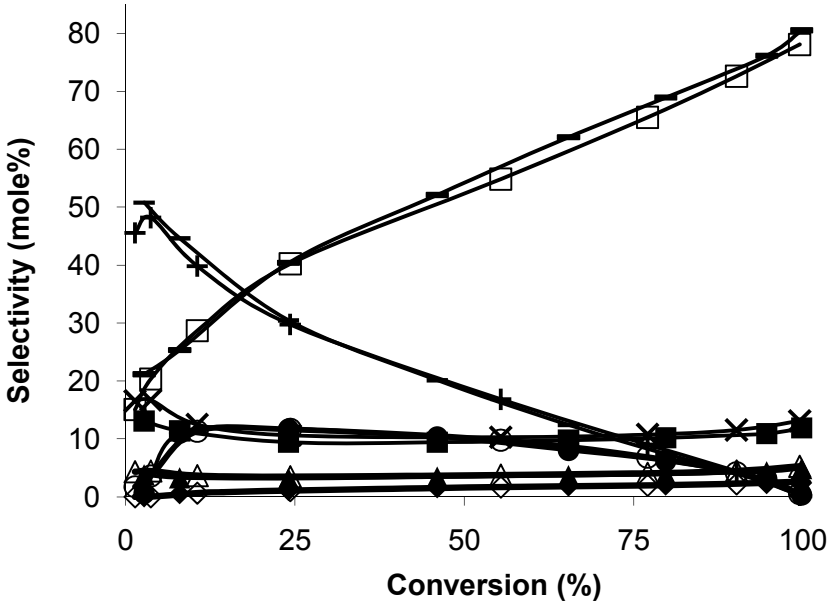

Figure 42: Comparsion of conversion selectivity plots of two layer and three layer experiments; where TA (+), MA (◊), CO_2 (x), PA (□), CO (Δ), and PD (O) are results of the three layer experiment and TA (−), CO_2 (■), PA (-), PD (●) CO(▲), and MA (♦) are results of the two layer experiment

A slight deviation between the selectivity profiles of the two- and the three layer experiments becomes visible at nearly full conversion, when the layer three catalyst begins. The most significant difference in selectivity can be observed in the PA selectivity profile. While the selectivity profile applying layer two catalyst rises continuously and even increases further at full conversion, in layer three catalyst the increase of PA selectivity at this point has a smaller gradient. At this point, CO and CO_2 selectivities rise. This suggests that in layer three, PA is consumed and mainly CO and CO_2 are formed. Also, the MA selectivity is slightly higher with layer three catalyst.

Other selectivity profiles, particularly TA and PD selectivities do not show any deviation between the experiments. In both experiments the selectivities drop to zero. In the two layer experiment, a conversion of nearly 99.8% is reached, while layer three completely converts the o-xylene. In the industrial application this is highly important due to hazards of explosive atmospheres downstream of the reactor.

Additionally to the general experimental plan, the reason for the development of the described temperature profiles was investigated in more detail in the three layer experiment. One possible reason for this comportment could be a strong adsorption of o-xylene and therefore an inhibiting effect. Consequently, the influence of varying o-xylene inlet concentrations was studied, by gradually decreasing the o-xylene load at constant space velocity and cooling temperature. The resulting temperature profiles are shown in figure 43.

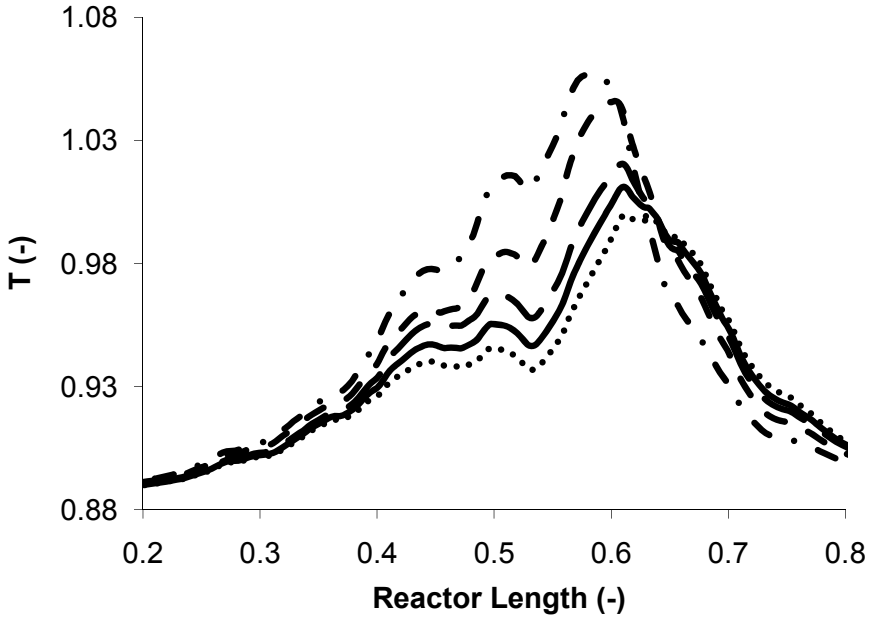

Figure 43: Temperature profiles of different o-xylene inlet concentrations at a constant SBT; o-xylene loads are 90 g/Nm³ (– · –), 86 g/Nm³ (- -), 78 g/Nm³ (– –), 74 g/Nm³ (——), 70 g/Nm³ (···) at a constant air flowrate of 4 Nm³/h

The overall hot spot at such low SBTs, without layer zero filling is in the second catalyst layer for all operating conditions. The highest hot spot is recorded for the highest o-xylene inlet concentration. It gradually decreases with decreasing load and also changes its position to an even deeper bed position. Higher catalyst activity due to lower o-xylene concentrations at the reactor inlet cannot be derived. Particularly strong o-xylene inhibition apparently is not the only cause for the formation of such temperature profiles.

The catalyst is also not completely deactivated at the reactor inlet. With rising SBT, a similar comportment is observed, as in the previous two layer experiment. The hot spot moves back into layer one catalyst.

8. Reaction Kinetics

8.1 Parameter Estimation

Kinetic parameters are evaluated for the main reaction steps taking into account the concentrations of the components which appear in sufficiently large quantities. The evaluation of more intermediate reaction steps significantly raises the number of parameters, while the significance of estimated kinetic parameters for those reactions with reactants of very small quantities remains low.

The estimation of kinetic parameters is conducted with the parameter estimation module of gPROMS™. In the course of parameter estimation the reactor model previously described (chap. 6.2) is solved for each of the experimental operating conditions, at which measurements are available. The resulting modeled process data, such as temperatures and concentrations is compared to experimental data. The operating conditions are introduced to the parameter estimation as controlled parameters. In specific these are:

- salt bath temperature (SBT)
- total molar flowrate at the reactor inlet
- composition of the inlet flow in molar fractions of each component (o-xylene, TA, PD, PA, MA, O_2, CO, CO_2, N_2, H_2O)
- reactor inlet temperature

The measured variables which are compared to the model data are:

- temperature profile with up to 150 measured temperatures per operating condition
- concentration profiles of all measured components important for the kinetic model; these are o-xylene, TA, PD; MA, PA, CO and CO_2

The objective function chosen to be minimized is a maximum likelihood function (eq. 8.1.1), where not only the model error term is relevant, but also the variance of measurements is taken into account [142,143].

$$\Phi = \frac{N}{2} \cdot ln\,(2\pi) + \frac{1}{2} \cdot min\left[\sum_i \left(ln\left(\sigma_i^2\right) + \frac{(\tilde{x}_i - x_i)^2}{\sigma_i^2} \right)\right] \tag{8.1.1}$$

The measured data entered to the parameter estimation corresponds to the raw concentration data evaluated, i.e. the molar composition of the organic compounds measured in the GC is entered directly as well as the gas phase concentrations of CO and CO_2 measured in the IR spectrometer. In addition, the measured temperatures are entered as centigrade values.

The variance models and respective parameters chosen have been optimized in order to avoid inappropriate weighting of one or the other measurement. In case of concentration measurements which can reach values close to zero, a linear variance model (8.1.2) appears most suitable. In this model, a certain offset at very low concentration measurements avoids the overrepresentation of these low concentration measurements in their contribution to the objective function.

$$\sigma^2 = (\alpha \cdot x + \beta)^2 \tag{8.1.2}$$

For simplification reasons, the measured variables were scaled to reach numeric values in the range between 0 and 100. Assuming an equal measurement error for all concentration measurements, which is justified by the calibration data (see annex), one single set of variance model parameters needs to be defined. The value for α was optimized to 0.03, equivalent to a relative measurement error of 3% and the value for β equals a scaled value of 0.1 for all measurements.

Since the temperature measurement does not reach values inferior to 300 °C a constant variance model was chosen (8.1.3).

$$\sigma^2 = \alpha^2 \tag{8.1.3}$$

For temperature measurement in this temperature range, the applied K-type thermocouples have a measurement error of ±2 K. Due to inaccuracies in the axial positioning of the thermocouple, the measurement error for temperature measurement is assumed double this value, α for temperature measurement equals 4 K.

The values of the variance model parameters have been gradually optimized in order to reach an equally good description of both temperature and concentration profiles.

The parameter estimation module in gPROMS® the measured data is compared to simulated values. The algorithm implemented in gPROMS® first solves the reactor model for each operating condition with the initialization for the parameter values. The numerical solver for parameter estimations then varies the model parameters according to a combined search- and gradient method. The reactor model is then solved again for each operating condition and the value of the objective function is compared to the previous iteration. Is an improved parameter set is not found, the search step length is decreased until this is the case. The iteration is continued until the precision criterion is reached.

8.2 Evaluation of Estimation Results and Estimation Strategy

The kinetics of the different catalyst layers are evaluated independently. Most of the o-xylene conversion takes place in the layers zero and one. Thus, the proper description of temperature profiles is strongly related to the kinetics of these layers. The kinetics of layer 1 catalyst are therefore evaluated prior to layer 2 and 3 kinetics. For each of the kinetics, thorough model discrimination is conducted in order to evaluate the best possible description of the reactor comportment applying the lowest possible number of kinetic parameters. This involves the formulation of the kinetic model on the one hand and the evaluation of kinetically significant reaction steps on the other hand.

The requirements for a good parametric fit are multifold. Apart from the visual evaluation of the parameter estimation results through parity plots and comparison of measured and modeled process variables, several statistic criteria are applied in order to evaluate the accuracy of the parameter fit. Amongst these are:

- Value of the objective function: The objective function includes the cumulative deviation of the reactor model from the measured concentrations and temperatures. Consequently, the smaller the value of the objective function becomes, the more accurate is the parameter estimation. This value should lie in a sensible range [142,144]. If this value is too high, the model is not described sufficiently well. A value too low indicates that the model is over-parameterized. Extremely high values of the objective function imply either the inclusion of obvious measurement errors in the estimation or a variance model with insufficient scaling.
- Number of parameters: one aim is to identify the minimum number of parameters to describe the reaction kinetics.
- Correlation: Strong statistical correlation of parameters indicates that at least one of these parameters may be insignificant for the proper mathematical description of the model. The aim of all parameter estimations is to omit any strong parameter correlations. Correlation values above 0.9 are considered weak correlations with values above 0.95 are considered strong correlations [144,145].
- Significance: Each parameter has a range of validity dependent on the statistical confidence interval. If this range exceeds 50% of the parameter value, the estimated parameter is not significant for the mathematical model and can therefore be dropped. Also when the value zero is included in the validity range, this parameter is not significant.
- Distribution of model errors: If a good model description is achieved, the model errors show a normal distribution [146]. The control of the distribution of model errors allows the identification of systematic model errors.

In order to discriminate between different model formulations, the parameter estimations are compared according to the named criteria. The aim is to achieve the minimum objective function with the minimum number of model parameters. The decision

which model parameter is necessary for the description is derived from the statistical analysis of the parameter estimation results.

8.3 Comparison of Catalysts through their Kinetics

The different catalyst layers are compared through the resulting reaction kinetics. The two main factors in this respect are selectivity and activity of each layer. In general, the activity of a catalyst is to be seen as a relative value when comparing this catalyst to another catalyst [54]. In general higher activity means that under the same operating conditions, constant control volume and the same amount of active catalyst, one catalyst has the ability to convert a larger amount of reactant than another catalyst. The relative activity of two catalysts is dependent on the precise operating conditions chosen. In addition, an activity can only be defined for certain reaction steps or the consumption of certain reactants.

In comparing activities from isothermal experiments, the approach frequently taken is to evaluate the rate constant for a first order reaction [79]. Since in this work polytropic measurements are applied for the evaluation of kinetics, this approach alone is not sufficient to characterize the activity. Over the broad range of operating conditions, different relative activities are observed. Therefore, the term activity of a catalyst is applied in this work as a lumped value considering different relative activities throughout the range of operating conditions, particularly temperatures. Since this is only a relative approach any inhibiting terms are neglected for simplification reasons in this consideration. The activity is compared for several reactions according to the following correlation (eq. (8.3.1))

$$A_{rel} = \frac{dn_{cat1}}{dn_{cat2}} = \frac{r_j(T)_{cat1}}{r_j(T)_{cat2}} \tag{8.3.1}$$

where $r_j(T)_{cat}$ represents the first order reaction rate of a certain reaction on one catalyst without consideration of inhibition terms. If the value of the relative activity at a particular operating condition is greater than unity, the activity of the catalyst considered in the numerator has a higher activity than the other catalyst.

When comparing catalysts from their reaction kinetics in terms of selectivity, the differential selectivity (eq. (8.3.2)) of a specific product or a group of products are evaluated in detail and compared individually.

$$s_{ki} = \sum_k \frac{\nu_i}{\nu_k} \cdot \frac{dn_k}{dn_i} \tag{8.3.2}$$

The differential selectivity s_{kj} is defined as the sum of the relations of production rates of selective reaction products *k* from a reactant *i* under consideration of stochiometric coefficients *v* [54].

8.4 Layer 1 Kinetics - Model Discrimination

8.4.1 Initial Kinetic Model

As discussed previously (chap. 6.3), the Skrzypek model is the literature model which with some modifications allows the most precise and coherent representation of the reactor performance of the pilot reactor, both in terms of temperature and concentration profiles. Thus, this general model was chosen as initial model to begin the estimation of kinetic parameters. Certain simplifying assumptions and modifications were made. According to Froment [107], in a system with numerous components which are chemically similar, the adsorption constants in a Langmuir Hinshelwood type rate expression can be lumped. For first estimations, it is assumed that all products and intermediates have similar inhibiting effects, while the effect of oxygen inhibition is assumed constant in the applied concentrations and temperature ranges and is therefore not taken into account. This significantly reduces the number of parameters to be evaluated during first estimations, where the aim is generally to be able to describe the overall reactor comportment.

$$r_j = \frac{k_j \cdot p_i \cdot p_{O_2}}{\left(1 + K_{oX} \cdot p_{oX} + K_P \cdot (p_{TA} + p_{PD} + p_{PA} + p_{MA})\right)^2} \tag{8.4.1}$$

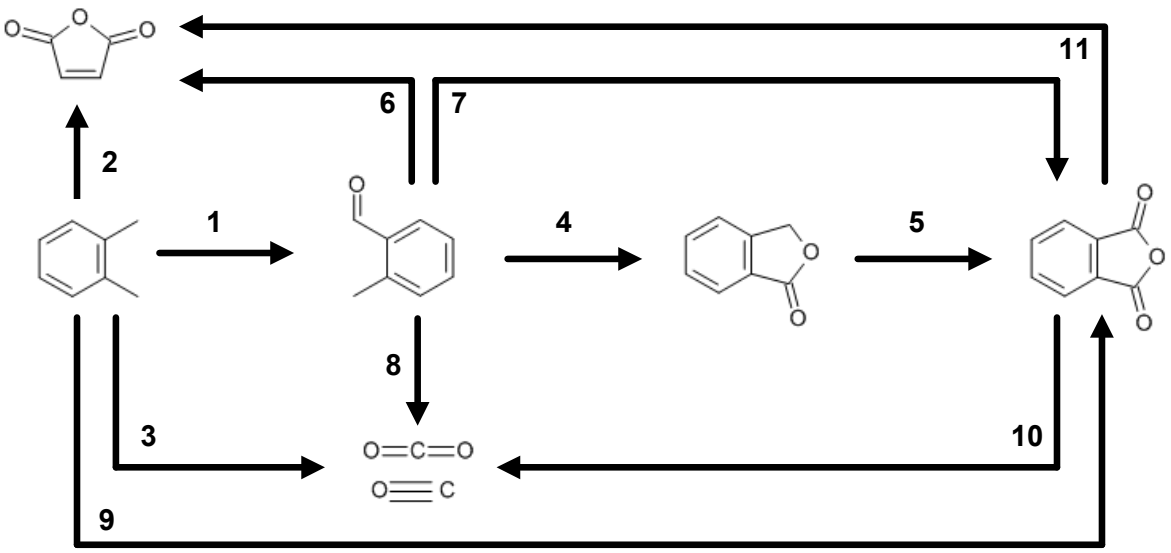

Figure 44: Reaction scheme for kinetic modeling, taking into account both reaction paths described in literature and possible formation paths of by-products MA, CO and CO_2 evaluated in dosage experiments

In recent literature [147-151], it is commonly accepted that reparameterization of the Arrhenius type temperature dependency in the rate equation is favorable for finding the optimal parameter set in application of numerical estimators. The temperature dependency of both frequency factors and adsorption constants is modified according to the following equation.

$$k_j = k_{0,j} \cdot exp\left(-\frac{E_{A,j}}{R \cdot T}\right) = k_{0,j,ref} \cdot exp\left(-\frac{E_{A,j}}{R} \cdot \left(\frac{1}{T} - \frac{1}{T_{ref}}\right)\right) \tag{8.4.2}$$

The optimal reference temperature was evaluated according to the strategy suggested by Schwaab et al. [148] and valued 667.3 K for all frequency factors and adsorption constants.

Table 12: Kinetic parameters of the initial kinetic model; reaction paths are enumerated according to the paths in figure 44

Path Nr.	$k_{0,j} / k_{ref}$	$E_{A,j}$ (kJ mol^{-1})
1	27.4	108
2	0.8	96.7
3	29.8	85.4
4	50.0	85.4
5	53.3	93.8
6	0	0
7	17.5	109
8	0	0
9	52.6	96.3
10	0	0
11	0	0

Table 13: Adsorption parameters of the initial kinetic model

Component	$K_{0,i}$ (10^{-5} Pa^{-1})	$\Delta H_{Ads,i}$ (kJ mol^{-1})
oX	154	28
P	536	25

The resulting initial parameter set applied in first parameter estimations is documented in tables 12 and 13. As in the original Skrzypek model, seven reaction steps are accounted for. This comprises the sequential PA formation via TA and PD as well as direct PA formation from o-xylene and from TA. CO, CO_2 and MA are produced only in parallel reaction paths.

Table 14: Stochiometric coefficients applied in kinetic modeling; reaction paths are according to figure 44

Reaction Nr.	oX	TA	PD	PA	MA	O_2	CO	CO_2	H_2O
1	-1	1	0	0	0	-1	0	0	1
2	-1	0	0	0	1	-7	1	3	4
3	-1	0	0	0	0	-9.45	2.1	5.9	5
4	0	-1	1	0	0	-1	0	0	1
5	0	0	-1	1	0	-1	0	0	1
6	0	-1	0	0	1	-6	1	3	3
7	0	-1	0	1	0	-2	0	0	2
8	0	-1	0	0	0	-8.45	2.1	5.9	4
9	-1	0	0	1	0	-3	0	0	3
10	0	0	0	-1	0	-6.45	2.1	5.9	2
11	0	0	0	-1	1	-4	1	3	1

Taking into account the reaction paths suggested in literature and the results of dosage experiments for the formation of by-products, the reactions scheme shown in figure 44 is accounted for in kinetic modeling. The reaction paths shown include all possible reaction paths which are discriminated. In order to distinguish between CO and CO_2 formation which has a significant impact on both mass and energy balances, the stochiometry in the total oxidation steps is weighted according to the relations of selectivities (CO : CO_2 = 2.1 : 5.9). The stochiometric coefficients applied are shown in table 14.

8.4.2 Description of Temperature Profiles

In first parameter estimations, most difficulties were encountered with the description of temperature profiles for a wide range of operating conditions. As shown in chap. 7, unexpected effects were encountered in experiments where temperature profiles recorded at low SBTs yielded hot spots in a deeper bed position, but significantly sharper and higher in magnitude than temperature profiles recorded at higher SBTs.

Numerous approaches were made to describe this effect kinetically. This includes the broad variation of the reaction scheme, different kinetic approaches (Mars-van-Krevelen, Langmuir Hinshelwood, Eley-Rideal models), variation of kinetic parameters and also the adjustment of reactor model parameters. The kinetics can be described by the Langmuir-Hinshelwood type rate expression as shown above for limited sets of operating conditions. One set of kinetic parameters can describe low SBTs well, while another set provides a good description at high SBTs.

In order to study this systematically, the results of independent estimations at different operating conditions were compared with the aim of finding correlations between the parameter estimates and operating conditions. Generally, all experiments could be described by a Langmuir-Hinshelwood type rate expression. However, with values of the adsorption energy ranging around 300 kJ/mol, the estimated temperature dependency of the o-xylene inhibition lay significantly higher than literature values [24,109].

Comparing the different parameter sets, the relations between pre-exponential factors remain nearly constant for all operating conditions. The main differences can be observed in magnitude of pre-exponential and inhibiting factors on the one hand and in the temperature dependencies on the other hand.

Kershenbaum and Lopez-Isunza et al. [30,111-113,116,117] as well as Georgieva et al. [152-154] have studied the formation of hot spots in pilot reactors loaded with industrial catalysts in correlation with the activity status of the catalyst. In application of the Calderbank reaction kinetics, the temperature profiles of polytropic pilot reactors could be described with sufficient accuracy when applying activity profiles.

In fact, the start-up of an o-xylene oxidation reactor is conducted at very low inlet concentrations, which are then gradually increased over a time of around 50 days [152], until the design load is reached and steady state operation of the reactor begins. During this period, it was reported that the catalyst activity decreases significantly [127,155-157], particularly around the hot spot region at the reactor inlet. This comportment is also observed in experiments with the applied catalytic system without layer 0 filling. This leads to the conclusion that an activity profile is formed during the ramp-up period, which needs to be taken into account also in the kinetic model.

Kershenbaum et al. [112] attempted to describe this type of activity profile through the oxidation status of the catalyst, since this deactivation is somewhat reversible. This approach was also applied in this investigation. However, the parameters of this type of activity profile strongly correlate with other inhibition parameters.

The aim of this study is to describe the reaction kinetics of o-xylene oxidation at steady state conditions. Consequently, the dynamic behavior which leads to said activity profile is not studied closely. The activity profile is described by an empirical polynomial function of the dimensionless reactor length z.

$$A(z) = A_0 + (1 - A_0) \cdot \left(\frac{z}{C_z}\right)^n \tag{8.4.3}$$

The three parameters of the activity profile are the initial activity A_0, the dimensionless bed position C_z, always within layer 1, at which the activity reaches unity and the exponent of the polynomial function. It was found that with the described start-up procedure (chap. 4.2), a constant activity profile within layer 1 catalyst develops in all experiments. Experimental data

obtained from different fillings could be fitted accurately with one activity profile. In addition, the activity profile evaluated independently for data recorded with different catalyst fillings also yields the same parameter results.

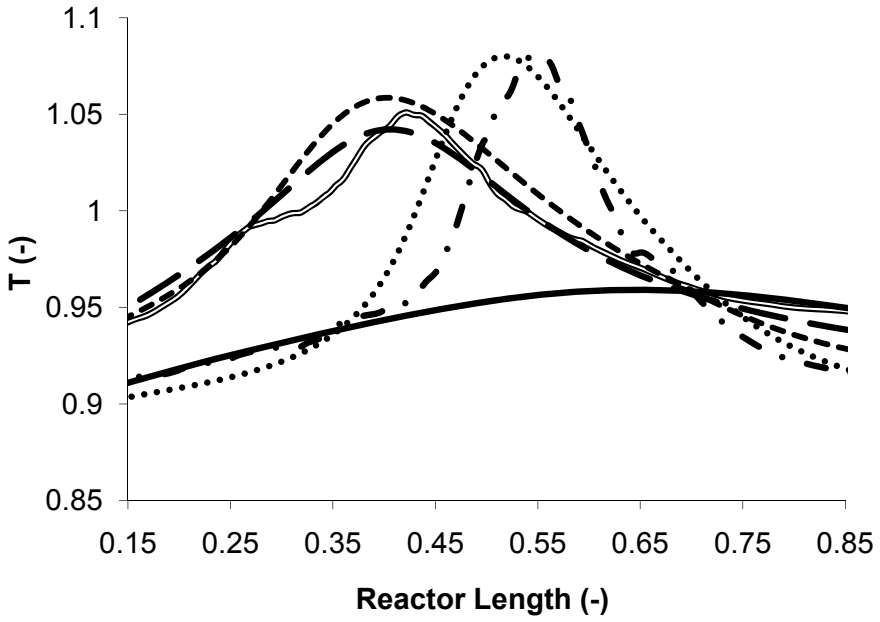

Figure 45: Comparison of measured and modeled temperature profiles at different SBTs with and without the application of activity profiles; T_1 measured (– · –), T_1 without activity profile (——), T_1 with activity profile (···), T_2 with activity profile (- -), T_2 without activity profile (– –), T_2 measured (=) with $T_1 < T_2$

Figure 45 shows the comparison of temperature profiles measured and modeled with and without activity profile. Temperature profiles at high SBTs can be described reasonably well in both cases. However, the accuracy of the description of temperatures resulting with low SBTs is very limited. In application of an activity profile, both the effect of higher hot spot temperatures at low SBTs and the magnitude of the hot spot are represented very well.

In the pilot reactor without layer 0 filling, the fitted activity profile implies that the initial activity at the reactor inlet values around 20% of the full activity, which is reached within the first layer catalyst. The activity function is nearly linear, the exponent n values 1.2. With this activity function, it becomes possible to accurately describe temperature and concentration profiles for various operating conditions.

8.4.3 Reactor Model

The concentration profiles as well as selectivity profiles are represented reasonably well with the adjusted parameters and an imposed activity profile. Nevertheless, the direct formation path of PA from o-xylene (path 9 in figure 44) implies an ill description of the actual reaction kinetics taking place on the catalyst surface. In dosage experiments, a direct PA formation path was not identified. In addition, this path lacks chemical sensibility, considering the surface reaction mechanism [11,19], with which this reaction is assumed to proceed.

In addition, the activation energies obtained when estimating kinetic parameters with the standard heterogeneous model, which accounts for film diffusion to the catalyst pellet, but not for reactant diffusion within the catalyst pellet, are comparatively low (table 15). With values around or below 10 kJ/mol the activation energies of the selective, sequential formation path of phthalic anhydride (3 and 4) indicate mass transfer limitation [61].

Table 15: Activation energies of the standard heterogeneous model; reaction paths according to figure 44

Path Nr.	$E_{A,j}$ (kJ mol^{-1})
1	39
2	118
3	6.7
4	15
5	65
7	80
9	84

The fact that mass transfer limitations persist is somewhat surprising, since the catalyst is an egg shell catalyst with a thin layer of active component. It seems however, that only several reaction steps are actually limited by mass transfer. Nevertheless, the actual intrinsic kinetics can apparently only be evaluated with a reactor model accounting for heat and mass transfer gradients within the catalyst pellet.

Consequently, the reactor model was extended to include also these phenomena. The model implementation in gPROMS® [137] was done based on model libraries available, which were modified in order to properly describe the applied catalyst. The following assumptions and simplifications were taken into account for this model:

- Diffusion within the particle is considered equimolar Fick diffusion with the pore structure accounted for in an effective diffusion coefficient including binary and Knudsen influence [55].

- The thickness of the layer of active mass is constant at both inner and outer surface of the catalyst ring.
- The diffusion length is defined by approximating the ring geometry by a cylinder, accounting for the inner surface area through the specific volumetric particle surface.
- The inert core of the catalyst pellet is taken into account through the inner boundary condition.
- Fluid flow conditions at both inner and outer surface are considered nearly equivalent leading to the constant heat and mass-transfer coefficients for both inner and outer surface.

The basic reactor model (eqs. (8.4.4) - (8.4.9) in table 16) for the catalyst bed is not changed significantly to the heterogeneous model (chap. 6.2) applied. Heat and mass balances of the fluid are modified for the transfer term between solid and fluid, where the solid temperature is no longer a constant solid temperature, but the temperature of the solid at the solid-gas interface (eqs. (8.4.4) and (8.4.6)).

Since the pellet is no longer considered uniform in temperature and concentration distribution, heat and mass balances of the solid (eqs. (8.4.7) and (8.4.8)) are slightly different. Both balances include each a conductive term and consumption or production of reactants in the mass balance and the heat production through the reaction enthalpy in the heat balance respectively.

Table 16: Model equations of the reactor model accounting for mass transfer limitations within the catalyst pellet

mass balance of component *i* in the fluid phase	$\frac{\partial \dot{N}_z^i}{\partial z} = \varepsilon \cdot D_r \cdot \left(\frac{\partial^2 C_f^i}{\partial r^2} + \frac{1}{r}\frac{\partial C_f^i}{\partial r}\right) - k_f \cdot a_v \cdot \left(C_{s,r_p=R_p}^i - C_f^i\right)$	(8.4.4)
overall mass balance fluid	$\dot{M}_{z,tot} = \sum_i \dot{N}_z^i \cdot M_W^i = \rho_f \cdot u_z$	(8.4.5)
heat balance fluid phase	$u_z \cdot \rho_g \cdot c_p \cdot \frac{\partial T_f}{\partial z} = \frac{1}{r} \cdot \frac{\partial}{\partial r} \cdot r \sum_i D_r \cdot \frac{\partial C_f^i}{\partial r} \cdot c_p^i \cdot M_W^i \cdot T_f + h_f \cdot a_v \cdot \left(T_{s,r_p=R_p} - T_f\right)$	(8.4.6)
mass balance of component *i* solid phase	$-\frac{1}{r_p} \cdot \frac{\partial}{\partial r_p} \cdot r_p \cdot D_{eff}^i \cdot \frac{\partial C_s^i}{\partial r_p} + \sum_j \nu_i \cdot r_j \cdot \rho_{cat} = 0$	(8.4.7)
heat balance solid phase	$\frac{1}{r_p} \cdot \frac{\partial}{\partial r_p} \cdot \lambda_s \cdot r_p \cdot \frac{\partial T}{\partial r_p} - \sum_i \sum_j \Delta H_R^j \cdot \nu_i \cdot r_j \cdot \rho_{cat} = 0$	(8.4.8)
Momentum conservation	$\frac{\partial P}{\partial z} = -150 \cdot \frac{\eta_f \cdot u_z}{d_p^2} \cdot \frac{(1-\epsilon)^2}{\epsilon^3} - 1.75 \cdot \frac{\rho_f \cdot u_z^2}{d_p} \cdot \frac{(1-\epsilon)}{\epsilon^3}$	(8.4.9)

The effective diffusion coefficient in eq. (8.4.7) is approximated by the combination of binary and Knudsen diffusion as suggested by Baerns et al. [55].

$$\frac{1}{D_{eff}^i} = \frac{1}{D_{12}^i} + \frac{1}{D_{Knudsen}^i} \tag{8.4.10}$$

The description of binary diffusion coefficients remains the Fuller type estimation corrected with porosity and tortuosity. The tortuosity τ_s is 3 for first estimations with this model. The Knudsen diffusion is estimated according to correlations presented by Baerns et al. [55].

$$D_{Knudsen}^i = \frac{\epsilon_s}{\tau_s} \cdot \frac{d_{pore}}{3} \cdot \sqrt{\frac{8 \cdot R \cdot T}{\pi \cdot M_W^i}} \tag{8.4.11}$$

The boundary conditions for this reactor model are shown in table 17. At the inner perimeter of the catalyst pellet, the reaction temperature equals the temperature of the inert carrier ring, while mass transfer across this barrier is not possible. Radial heat dispersion within the catalyst bed is again considered within the solid. This is visible in the boundary condition at the outer perimeter, where apart from heat transfer to the fluid and conduction within the catalyst pellet, also the radial dispersion term is considered.

Table 17: Boundary conditions for the applied reactor model accounting for mass transfer limitations within the catalyst pellet

for *z = 0*	$T_f = T_s = T_0, \qquad C_f^i = C_{f,0}^i, \qquad \frac{\partial C}{\partial r} = 0,$ $u_z = \frac{\dot{M}_{z,tot,0}}{\rho_f}, \qquad \dot{M}_{z,tot} = \dot{M}_{z,tot,0}$	(8.4.12)
for *r = 0*	$\frac{\partial u_z}{\partial r} = \frac{\partial \dot{M}_z^i}{\partial r} = \frac{\partial T_f}{\partial r} = \frac{\partial T_{s,r_p=R_p}}{\partial r} = 0$	(8.4.13)
for *r = R*	$\alpha_W \cdot \left(T_W - T_{s,r_p=R_p}\right) = \lambda_r \cdot \frac{\partial T_{s,r_p=R_p}}{\partial r}, \qquad \frac{\partial T_W}{\partial r} = 0,$ $\frac{\partial C_f^i}{\partial r} = 0$	(8.4.14)
for $r_p = 0$	$T_{s,rp=0} = T_{inert}, \qquad \frac{\partial C_s^i}{\partial r_p} = 0$	(8.4.15)
for $r_p = R_p$	$h_f \cdot a_v \cdot \left(T_{s,r_p=R_p} - T_f\right) = \frac{1}{r} \cdot \frac{\partial}{\partial r} \cdot r \cdot \lambda_r \cdot \frac{\partial T_{s,r_p=R_p}}{\partial r} + \lambda_s \cdot a_v \cdot \frac{\partial T_s}{\partial r_p}$ $k_f \cdot \left(C_{s,r_p=R_p}^i - C_f^i\right) = D_{eff}^i \cdot \frac{\partial C_{s,r_p=R_p}^i}{\partial r_p}$	(8.4.16)

Results of simulations of both pellet and standard reactor model, with kinetics evaluated with the standard heterogeneous reactor model are depicted in figure 46. The simulated hot spot of the pellet model is of the same magnitude as of the standard model. However, the position is significantly different. In transport limited reactions, catalyst efficiency factors for consecutive reactions are larger than unity. This is due to elevated concentrations of intermediates within the catalyst pellet, compared to the surrounding fluid. In the effective kinetic model, the reaction velocities of intermediate reaction steps are consequently overestimated. This leads to the significant difference in the formation of

temperature profiles and also implies that the application of the pellet model yields an improved description of the physical system.

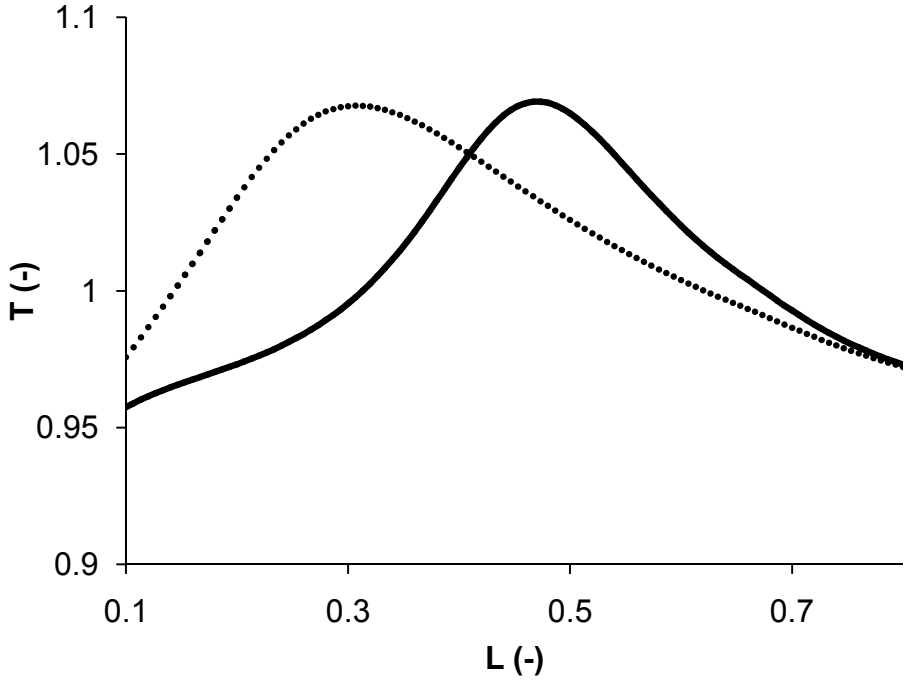

Figure 46: Comparison of temperature profiles modeled in application of reaction kinetics evaluated with the standard reactor model for the same operating conditions; pellet model (⋯), standard heterogeneous model (—)

Figure 47 compares the selectivity profiles of PA and TA at low conversions obtained from the effective kinetic model, with and without direct formation path on the one hand and the pellet model, only without direct PA formation, on the other hand to experimental data. The selectivity profile of TA simulated with the effective kinetic model without direct PA formation significantly overestimates the respective selectivity at low conversions. Opposite to this comportment, the equivalent PA profile begins at nearly zero selectivity and only at conversions of about 50%, it properly describes the experimental data.

In comparison, the selectivity profiles modeled with the effective kinetic model and a direct PA formation path represent the experimental data of TA and PA selectivities reasonably well. In the pellet model, the formation of PA is modeled by a combination of parallel and consecutive reaction paths (paths 4, 5 and 7 in figure 44). The simulated data of the pellet model does not involve direct PA formation (path 9). Nevertheless, non-zero selectivity of PA is represented with very good accuracy in application of this model. Also the TA selectivity profile yields a significantly improved simulation result.

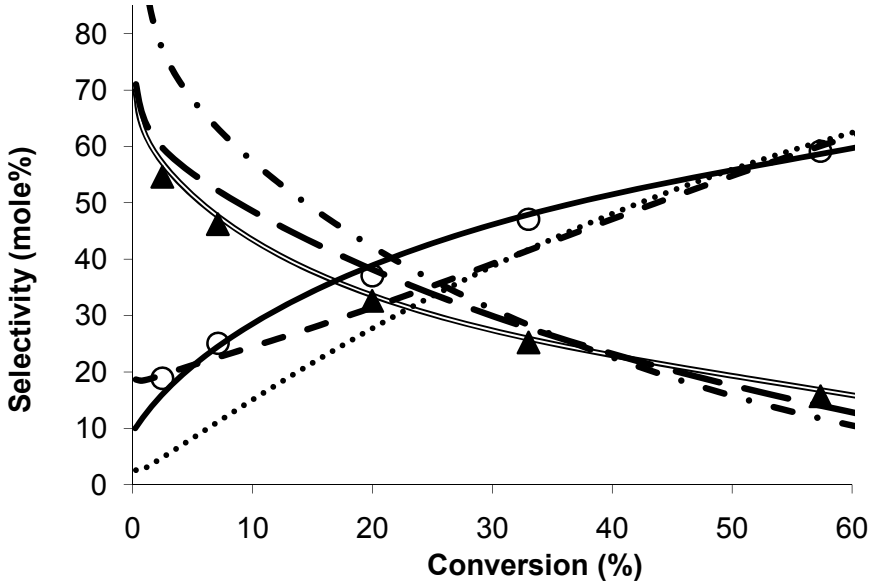

Figure 47: Comparison of selectivity profiles of PA and TA modeled with the pellet model and the effective model; TA effective model (– · –), PA pellet model (——), PA effective model (···), PA effective model, direct PA formation (- -), TA effective model, direct TA formation (– –), TA pellet model (=), PA measurement (O), TA measurement (▲)

The reaction paths necessary for the representation of this effect are also backed by the results of dosage experiments. While a direct formation of PA is chemically not sensible, the formation of PA via TA and PD is commonly accepted as the main formation path. A direct path from TA (path 7 in figure 44) is the model representation of the second selective PA formation route via phthalaldehyde and phthalic acid described in chap. 5.6. Due to low measured phthalaldehyde and phthalic acid concentrations within this consecutive reaction is lumped to one single reaction path.

Riekert [80] has derived theoretically that non-zero initial selectivities of consecutive reaction products can be observed in transport limited reactions due to elevated intermediate concentrations within the catalyst pellet. Within the experimental setup, concentrations are measured of the gas phase only, while concentrations in the catalyst pellet remain widely unknown. In this case o-xylene diffuses into to the pore structure of the catalyst pellet and is quickly converted to TA. o-Xylene which reaches the inner perimeter of the active mass is converted similarly. While TA is transferred in the pores towards the catalyst surface, it can adsorb again and be converted further to PD or PA. Therefore, even at low o-xylene conversions and small values of the GHSV, non-zero PA selectivities are observed in the gas phase.

The model discrimination above shows clearly that the observation of non-zero PA selectivities at low conversions is an effect which can be explained by transport phenomena within the catalyst pellet.

In conclusion, it is possible to describe the reactor performance more accurately with chemically sensible reaction paths applying the pellet model. Additionally, the values of activation energies have increased significantly to reach more reasonable values. Hence, the pellet model is applied for all further model discrimination.

8.4.4 Heat Transfer Parameters

The simulated temperature profiles in figure 45 indicate that temperature values, particularly in the hot spot area are systematically overestimated. With the kinetic model applied, the hot spot temperatures are regularly around 15 – 20 K above the measured values. The main influence on the hot spot formation is surely the reaction kinetics together with different reaction paths and selectivities of these reaction paths. The estimation of the parameter values of the kinetic model alone does not allow accurate description of temperature profiles.

Other influencing factors on the simulation of hot spots are the heat transfer parameters in the reactor model as well as reaction enthalpies. Reaction enthalpies are evaluated from standard enthalpies of formation of each of the chemical compounds along with their heat capacity. The values enthalpies of formation are compared with several literature values [67,138]. The heat capacities, which have only a very small influence on the reaction enthalpies, are evaluated with the commercial Multiflash^{TM} module. Hence, the values of reaction enthalpies can be trusted.

Heat transfer parameters of the fixed bed, heat transfer from gas to solid phase and to the reactor wall are estimated from literature correlations. The heat conductivity of porous active mass of the catalyst pellet ranges between 0 and 1 W/m K [159]. Sensitivity analysis has shown that the influence of this transfer parameter on simulation results is only minimal. It was therefore set to 1 W/m K.

The sensitivity of the remaining transfer parameters however is significant on the description of hot spots. In a series of parameter estimations the influence of each of these parameters was studied. Since the correlations for transport parameters include the influence of temperature and hydrodynamics on these parameters, proportional factors were introduced to adjust these parameters.

The following estimations were conducted:

1. Base case, considering that all heat transfer parameters are correctly estimated by literature correlations; the pellet model is applied along with an activity profile and the kinetic scheme described in chap. 8.4.1.
2. Modification of the radial heat conductivity (λ_r) only; in this estimation an additional model parameter is applied. The value of the objective function decreases

significantly, which can be directly tracked to an improved description of temperature profiles. The additional parameter is significant and is not correlated with any other parameter

3. Modification of the tube-wall heat transfer parameter (α_W) only; with this estimation the base case is improved significantly. However, the modification of the radial heat conductivity yields better results both in resulting temperature profiles and in objective function value.
4. Modification of the solid-gas heat transfer coefficient (h_f) only; this measure improves the estimation only to a rather small extent.
5. Simultaneous estimation of radial heat conductivity and tube-wall heat transfer coefficient (λ_r and α_W); when estimating these two parameters simultaneously, the factor of the tube-wall heat transfer coefficient is estimated to a value of nearly unity, while the radial heat conductivity is modified significantly. In addition, the estimated parameters are strongly correlated.
6. Simultaneous estimation of radial heat conductivity and solid-gas heat transfer coefficient (λ_r and h_f); in this case both transfer parameters are modified to slightly elevated values. The overall estimation accuracy is not improved compared to case 2. Consequently, the additional parameter is not justified.
7. Simultaneous estimation of tube-wall heat transfer coefficient and solid-gas heat transfer coefficient (α_W and h_f); estimating these two parameters simultaneously yields an improved description when compared to the base case, but not when compared to the estimation of only the radial heat conductivity.
8. Simultaneous estimation of all heat transfer parameters (λ_r, α_W and h_f); in this case all additionally estimated parameters are strongly correlated. Since the model representation is not significantly improved, the estimation of all three heat transfer parameters seems unfavorable.

The results of these estimations are summarized in table 18. The values of the objective functions are normalized to the value of the optimal estimation. In addition, the total number of estimated parameters, including kinetic, reactor model and activity profile parameters, as well as the number of insignificant parameters and parameter correlations is indicated.

Clearly, the modification of the radial heat conductivity yields the most precise description with the minimum number of parameters necessary. The resulting value of this parameter is optimized to 1.8 times the value predicted by model correlations. For the tube-wall and solid-gas heat transfer coefficients, the values of literature correlations appear to describe the reactor comportment sufficiently well.

Table 18: Summary of estimation results of the investigation of heat transfer parameters where the value of the objective function relative to the optimum case, the total number of estimated parameters, the number of insignificant model parameters and the total number of parameter correlations are compared.

Model	rel. OF	N_P	N_{in}	N_c
1	1.44	21	0	1
2	1	22	0	1
3	1.22	22	0	1
4	1.33	22	0	1
5	1.01	23	0	2
6	0.99	22	0	1
7	1.19	22	0	1
8	0.99	24	0	3

This finding is somewhat surprising, since the literature correlations by Nilles [160] are based on very broad data set. Two major differences can be found between the experimental set-up applied in this study and in studies conducted to evaluate correlations for heat transfer parameters. This is the low aspect ratio of particle diameter to tube diameter as it is applied in industrial reactors for the oxidation of o-xylene on the one hand. On the other hand, correlations for heat transfer parameters are usually evaluated in systems without catalytic reaction.

Generally, two types of heat transfer models for fixed beds are frequently cited in literature. Traditionally, ideal plug flow is assumed and a pseudohomogeneous model with effective radial conductivity and apparent tube-wall heat transfer coefficient is developed. Over the last decades numerous publications [28,62,160-171] have presented correlations for heat transfer parameters needed for such models, which themselves yield large differences in parameter predictions [162,163].

More recently, efforts have been made to find a physically more precise model description of the transport phenomena. Vortmeyer et al. [172,173], Tsotsas [174] and Eigenberger et al. [175,176] have introduced fluid flow patterns and the nature of the fixed bed to the description of heat transfer. This approach has been taken up and extended by various research groups [177-181]. There is however a continuing debate on whether to apply these effects to the classical heat transfer models with constant radial heat conductivity and a wall heat transfer coefficient, or instead applying varying radial heat conductivity dependent on flow profile and voidage of the fixed bed at the radial position is introduced. In the second case, the so-called *λ(r)*-model, the boundary condition at the wall can be modeled through the physically more coherent boundary condition of $T(r=R) = T_W$.

Such models require detailed knowledge of the fluid flow profile in the packed bed, which for low aspects ratios and random particle shapes has yet not been investigated with

sufficient detail [179]. Hence, similar deviations as observed with the more basic model are to be expected.

Unfortunately, the influence of catalytic reaction on the heat transfer within a fixed bed has only been studied scarcely in literature. Hofmann [54] reports of a study where experimental data from a fixed bed catalytic reaction was fit to a kinetic model. In this study the kinetic parameters were estimated first with fixed heat transfer parameters, which were then also released for estimation. While kinetic parameters hardly change, the heat transfer parameters rise in 30%. Hofmann states that each catalytic reaction has an influence on heat transfer parameters, which is reaction specific. In this context the approach taken above appears the most consequent approach.

Westerterp et al. [182] studied the effects of chemical reaction on heat transfer directly. He established that when applying a homogeneous model, heat transfer coefficients appear higher due to heterogeneity effects. Since in this work a heterogeneous model is applied, this effect does not influence the transfer parameters.

In another study of heat transfer parameters, Westerterp et al. [183] employed industrial Raschig ring catalysts with dimensions similar to the catalyst applied in this study in order to study the predictions of literature correlations in different geometrical setups. Particularly for small aspect ratios of tube diameter to particle diameter, the resulting Biot number was significantly lower than Biot numbers from literature correlations. With the modified radial heat conductivity, the Biot numbers range between 0.75 and 0.86, while the values obtained from the applied literature correlations are between 1.45 and 1.65. This decrease corresponds to the findings described by Westerterp for Raschig rings and small aspect ratios, both in magnitude and direction.

In consequence, the modification of heat transfer parameters, particularly of the radial heat conductivity, appears justified with the geometrical conditions under which the oxidation of o-xylene is conducted under industrial conditions. For further model discrimination, the factor of 1.8 is applied for the radial heat conductivity.

8.4.5 Reaction Scheme

Another part of model discrimination looked into in detail is the reaction scheme. Dosage experiments have shown via which intermediates both selective and non selective oxidation products are formed. In this part of model discrimination the kinetic significance of these reaction paths is investigated. Generally the questions focused on in this study are:

- What is/are the significant reaction path(s) forming CO and CO_2?
- Which way of maleic anhydride formation is significant?
- Which selective reaction paths for PA formation are necessary to properly describe both temperature and concentration profiles?

In terms of CO and CO_2 formation the measured selectivity profiles imply that there is a parallel formation path directly from o-xylene and also one or more consecutive reaction path(s). Dosage experiments have shown that CO and CO_2 are formed in consecutive reaction paths by total oxidation of tolualdehyde or its oxidation intermediates on the way to MA. In addition, PA total oxidation is possible, via intermediates like benzoic acid or directly at high residence times.

In order to investigate CO and CO_2 formation, several estimations were conducted. The corresponding results are summarized in table 19. Starting from the initial model CO and CO_2 formation were assumed only from o-xylene (path 3 in figure 44). The number of parameters is smaller when only this total oxidation path is taken into account (model 1 in table 19). However, due to slightly rising CO and CO_2 selectivity profiles at high conversions, the addition of a consecutive reaction path improves the model description in terms of objective function. Therefore, total oxidation of tolualdehyde (path 8 in figure 44) and total oxidation of PA (path 10 in figure 44) were added to the model in order to obtain an improved description.

Table 19: Comparison of parameter estimations evaluating the necessary CO and CO_2 formation paths; (1) path 3, (2) paths 3, 8 and 10, (3) paths 3 and 8 and (4) paths 3 and 10 in figure 44

Model	rel. OF	N_P	N_{in}	N_c
1	1.18	22	0	1
2	1	26	2	3
3	1.07	24	0	1
4	1	24	0	1

Estimating parameters for both TA and PA total oxidation path leads to a strong correlation of activation energies and pre-exponential factors of these two reaction paths (model 2 in table 19). In addition, both pre-exponential factors are not significant, their error range is larger than the parameter value itself. Consequently, only one of these paths is necessary to properly describe the reaction.

In the evaluation which of these two paths yields an improved result, it clearly shows that the total oxidation of TA is kinetically insignificant (model 3 in table 19), while the total oxidation of PA yields a sufficiently good estimation result (model 4 in table 19).

In terms of maleic anhydride formation paths, the dosage experiments have shown that again two reaction paths are possible. Sources are again o-xylene, with the path via DMBQ, and tolualdehyde, with toluene and several other compounds as intermediates.

The summary of conducted estimations is shown in table 20. When assuming that MA is formed only from o-xylene directly, the rising run of the MA selectivity profile cannot be

properly represented (model 1 in table 20). Therefore, the objective function shows a high value, particularly due to higher modeled MA concentrations at low conversions.

Table 20: Comparison of estimations evaluating the kinetically significant MA formation; (1) path 2, (2) paths 2 and 6 and (3) path 6 in figure 44

Model	rel. OF	N_P	N_{in}	N_c
1	1.2	22	0	1
2	1.02	24	2	1
3	1	22	0	1

Assuming direct formation from o-xylene and from TA, the latter a clear result of dosage experiments, the objective function value improves significantly. However, in this case the kinetic parameters for the direct formation path become kinetically insignificant (model 2 in table 20). Consequently, this path is dropped and MA formation is modeled only from TA (model 3 in table 20). This reduces the number of parameters and eliminates the insignificancies and thereby significantly improves the model description.

In chap. 8.4.2 it was shown that the direct formation path of PA is generally not necessary to properly describe the selectivity profile of PA. This is also backed by estimation results. Table 21 compares the results of this investigation. Taking in account all possible PA formation paths as Skrzypek suggests, the number of parameter correlations as well as insignificancies rises, while the objective function reaches a nearly optimal value (model 1 in table 21). Dropping only the direct formation path of PA from TA (path 7 in figure 44) but keeping the direct PA formation from o-xylene also eliminates any correlations and insignificancies (model 2 in table 21).

Dropping also the direct formation of PA (path 9 in figure 44) further reduces the number of parameters, but weakens the accuracy of the model description (model 3 in table 21). Since an independent PA formation path from tolualdehyde via phthalaldehyde has been evaluated in dosage experiments, this path (path 7) is reintroduced. The number of parameters rises again, but the model description improves substantially (model 4 in table 21).

Table 21: Comparison of estimation results investigating the necessary formation paths of PA; (1) paths 5, 7 and 9, (2) paths 5 and 9, (3) path 5, (4) paths 5 and 7 in figure 44

Model	rel. OF	N_P	N_{in}	N_c
1	1.01	24	1	2
2	1.01	22	0	0
3	1.06	20	0	1
4	1	22	0	1

Models 2 and 4 yield nearly the same accuracy in terms of objective function. Including the direct formation path even omits the correlation between consecutive and parallel PA formation from TA, which persists in all parameter estimations. Nevertheless, the direct PA formation is not necessary for the representation of the measured data. Consequently, the chemically more coherent model formulation is chosen over the purely numeric model with direct PA formation path. In this kinetic model, the formation of PA from TA is modeled as one lumped reaction. It is assumed that this path goes via several microkinetic steps which are not explicitly taken into account.

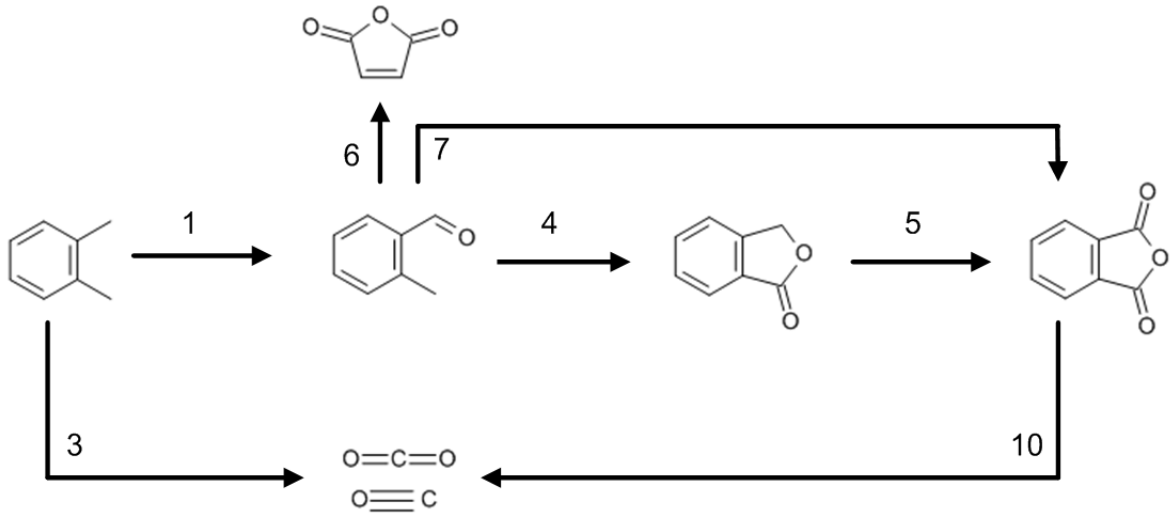

Figure 48: Final reaction scheme for kinetic modeling of layer 1 catalyst

The finally evaluated reaction scheme necessary for the description of layer 1 catalyst is depicted in figure 48. The reaction scheme of possible reactions evaluated in dosage experiments has been reduced from 11 to 7. Compared to the Skrzypek literature model, this amounts to the same number of reactions, but yields a significantly improved description of the reactor comportment. All of the modeled reactions are lumped reactions, which in reality have several reaction intermediates and all of these reactions also have a chemical background based on the findings of dosage experiments.

8.4.6 Kinetic Model

Apart from the reaction scheme and the reactor model, one very important point of interest is the kinetic model that describes this reaction with sufficient accuracy. The aim is to find the best possible description with the simplest kinetic model. As described in chap. 6.1, different model types have been applied to describe o-xylene oxidation kinetics. Amongst these are simple power law rate expressions, Langmuir-Hinshelwood type rate expressions and Mars-van-Krevelen type rate expressions.

In order to study this systematically, the initial rate expression was extended to a full Langmuir-Hinshelwood type rate expression, with the organic compounds with high concentrations in the inhibition term (eq. (8.4.17)). All rate constants and inhibition constants are temperature dependent.

$$r_j = \frac{k_j(T) \cdot p_i \cdot p_{O_2}}{(1 + K_{oX}(T) \cdot p_{oX} + K_{TA}(T) \cdot p_{TA} + K_{PD}(T) \cdot p_{PD} + K_{PA}(T) \cdot p_{PA})^2} \tag{8.4.17}$$

Estimations with this type of rate expression lead to strong correlations of the inhibition constants (model 1 in table 22). Particularly adsorption constants of PA and PD are strongly correlated. In addition, the PA inhibition parameters are kinetically insignificant.

$$r_j = \frac{k_j(T) \cdot p_i \cdot p_{O_2}}{(1 + K_{oX}(T) \cdot p_{oX} + K_{TA}(T) \cdot p_{TA} + K_{PD}(T) \cdot p_{PD})^2} \tag{8.4.18}$$

Consequently, the PA inhibition term was dropped and the kinetic rate equations were reduced to the expression shown in eq. (8.4.18). The results of this estimation (model 2 in table 22) show a slight improvement of the objective function. The major advantage of the other model formulation is however the reduction of insignificant parameters and correlations. In this type of rate expression, the temperature dependency of the phthalide inhibition is repeatedly estimated zero and is therefore kinetically insignificant.

$$r_j = \frac{k_j(T) \cdot p_i \cdot p_{O_2}}{(1 + K_{oX}(T) \cdot p_{oX} + K_{TA}(T) \cdot p_{TA})^2} \tag{8.4.19}$$

Further reduction of the inhibition terms as shown in eqs. (8.4.19) and (8.4.20), leads to higher objective function values and also more parameter correlations (models 3 and 4 in table 22).

$$r_j = \frac{k_j(T) \cdot p_i \cdot p_{O_2}}{(1 + K_{oX}(T) \cdot p_{oX})^2} \tag{8.4.20}$$

The effect of diffusion models for pore diffusion within the catalyst pellet on the formulation of the rate equation was studied by releasing the tortuosity for estimation. Initially this parameter was set to three. However, values between 2 and 7 [159] appear realistic. A measured value is not available for the applied catalyst.

Table 22: Comparison of estimations with various kinetic models

Model	rel. OF	N_P	N_{in}	N_c
1	1.03	26	2	3
2	1.02	24	1	0
3	1.04	22	0	1
4	1.06	20	0	3
5	1.02	22	0	1
6	1.01	22	0	2
7	1	22	0	1

The estimation of the tortuosity leads to a value for this parameter of 4.3, which is within the cited range. In this case however, the inhibition term of phthalide not only becomes independent of temperature, but completely insignificant kinetically. In addition, the temperature dependency of the TA inhibition term reaches values of zero. The rate equation can be simplified to the correlation shown in eq. (8.4.21). The corresponding estimation (model 5 in table 22) yields objective function values which are equivalent to a model with phthalide inhibition, but with an inferior number of parameters.

$$r_j = \frac{k_j(T) \cdot p_i \cdot p_{O_2}}{(1 + K_{oX}(T) \cdot p_{oX} + K_{TA} \cdot p_{TA})^2} \tag{8.4.21}$$

In a next step, it was investigated whether the Langmuir-Hinshelwood type rate expression is necessary, or whether the system can also be described with a Eley-Rideal type rate expression. Consequently, the exponent in the denominator was dropped to obtain the rate expression shown in eq. (8.4.22).

$$r_j = \frac{k_j(T) \cdot p_i \cdot p_{O2}}{1 + K_{oX}(T) \cdot p_{oX} + K_{TA} \cdot p_{TA}} \tag{8.4.22}$$

Estimations with this type of rate expression yield results which in terms of statistical accuracy and objective function value show only minimal difference (model 6 in table 22). An additional correlation must be taken into account, while the objective function value decreases slightly. In order to decide which of the rate expressions appears more sensible, the dependency of the reaction rate on oxygen partial pressure was investigated by introducing an exponent to this variable as shown in eq. (8.4.23).

$$r_j = \frac{k_j(T) \cdot p_i \cdot p_{O2}^n}{1 + K_{oX}(T) \cdot p_{oX} + K_{TA} \cdot p_{TA}} \tag{8.4.23}$$

At the concentrations at which the industrial process is run, the oxygen partial pressure apparently does not have a direct influence on the reaction rate. The exponent takes values around zero. Applying the Eley-Rideal type rate expression the estimation results in a smaller objective function value and improved statistical accuracy, particularly considering the number of correlations.

The Langmuir-Hinshelwood rate expression implies that both reactants adsorb at the surface of the catalyst. This is surely the case for both oxygen and the organic compounds in selective oxidation on vanadia catalysts. Nevertheless, since the oxygen concentration does not influence the reaction kinetics at these concentrations, also the adsorption of oxygen does not have an influence on reaction rates. Since also parameter estimations with Langmuir-Hinshelwood and Eley-Rideal type rate expression yield equivalently accurate estimation results, the Eley-Rideal type model appears more consistent.

The final, optimized rate equation for all reaction steps is shown in eq. (8.4.24).

$$r_j = \frac{k_j(T) \cdot p_i}{1 + K_{oX}(T) \cdot p_{oX} + K_{TA} \cdot p_{TA}} \tag{8.4.24}$$

Simple mathematical manipulation of this expression yields a type of rate equation, as suggested by Mars and van Krevelen. Introducing a kinetic parameter, equivalent to the oxidation rate of the catalyst in the Mars-van-Krevelen approach, the rate equation can be transformed to the expression shown in eq. (8.4.25).

$$r_j = \frac{k_j \cdot k_o \cdot p_i}{k_o + (k_1 + 9.45 \cdot k_3) \cdot p_{oX} + (k_4 + 6.5 \cdot k_6) \cdot p_{TA}} \tag{8.4.25}$$

with

$$K_{oX} \cdot k_o = k_1 + 9.45 \cdot k_3 \tag{8.4.26}$$

and

$$K_{TA} \cdot k_o = k_4 + 6.5 \cdot k_6 \tag{8.4.27}$$

This shows that o-xylene oxidation can be described with a rate equation which is derived from adsorption kinetics, as the Langmuir-Hinshelwood or Eley-Rideal rate equations as well as with a model based on oxidation and reduction of the catalyst surface, as the Mars-van-Krevelen model. However at the industrial process conditions, an influence of oxygen partial pressure on the reaction rates could not be derived and the Eley-Rideal type rate expression is chosen to describe the reactor comportment.

8.4.7 Final Kinetic Model Layer 1

The parameters of the final kinetic model of layer 1 catalyst are shown in table 23 and table 24. In total the number of kinetic parameters amounts to 17. This includes a total of seven reaction steps. Inhibiting parameters are o-xylene inhibition with temperature dependency and tolualdehyde inhibition, which is constant with temperature.

Table 23: Parameters of the layer 1 kinetic model with the error for a confidence interval of 95%

Path Nr.	$k_{0,j}$ / k_{ref}	$E_{A,j}$ (kJ mol^{-1})
1	55 ± 0.1	156 ± 4
3	5.8 ± 0.2	89 ± 6
4	95 ± 5	62 ± 9
5	116 ± 7	65 ± 12
6	11.4 ± 0.2	73 ± 12
7	135 ± 3	39 ± 9
10	1 ± 0.05	152 ± 8

Table 24: Adsorption parameters of layer 1 kinetic model

Component	$K_{0,j}$ (10^{-5} Pa^{-1})	$\Delta H_{Ads,j}$ (kJ mol^{-1})
oX	15 ± 2	144 ± 10
TA	130 ± 20	-

The activation energies evaluated show quite a broad distribution. While the activation energy of the selective oxidation step from o-xylene to TA takes an unexpectedly high value, the further conversion to PA directly or via PD seems to be very rapid also at low temperatures, due to relatively low activation energies. Particularly striking is the observation that the activation energy of the total oxidation step is significantly lower than the selective oxidation step. This explains the unusual runs of the CO and CO_2 selectivity profiles, which in the polytropic measurement show relatively high initial selectivities which then decrease, reach a minimum and increase again.

The inhibition term of o-xylene has a very strong temperature dependency. Along with the activity profile, this accounts for the rather unusual shape of the temperature profile. Comparatively strong adsorption energies of around 50 kJ/mole for different components such as oxygen and CO on vanadia are documented by Somorjai [184], while for other metal oxides these values range around 20 kJ/mole. Unfortunately, adsorption energies of organics are not documented. However, the relatively strong temperature dependency of adsorption on vanadium seems coherent with the findings above.

In terms of activity, the pre-exponential factor of o-xylene conversion to tolualdehyde has a value roughly half the pre-exponential factors of all TA consuming reactions (4, 6 and 7). By this way, the strong decrease of TA selectivity at low conversions can be described kinetically. Generally, the activity of the total oxidation reactions is one magnitude lower in case of o-xylene oxidation or two magnitudes lower than the selective reaction steps. This accounts for the high selectivities this catalyst shows to PA.

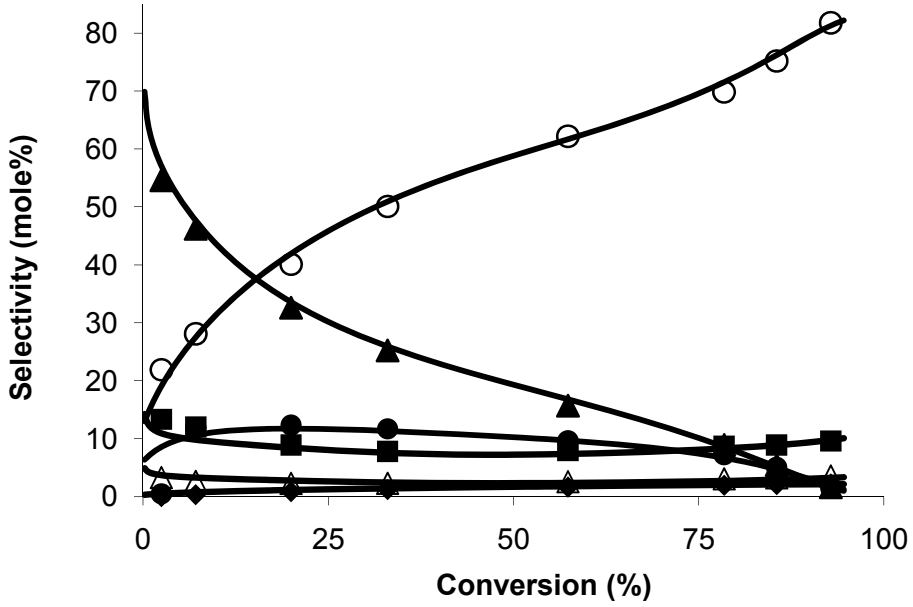

Figure 49: Comparison of measured and modeled selectivity profiles for layer 1 catalyst; lines are modeled runs while dots are measured values; TA (▲), MA (♦), CO_2 (■), PA (O), PD (●) and CO (Δ)

Figure 49 depicts the comparison of measured and modeled selectivity profiles. The rising PA selectivity profile is represented with very good accuracy throughout the entire range of conversion. The discussed non-zero initial selectivities are represented equally well as the high above 80% values at high conversions. The high TA selectivities at low o-xylene conversion, with very strong decrease until conversions of about 10% can be simulated very well with this kinetic model. The simulated PD selectivity profile reaches its maximum at an o-xylene conversion of about 10%. The strong increase, which is observed in measured values is not shown with the same severity in the simulated profile. However, both TA and PD selectivities reach values of nearly zero at the reactor outlet, equivalent to measured values.

CO and CO_2 selectivity profiles are represented extremely well. The decrease due to temperature effects in non-isothermal operation is represented equally well as the rise in selectivity at higher conversions. The simulated MA selectivity profile shows the constantly rising run that measurements also show. At the reactor outlet the selectivity of MA reaches values around 2.5%, equivalent to the measured values.

In experiments with a full filling of first layer catalyst, the conversion reaches a maximum of around 95%. This is also the maximum simulated conversion. Generally, the conversion profiles fit the measured profiles very well.

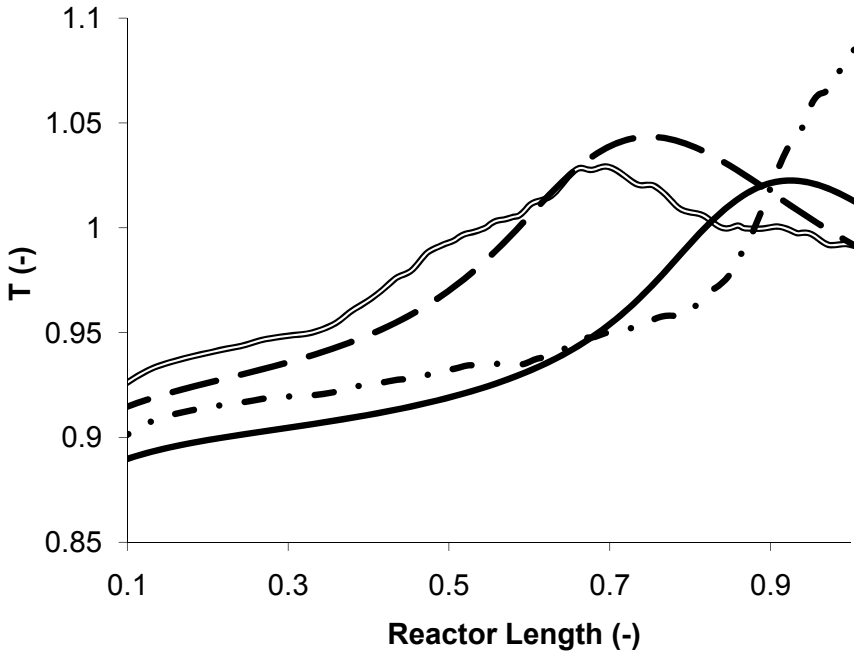

Figure 50: Comparison of measured and simulated temperature profiles for layer 1 catalyst; T_1 measured (– · –), T_1 simulated (—), T_2 measured (=), T_2 simulated (- -), where $T_1 < T_2$

Figure 50 compares measured and simulated temperature profiles. The strongest deviation of temperature profiles is observed at low SBTs. The simulated profiles at high SBTs are represented with very good accuracy both in hot spot position and magnitude. At low SBTs, the temperatures are represented very well until a certain reactor length. It must be stated that the temperature profile shown here represents the worst fit of all fitted temperature profiles. Since a strong deviation is only apparent on a very short reactor length, this deviation is considered acceptable.

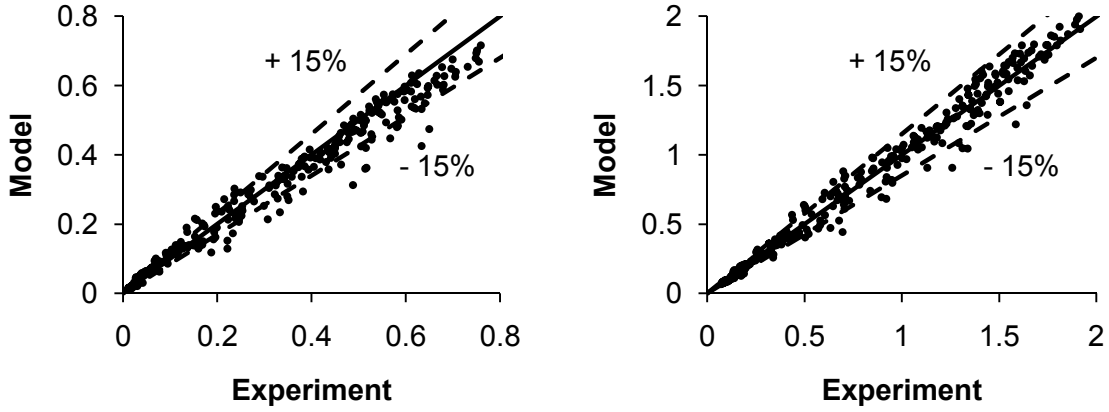

Figure 51: Parity plots of CO (left) and CO_2 (right) for layer 1 catalyst; compared are measured gas phase concentrations of CO and CO_2

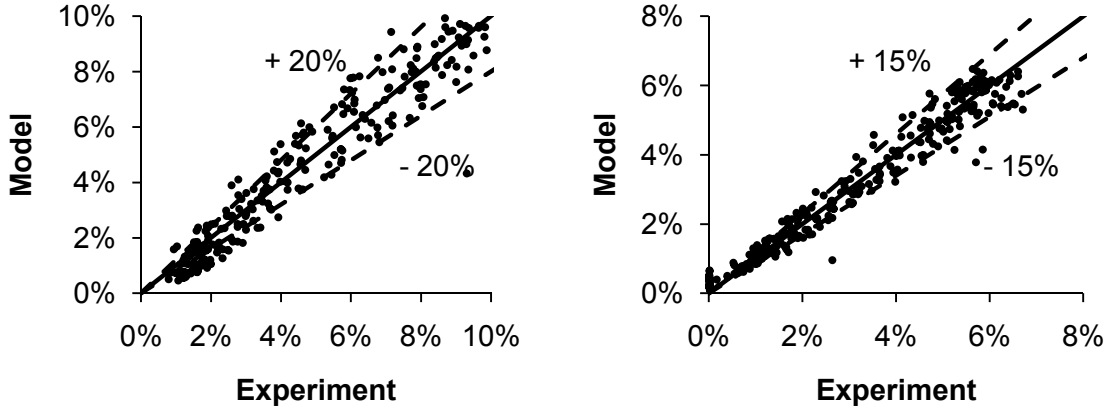

Figure 52: Parity plots of TA (left) and PD (right) for layer 1 catalyst; compared are the raw measured data in terms of composition of the organic compounds as entered to the parameter estimation

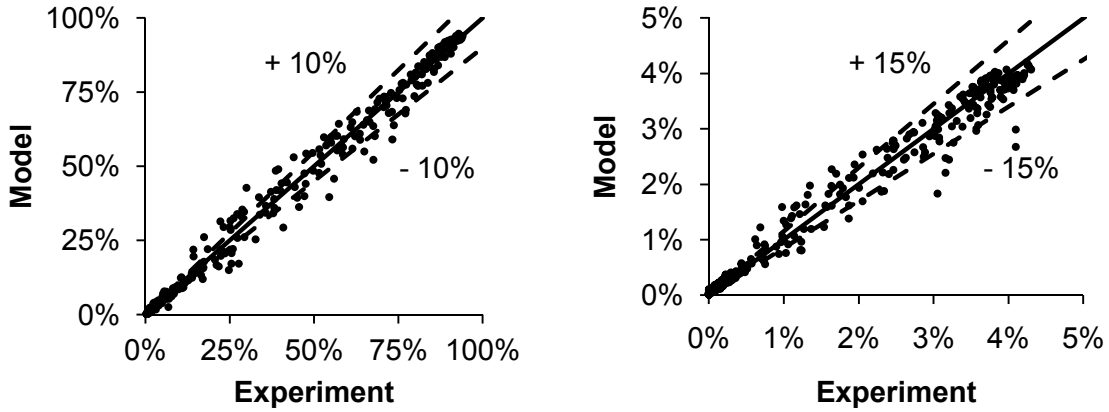

Figure 53: Parity plots of PA (left) and MA (right) of layer 1 catalyst

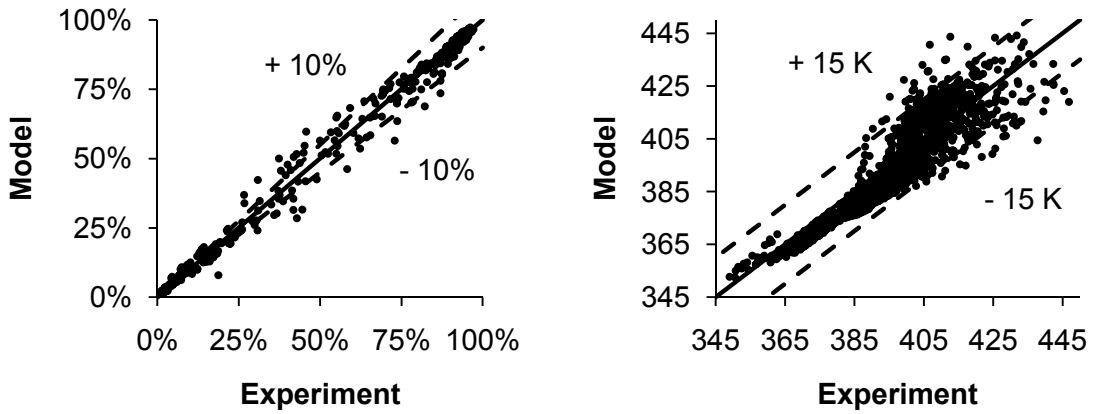

Figure 54: Parity plots comparing experimental and modeled values for o-xylene conversion (left) and reaction temperature (right) for layer 1 catalyst

Judging by the parity plots for layer 1 catalyst, the CO and CO_2 concentrations are represented very well (figure 51). The range of 15% is a good value [146,185,186] for parameter estimations of heterogeneous catalyzed processes with data acquired at non-isothermal conditions. Particularly at low and high concentrations the model fits the experimental values very well, even accuracies of up to 5% are achieved. At intermediate concentrations, which are measured in the hot spot region, the deviation is slightly larger.

The TA concentration runs basically parallel to the temperature profile. Consequently, the TA concentrations show a larger deviation (20%) between measured and modeled values (figure 52). The accuracy of PD representation is somewhat better (15%), although also PD is formed mainly in the hot spot region. In the PD parity plot, the previously discussed deviations at very low concentrations are apparent, where the model overestimates PD. While the model representation at the reactor outlet is very good, the concentrations at low conversions are estimated too high.

The accuracy of the description of PA concentrations ranges within 10%. At high conversions, this value is reduced to 5% (figure 53). This shows the excellent agreement between model and experiment. Also for MA concentrations, this can be observed. Over the entire range of MA concentrations the scattering of modeled values is minimal.

Comparing experimental and modeled temperature values, a larger scattering of points becomes visible (figure 54). In the hot spot area, where the largest deviations are visible, several different errors overlap. Due to the large axial gradient within the temperature profile, only the slightest deviation in hot spot position creates a large error between measured and modeled value. In the comparison of hot spot profiles, this does not necessarily have a large effect, but strongly influences the judgment of parity plots. The difference in magnitude of modeled and experimental hot spot profiles, which in most cases is inferior to 8 K, adds to the total modeling error. Nevertheless, most temperature measurements are represented

within ±15 K, which compared to literature kinetic models of o-xylene oxidation is an excellent improvement.

The parity plot of o-xylene conversion yields a picture similar to other concentration measurements. While around the hot spot region, the deviation between model and experiment reaches errors of up to 10%, in some cases slightly higher, high conversions at the reactor outlet are represented with excellent accuracy.

8.5 Layer 2 Kinetics – Model Discrimination

8.5.1 General

Layer 2 kinetic parameter estimations were started with the layer 1 kinetics. In layer 1 estimations it became clear that the pellet model is most suitably applied to describe this reaction properly.

In kinetic experiments with several layers, the catalyst filling was optimized in order to have a sampling point at the axial position where the next layer begins. At this point, the concentrations are measured at the outer perimeter of the reactor tube, while temperature is only measured in the center of the reactor. For parameter estimations there are two possible approaches. On the one hand, the simulated entry condition of layer 1 catalyst can be applied. On the other hand, the measured temperature and concentrations at the border between the two layers can be chosen as the entry condition. The former leads to an influence of the model error of layer 1 catalyst on the parameter estimations of layer 2 catalyst. The assumption of constant inlet temperature leads to a measurement error of the entry conditions for all experiments in parameter estimations for kinetics of layer 2 catalyst.

The two possibilities were evaluated and it was found that the measurement error is slightly less significant than the model error. The application of the measured entry condition also leads to less numerical effort and substantially shorter calculation times, since the first layer does not need to be solved. Kinetics of layer 2 catalyst is therefore evaluated taking the measurement error of the entry condition into account.

Another point of interest is the reactor model. For the estimation of layer 1 kinetics, reactor model parameters such as heat transfer coefficients or the tortuosity were fit to experimental data. This approach was also taken for layer 2 catalyst. However, both the factor of the radial heat conductivity and the tortuosity yielded values within the range of the results of layer 1 estimations. Consequently, the reactor model parameters are set to the values obtained in first layer estimations.

The introduction of an activity profile aids the description of hot spot profiles within layer 1 catalyst. The activity profile evaluated implies that for all catalyst fillings, the activity reaches unity at a reactor position within layer 1. Consequently, the activity profiling does not appear necessary for layer 2 catalyst.

In conclusion, the remaining factors to investigate for layer 2 catalyst kinetics are the kinetic model on the one hand and the necessary reaction scheme on the other hand. The model discrimination of these points will be described in detail in the following chapters.

8.5.2 Kinetic Model

The focus in investigations of the kinetic model is again the accurate description of measured data and reactor comportment with the simplest kinetic model possible, including the least necessary number of kinetic parameters. Since the concentrations in layer 2 are significantly different than particularly at the beginning of layer 1, all possible inhibiting factors are reintroduced to the kinetic model. As shown in eq. (8.5.1), the evaluated Eley-Rideal type rate expression, without dependency on the oxygen partial pressure is the starting point of this model discrimination.

$$r_j = \frac{k_j(T) \cdot p_i}{1 + K_{oX}(T) \cdot p_{oX} + K_{TA}(T) \cdot p_{TA} + K_{PD}(T) \cdot p_{PD} + K_{PA}(T) \cdot p_{PA}} \tag{8.5.1}$$

Parameter estimations with the shown rate equation lead to results, with numerous parameter insignificancies (model 1 in table 25). Although the number of parameters is significantly higher than the optimum case, the value of the achieved objective function remains significantly higher. Insignificant parameters are generally all inhibition parameters and several activation energies.

Table 25: Comparison of different parameter estimations for kinetics of layer 2 catalyst, model discrimination of the kinetic model with different inhibition terms and the influence of oxygen partial pressure

Model	rel. OF	N_P	N_{in}	N_c
1	2.13	22	12	3
2	2.24	17	4	2
3	1.49	16	2	2
4	1.32	14	1	3
5	1.00	14	1	2
6	0.98	15	2	21

The results of first layer 2 estimations show that there are generally too many inhibiting parameters. In order to identify which inhibition parameters are kinetically significant they

were gradually dropped. First PD and PA inhibition are omitted from the model again to reach a rate equation as shown in eq. (8.5.2).

$$r_j = \frac{k_j(T) \cdot p_i}{1 + K_{oX}(T) \cdot p_{oX} + K_{TA}(T) \cdot p_{TA}} \tag{8.5.2}$$

This measure results a slightly higher value of the objective function, but far less insignificant parameters (model 2 in table 25). Inhibiting parameters are then further reduced, first by dropping TA inhibition (model 3 in table 25), then by dropping also o-xylene inhibition (model 4 in table 25). While the first step already significantly improves the model representation, while also the number of parameters and number of insignificant parameters decreases, the second step means further improvement.

The resulting reaction rate equation for all reactions is then a simple first order power law rate equation (eq. (8.5.3)). Further optimization of model parameters, while keeping up the same reaction scheme leads to an even improved set of kinetic parameters (model 5 in table 25). Overall, the number of parameters is reduced to 14.

$$r_j = k_j(T) \cdot p_i \tag{8.5.3}$$

In measurements of differential reaction rates at conversions up to 10%, Vanhove and Blanchard [109] concluded that the consumption rate of o-xylene at concentrations inferior to 0.5% in air is directly proportional to the o-xylene concentration. In layer 2, the maximum o-xylene concentration reaches about that value. Also Calderbank et al. [41] states that the disappearance rate of o-xylene at low concentrations is directly proportional to its concentration. Consequently, the simple power law model for layer 2 seems applicable for the relevant concentration range.

Since at higher o-xylene conversions the oxygen concentration is substantially lower than at the reactor inlet, the influence of oxygen partial pressure was studied. The results of this parameter estimation are shown a model 6 in table 25. The objective function value improves minimally whereas the number of correlations rises unexpectedly. Nearly every kinetic parameter is correlated with the exponent of the oxygen partial pressure. Since the value for the exponent is estimated to the very low value of 0.05, the conclusion is that also for layer 2 catalyst, the oxygen concentration has no influence on the reaction kinetics. Consequently also the application of a Mars-van-Krevelen type rate expression is not favorable for layer 2 kinetics.

A general difficulty encountered in estimating layer 2 kinetics is the fact that with the initial parameter guess, far away from optimum values, the activation energies are estimated to values around 10 kJ/mol in case pre-exponential factors and activation energies are

estimated simultaneously. The objective function values thus obtained show that these minima are local minima. The gradual estimation of pre-exponential factors and activation energies, by fixing the other set of parameters, allows stepwise improvement of the parameter estimation and finally, once parameters close to the optimum are found, the estimation of all parameters simultaneously.

8.5.3 Reaction Scheme

Equivalent to the strategy chosen for the optimization of layer 1 kinetics, the reaction scheme was optimized also for layer 2 kinetics. The aim is to identify, which reaction paths are kinetically significant. The estimation of kinetic parameters as described in the previous chapter leaves the kinetic model with an insignificant parameter and two correlations. It turns out that these correlations are caused by the series and parallel reactions converting TA to PA (model 1 in table 26).

Table 26: Comparison of estimations with different reaction schemes for layer 2 catalyst kinetics

Model	rel. OF	N_P	N_{in}	N_c
1	1.03	14	2	3
2	1.00	12	0	0
3	1.30	14	2	2

Consequently, the direct PA formation path from TA (path 7 in figure 48) is omitted from the kinetic model (model 2 in table 26). The reduction of the number of parameters not only improves the objective function value, but also does not lead to any correlations between parameters.

The formation of CO and CO_2 was also studied and a total oxidation step from TA was added to the model. Not only is the rate constant of the TA total oxidation step two magnitudes smaller than the other total oxidation steps, but this specific step is again strongly correlated and both parameters of this reaction are kinetically insignificant (model 3 in table 26). This step was then dropped again from the reaction scheme.

The question of MA formation is posed again. Generally, the paths from o-xylene directly, from TA and from PA are chemically sensible. Since the direct formation of MA from o-xylene is kinetically insignificant already in layer 1 this path is also insignificant for layer 2 kinetics. The remaining paths to be discriminated are the formation of MA from PA and from TA (paths 6 and 11 in figure 44). The addition of path 11 to the model allows the optimizer to find a local minimum, where the objective function value is significantly higher than the

optimum case. In addition, MA formation from PA is kinetically insignificant and model parameters of this reaction path are strongly correlated with MA formation from TA.

In the end of the optimization, it has shown that CO concentrations are systematically underestimated by the layer 2 kinetic model, while CO_2 concentrations are systematically overestimated. This leads to the conclusion that the fixed relation of CO and CO_2 selectivities applied equally for all total oxidation reactions, may not appear applicable for layer 2 catalyst. Consequently the stochiometric coefficients of CO in both total oxidation steps were estimated along with the kinetic parameters.

Table 27: Stochiometric coefficients evaluated for layer 2 catalyst; reaction paths are according to figure 55

Reaction Nr.	oX	TA	PD	PA	MA	O_2	CO	CO_2	H_2O
1	-1	1	0	0	0	-1	0	0	1
3	-1	0	0	0	0	-7.2	3.6	4.4	5
4	0	-1	1	0	0	-1	0	0	1
5	0	0	-1	1	0	-1	0	0	1
6	0	-1	0	0	1	-6	1	3	3
10	0	0	0	-1	0	-6.6	1.8	6.2	2

Apparently, in the total oxidation of PA more CO_2 is formed than in the total oxidation of o-xylene. A similar effect was reported by Brandstädter [187] in a kinetic study of butane oxidation to maleic anhydride, where the oxidation of the anhydride results in higher formation of CO_2 than the oxidation of the reactant.

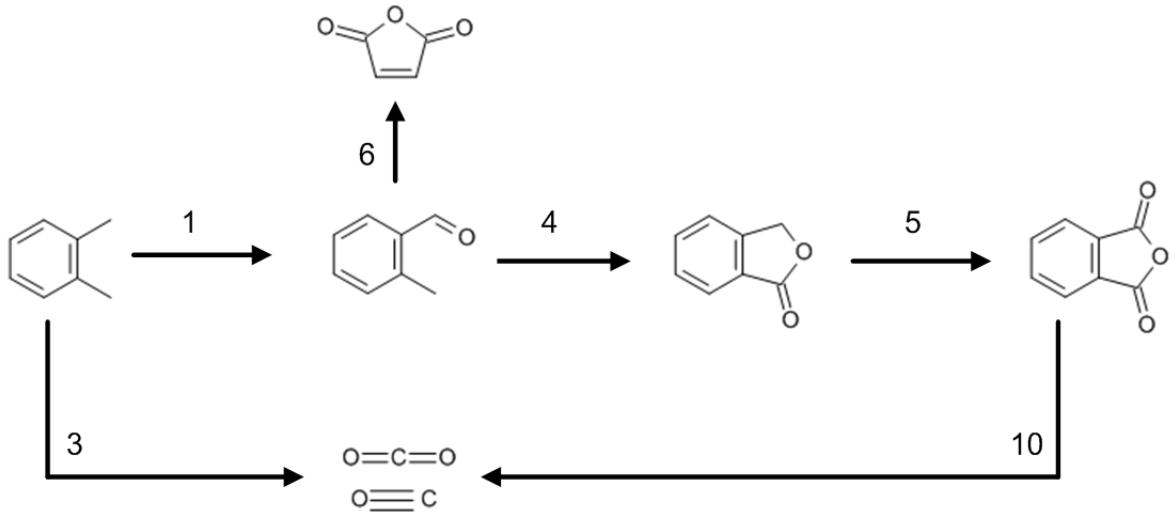

Figure 55: Final reaction scheme necessary to describe layer 2 kinetics

The optimized reaction scheme, containing all kinetically significant reaction steps for o-xylene oxidation on layer 2 catalyst is depicted in figure 55. Compared to the reaction scheme of layer 1 catalyst, this scheme involves one reaction step less, which is the direct PA formation from TA.

8.5.4 Final Kinetic Model Layer 2

The parameters of the final kinetic model for layer 2 catalyst are presented in table 28. Simple power law rate equations, which have pre-exponential factors and activation energies, are sufficient to describe the measured data. With the six necessary reaction paths, this adds up to a total of 12 kinetic parameters, 5 less than the layer 1 kinetic model. Comparing layer 2 kinetics to layer 1 kinetics, an unambiguous picture in terms of activity cannot be drawn. At low temperatures, the activity of layer 2 is relatively high compared to layer 1. While the activity of the selective oxidation step of o-xylene reaches up to three times layer 1 activity, the activity of the total oxidation reaches about four times the range of layer 1 catalyst. However, at higher temperatures, this effect does not persist. On the contrary, the far lower activation energies found for layer 2 catalyst, particularly for the selective reaction step from o-xylene, lead to the observation that the activity of layer 2 catalyst as defined in chap. 8.3 is actually smaller than the activity of layer 1 catalyst.

Table 28: Parameters of the layer 2 kinetic model with the error for a confidence interval of 95%; reaction paths according to figure 55

Path Nr.	$k_{0,j}$ / k_{ref}	$E_{A,j}$ (kJ mol^{-1})
1	149 ± 9	60 ± 14
3	23.3 ± 1.4	75 ± 16
4	512 ± 12	45 ± 8
5	454 ± 9	48 ± 7
6	38 ± 1	54 ± 12
10	0.70 ± 0.05	65 ± 20

When comparing both reaction kinetics, the intermediate reaction steps have the tendency to occur more quickly than in layer 1. Interestingly, as the only reaction, the total oxidation of PA decreases in activity over the complete range of operating conditions.

In experiments with layer 2 catalyst, full conversion is reached also at low reaction temperatures close to the SBT, which is not the case for layer 1 catalyst. This effect is reflected in the kinetic model by the higher activity at lower temperatures on the one hand, but mainly also by the far lower activation energies.

Since the range of measured reaction temperatures is smaller for layer 2 catalyst than for layer 1 catalyst, a result of the nature of the reaction, the activation energies have a larger error range. Opposite to layer 1 kinetics, in layer 2 kinetics the activation energy of the selective oxidation step is not larger than the activation energy of the selective oxidation.

All in all, it appears that layer 2 catalyst is less selective for o-xylene oxidation. However intermediates are more selectively converted to PA. Finally, the PA total oxidation appears less favored on layer 2 catalyst.

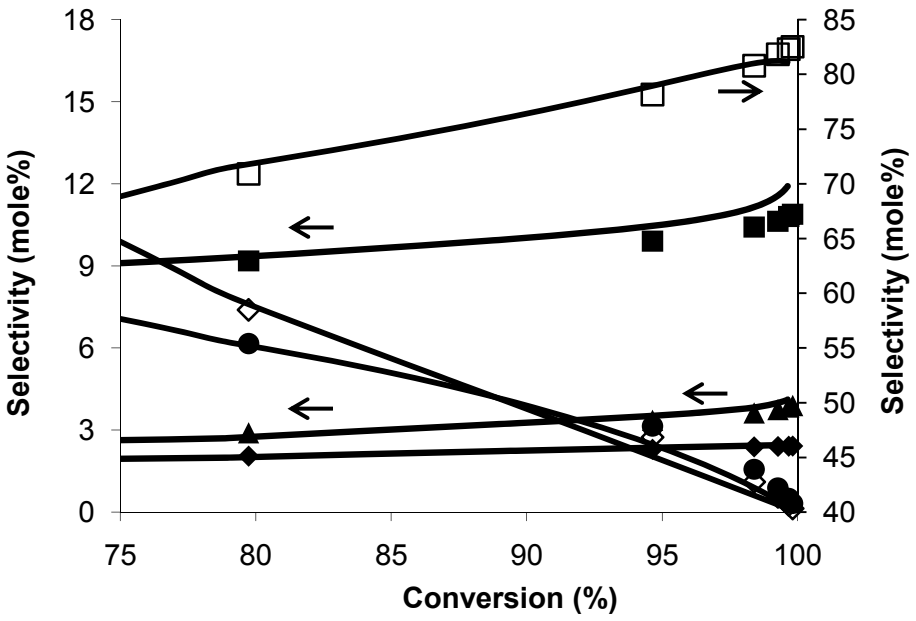

Figure 56: Comparison of measured and simulated selectivity profiles for layer 2 catalyst; complete lines are simulated runs while dots are measured values; TA (◊), MA (♦), CO_2 (■), PA (□), PD (●) and CO (▲)

Measured selectivity values are compared to simulated values in figure 56. Generally, the runs of the selectivity profiles are represented very well. The rise of PA selectivity decreases slightly at the transition from layer 1 to layer 2. At very high conversions (above 99%) the PA selectivity is systematically underestimated, while CO and CO_2 selectivities are overestimated. At the reactor outlet, where such high conversions are achieved, the reaction temperature is also underestimated by 3 - 4 K (figure 57). The estimator chooses to increase PA total oxidation in order to obtain an improved fit of the temperatures. However, the reaction temperatures are described very well, particularly in the hot spot region. Therefore, the small deviation in selectivity profiles is acceptable.

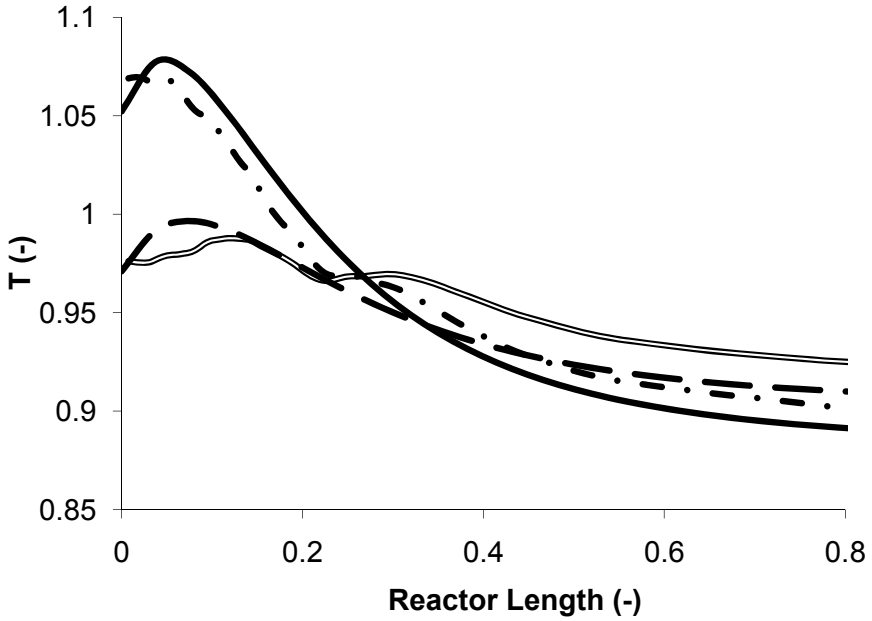

Figure 57: Comparison of measured and estimated temperature profiles at different operating conditions, where the entry conditions to layer 2 are the measured temperature and concentration values; T_1 measured (– · –), T_1 simulated (—), T_2 measured (=), T_1 simulated (- -) where $T_1 < T_2$

Considering the intermediates TA and PD, the strong decrease in selectivity is represented very well. Even the selectivities close to zero at full conversion can be modeled with very good accuracy. Equivalent to the layer 1 estimations, the MA selectivity profile is represented with excellent accuracy over the entire conversion range. In terms of conversion, full conversion which is measured in experiments cannot be represented completely by the model. However, conversions of up to 99.8% are simulated. Considering that o-xylene concentration goes through several orders of magnitude, the representation of conversion can also be considered sufficient.

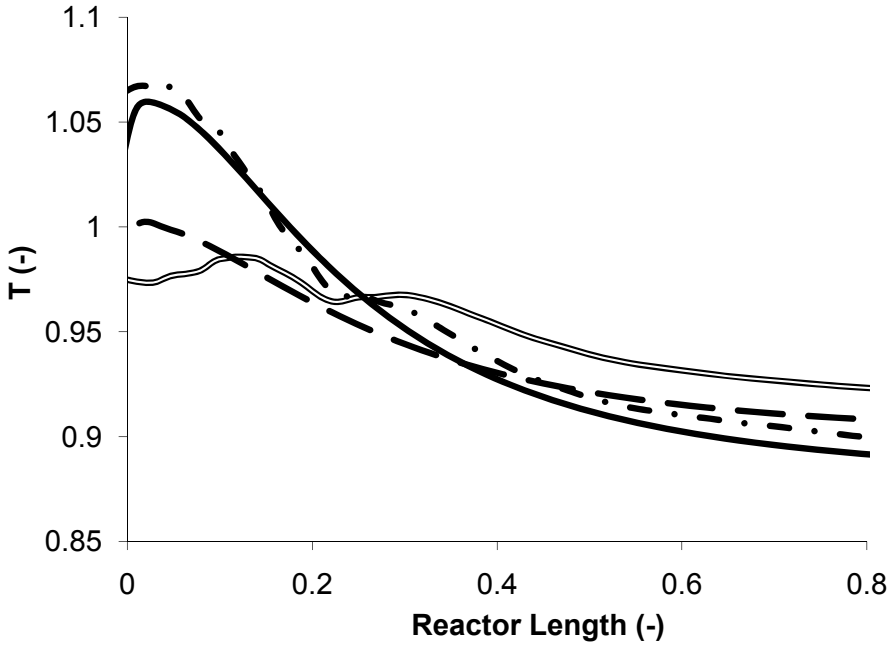

Figure 58: Comparison of measured and modeled temperature profiles at different operating conditions where both layer 1 and layer 2 are modeled; T_1 measured (– · –), T_1 simulated (—), T_2 measured (=), T_1 simulated (- -) where $T_1 < T_2$

Comparing the measured and modeled temperature profiles where both layers 1 and 2 are simulated, very good accordance can be seen (figure 58). Particularly at low SBTs, which yield the largest deviation between measured and simulated temperature profiles for layer 1, the representation of layers 1 and 2 together significantly improve the picture. Both magnitude and position of the hot spots in layers 1 or 2 are represented with very good accuracy.

The parity plots of CO and CO_2 show the very good representation of the measured values by the fitted kinetic model (figure 59). An accuracy of ±10% in general is very good for heterogeneous systems. Compared to layer 1 estimations this accuracy has also improved. A trend of errors in either measurement cannot be detected.

The intermediates TA and PD are very well represented at high concentrations, far better than the 20% deviation indicated (figure 60). However, at low concentrations, the deviations are around this value. Since it is generally difficult to properly represent data with large measurement error, which is the case for concentration measurements close to zero, the accuracy of description of both of these compounds can be considered exceptionally good.

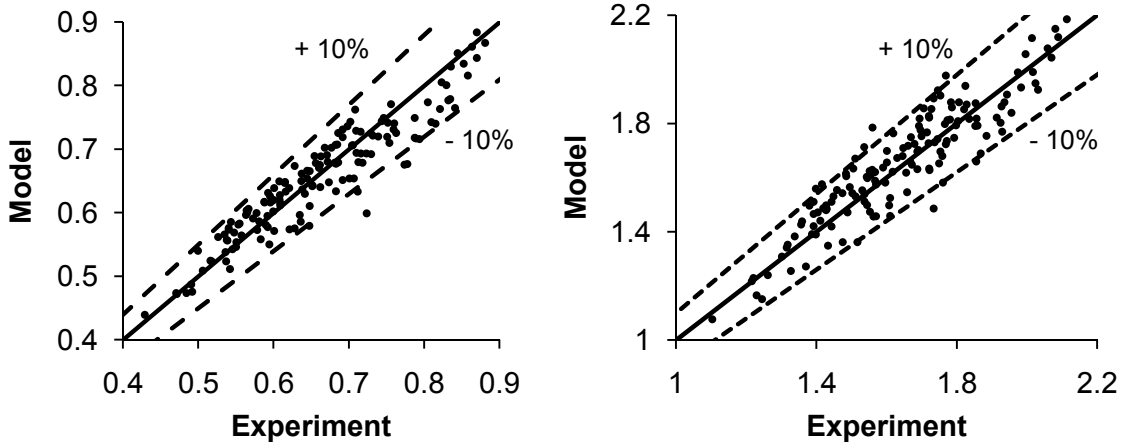

Figure 59: Parity plots of CO (left) and CO_2 (right) for layer 2 catalyst; compared are measured gas phase concentrations of CO and CO_2

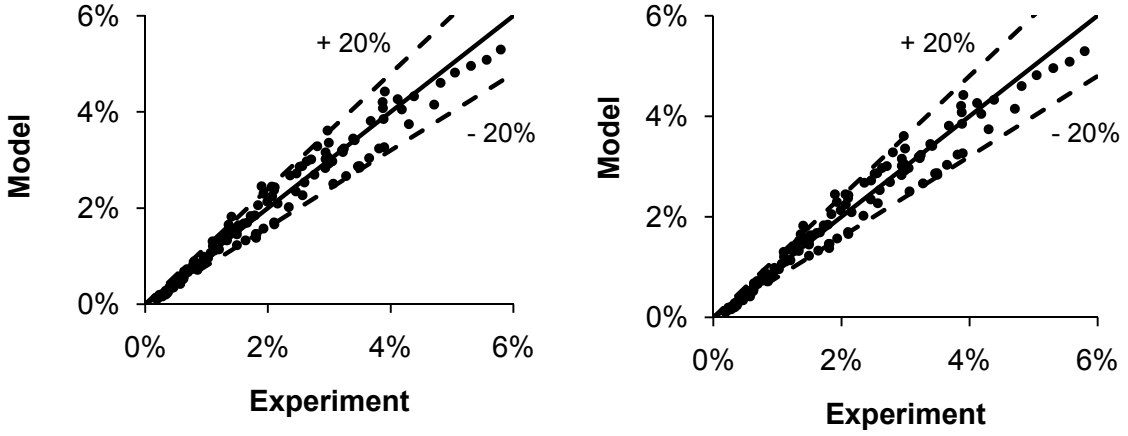

Figure 60: Parity plots of TA (left) and PD (right) for layer 2 catalyst; compared are the raw measured data in terms of composition of the organic compounds as entered to the parameter estimation

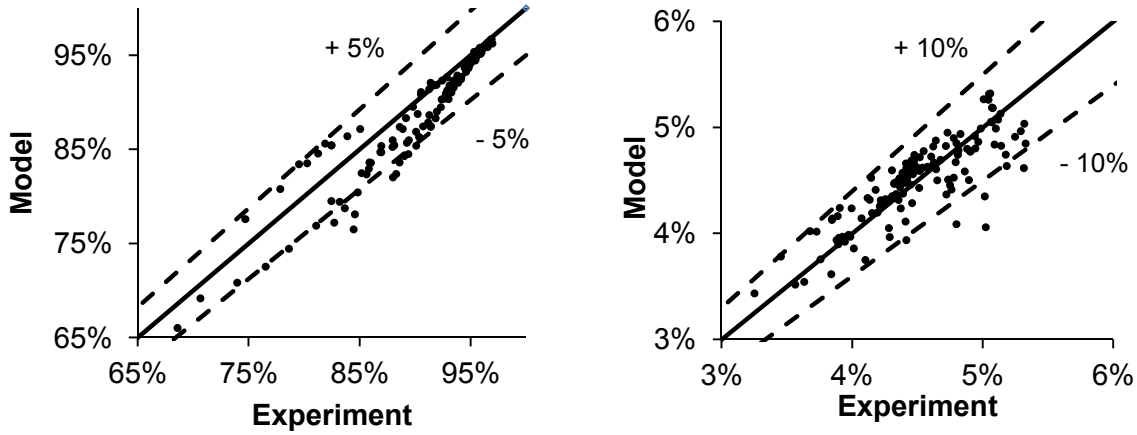

Figure 61: Parity plots of PA (left) and MA (right) of layer 2 catalyst

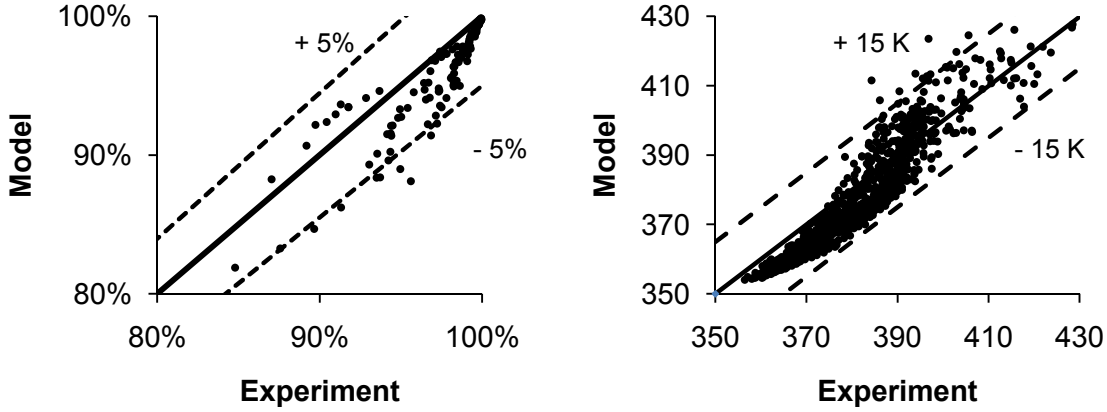

Figure 62: Parity plots comparing experimental and modeled values for o-xylene conversion (left) and reaction temperature (right) for layer 2 catalyst

In terms of PA concentration, ±5% accordance is achieved between measurement and model. At high conversions the accuracy is even ±2% (figure 61). For MA, the selectivity profiles appear more promising than the parity plots. However ±10% is again very good accuracy for a heterogeneous catalytic process.

Just as PA concentrations, the o-xylene conversion is also modeled with very good accuracy (figure 62). Around the hot spot region, the deviation is slightly larger than at nearly full conversion. Nevertheless, the model representation can be considered exceptionally good.

Parallel to the layer 1 estimations, the temperatures, particularly around the hot spot region are represented rather poorly, when considering only the parity plot (figure 62). The picture is substantially better when the actual comparison of measured and simulated temperature profiles is evaluated. However, again the multiple errors overlapping make it particularly difficult to simulate temperature profiles more precisely. Overall, the kinetic fit of layer 2 catalyst can be considered very good.

8.6 Layer 3 Kinetics – Model Discrimination

8.6.1 General

The strategies developed during layer 1 and layer 2 kinetic parameter estimation were followed also for layer 3 kinetics. Equivalent to layer 2, the reactor model was kept constant in order to maintain consistency and comparability between the layers. First layer 3 parameter estimations are initialized with the layer 2 kinetic model.

For layer 3 kinetics, the same question arises as for layer 2 considering which entry condition to apply. Simulated entry conditions, or layer 2 exit conditions contain a considerable model error while a measurement error in the entry condition persists, when considering uniform temperature over the complete pipe radius instead of a radial temperature profile. Since the measurement error proved less significant already for layer 2, also for layer 3 the policy chosen is to apply the measured entry condition with equal temperature for all radial positions, which in the experiment is actually only measured in the reactor center.

In the measured range of operating conditions, which is particularly wider than the industrial range of operating conditions, a hot spot is not encountered in layer 3. A general problem in layer 3 kinetics is to properly describe the temperature profiles. In the experimental profiles, the axial gradient in temperature is not particularly pronounced, the temperature slightly decreases from about 20 – 30 K above coolant temperature to about 8 K above the coolant temperature, where it only decreases very slowly. The main drop at the entrance to layer 3 is simulated decently, while close to the reactor outlet, the simulated temperature drops to 1 – 2 K above coolant temperature. This systematic error could not be finally eliminated and the description within a range of 5 – 10 K is far better than any literature model.

As described, the temperature variation in layer 3 is rather small. However, the concentrations, particularly of TA, PD and o-xylene do change significantly. The function of layer 3 catalyst is to remove these traces. Consequently, the aim of the kinetic model is also to describe these concentrations with good accuracy. Therefore, for the final parameter estimations of layer 3 catalyst, the measured temperature profiles were omitted from the experiments accounted for.

8.6.2 Kinetic Model

First parameter estimations with the simple power law rate equations already yield reasonable results. Therefore, the investigation of the kinetic model for layer 3 involves fewer steps than for layers 1 and 2. One point looked into is the existence of any inhibitions of organic compounds. TA, PD and o-xylene concentrations decrease considerably and reach values close to zero. Since these compounds do not have an inhibiting effect in layer 2

kinetics and concentrations in layer 3 are even lower, an inhibition of these compounds is ruled out.

Compounds with relatively high concentrations are PA, MA, CO and CO_2. Following literature suggestions [24,58,106,110], CO and CO_2 are not considered to have inhibiting effects since their desorption rate is assumed very fast. In layer 3, the PA concentration first rises strongly and then remains constant, while the MA concentration rises continuously. Consequently, these two compounds are taken into account when investigating possible inhibitions.

In addition, the oxygen concentration is again lower than in layer 2 and its influence on the reaction kinetics was studied as well. The results are shown in table 29.

Table 29: Estimation results for different kinetic rate equations for layer 3 catalyst

Model	rel. OF	N_P	N_{in}	N_c
1	0.95	14	3	8
2	0.98	14	3	2
3	1.00	12	1	0
4	0.99	13	6	10

The introduction of temperature dependent PA inhibition does not significantly improve the model description (model 1 in table 29). While the temperature dependency reaches a final value of zero, which makes this parameter kinetically insignificant, the pre-exponential factor reaches a significant value. However, this parameter is correlated with every other pre-exponential factor. In addition, it leads to strong correlations of other parameters as well. It is therefore dropped again from the formulation of the rate equation.

The introduction of MA inhibition yields a similar picture as for the PA inhibition (model 2 in table 29). The objective function improves minimally, while the number of insignificant parameters and parameter correlations increases. In both cases, two additional inhibiting parameters are not justified by the small improvement of description accuracy.

The introduction of oxygen partial pressure adds an additional parameter, its exponent. In the corresponding estimation, this parameter is correlated with numerous other model parameters. Due to these correlations, all pre-exponential factors are statistically insignificant. The objective function, in this estimation hardly improves. Consequently, the reaction rates can be considered independent of oxygen.

$$r_j = k_j(T) \cdot p_i \tag{8.6.1}$$

The final rate equation for layer 3 catalyst kinetics is a simple power law rate equation with direct proportionality to the concentration of organic compounds (eq. 8.5.1). Throughout the evaluation of the layer 3 kinetic model, a similar effect was observed for the activation energies as in layer 2 estimations. When estimating activation energies and pre-exponential factors simultaneously, the resulting values of activation energies are very small. The approach of estimating pre-exponential factors and activation energies separately also here leads to an improved set of initial parameter values, from which significant values for both activation energies and pre-exponential factors can be obtained.

8.6.3 Reaction Scheme

Just like the other catalyst layers, the evaluation of kinetically significant reaction paths is another aim of kinetic model discrimination. This particularly involves also the determination of the main by-product formation paths. In specific, the sources of MA, CO and CO_2 in layer 3 are studied. Additionally, kinetically significant PA formation paths are evaluated.

Table 30: Model discrimination of the reaction scheme for layer 3 catalyst

Model	rel. OF	N_P	N_{in}	N_c
1	1.00	12	1	0
2	1.02	10	0	0
3	0.99	12	2	0
4	1.00	10	0	0
5	1.33	12	1	3

The application of the layer 2 reaction scheme, which includes two total oxidation steps results in the insignificancy of the pre-exponential factor of the non-selective oxidation of o-xylene (model 1 in table 30). Dropping this reaction step from the kinetic scheme, reduces the number of parameters and only minimally raises the objective function value (model 2 in Table 30).

The formation of MA in layer 3 can be either from PA or from TA. In layer 1 and layer 2 kinetic models, MA formation is described by TA oxidation. Including also the formation path from PA, the model description improves slightly, while the TA oxidation step becomes insignificant (model 3 in table 30). Omitting TA oxidation to MA, the model description remains equally accurate, but the number of parameter is again reduced (model 4 in table 30).

The addition of the direct PA formation from TA raises the number of parameters and correlations. Instead of an improvement in terms of objective function, this measure actually

leads to a significant increase, or significantly inferior description of measured values. Consequently, this path is unnecessary for the proper description of the reaction within layer 3.

Table 31: Stochiometric coefficients evaluated for layer 3 catalyst; reaction paths are according to figure 63

Reaction Nr.	oX	TA	PD	PA	MA	O_2	CO	CO_2	H_2O
1	-1	1	0	0	0	-1	0	0	1
4	0	-1	1	0	0	-1	0	0	1
5	0	0	-1	1	0	-1	0	0	1
10	0	0	0	-1	0	-5.2	2.7	5.3	2
11	0	0	0	-1	1	-4	1	3	1

In order to properly describe the CO and CO_2 selectivities, the stochiometric coefficients of the total oxidation step were estimated, following the example of the layer 2 estimation strategy. In fact, a significant improvement was obtained.

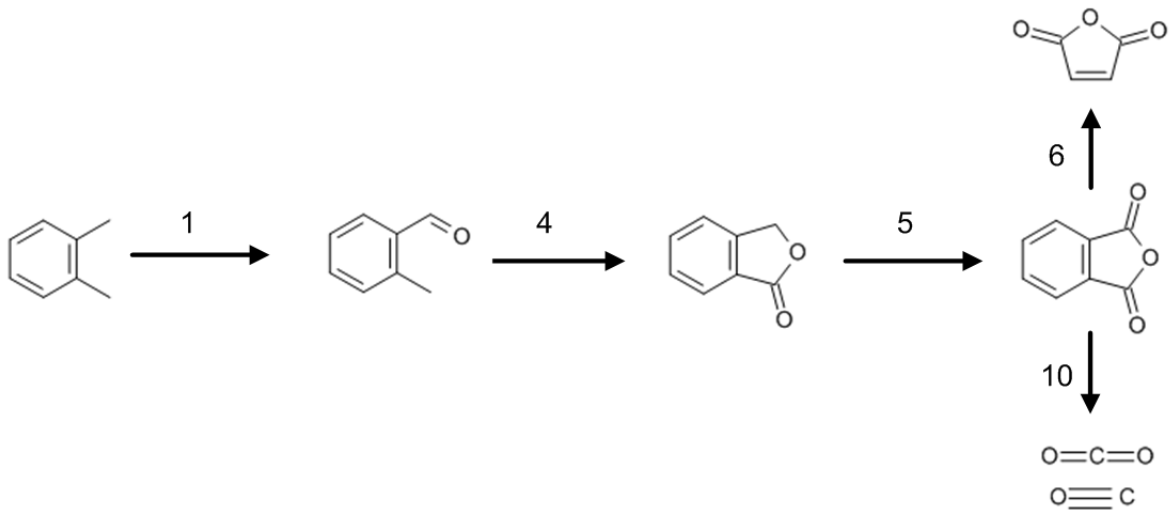

Figure 63: Final reaction scheme for layer 3 catalyst

The reaction scheme of layer 3 catalyst can be reduced to a total of five reactions. PA is formed only by the consecutive reaction via TA and PD. However, another path of PA consumption needs to be added.

8.6.4 Final Kinetic Model Layer 3

The final parameter values for layer 3 kinetics are shown in table 32. As for the layer 2 catalyst, a simple power law kinetic model is sufficient to describe layer 3 catalyst. With five reaction steps shown in figure 63, the total number of kinetic parameters is ten. Comparing the obtained parameter values to layer 2 kinetics, the activity rises by about 50% for the selective oxidation of o-xylene to TA. Although the parameter initialization for paths 4 and 5 were varied considerably, the pre-exponential factors as well as the activation energies change only minimally. However, the total oxidation of PA is considerably higher. Since the sources are different, the MA formation cannot be compared directly.

Table 32: Parameters of the layer 3 kinetic model with the error for a confidence interval of 95%; reaction paths according to figure 63

Path Nr.	$k_{0,j}$ / k_{ref}	$E_{A,j}$ (kJ mol^{-1})
1	228 ± 56	61 ± 30
4	488 ± 42	45 ± 11
5	437 ± 28	47 ± 8
10	1.2 ± 0.2	59 ± 22
11	4.4 ± 0.7	61 ± 26

The activation energies do not change much between the two models. Nevertheless, for layer 3, the error of activation energies is substantially higher than for layer 2 kinetics. This can be explained by the fact that the measured and simulated temperature range is smaller for layer 3 than for layer 2 kinetics. Possibly, the number of data points applied in parameter estimations for layer 3 catalyst is not sufficient to find a better description of the temperature dependency of this reaction at this point. The amount of data acquired for layer 3 catalyst corresponds to the largest possible range which can be obtained in the pilot reactor. Also in the industrial process, layer 3 catalyst will not be exposed to other conditions than those measured and applied for parameter estimations.

The comparison of temperature profiles measured and simulated with layer 3 kinetics is depicted in figure 64. The aforementioned deviation between temperatures becomes apparent in this plot. The kinetic model systematically underestimates the reaction temperatures.

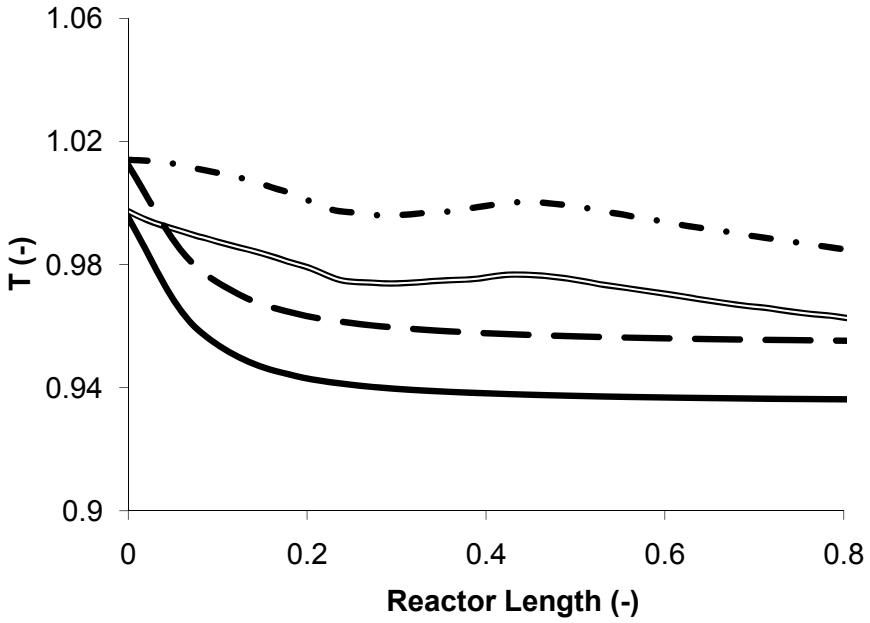

Figure 64: Comparison of measured and simulated temperature profiles for different operating conditions for layer 3 taking the measured data as entry condition; T_1 measured (– · –), T_1 simulated (- -), T_2 simulated (—), T_2 measured (=), where $T_1 > T_2$

In order to evaluate the reason for this deviation, also the heat transfer parameters were varied in a wide range. In layer 1 kinetic parameter estimations, it was found that the radial heat conductivity obtained from literature correlations needs to be multiplied with a factor of 1.8. This measure was revised for layer 3. It turns out the heat conductivity from literature correlations would have to be decreased in 90% in order to properly fit the measured temperature data. It is assumed that this deviation is caused by accumulating measurement errors and shortcomings caused by simplifications in the reactor model. However, since the aim of this kinetic model is to describe the reactor comportment. This includes the hot spot formation in layers 1 and 2 as well as selectivities over the complete reactor length.

Judging by the temperature profiles shown in figure 65, which compare temperature profiles over the complete reactor length, acquired in a three layer system to simulated temperature profiles. The general reactor comportment is represented with very good accuracy. Only the temperatures towards the reactor outlet are underestimated.

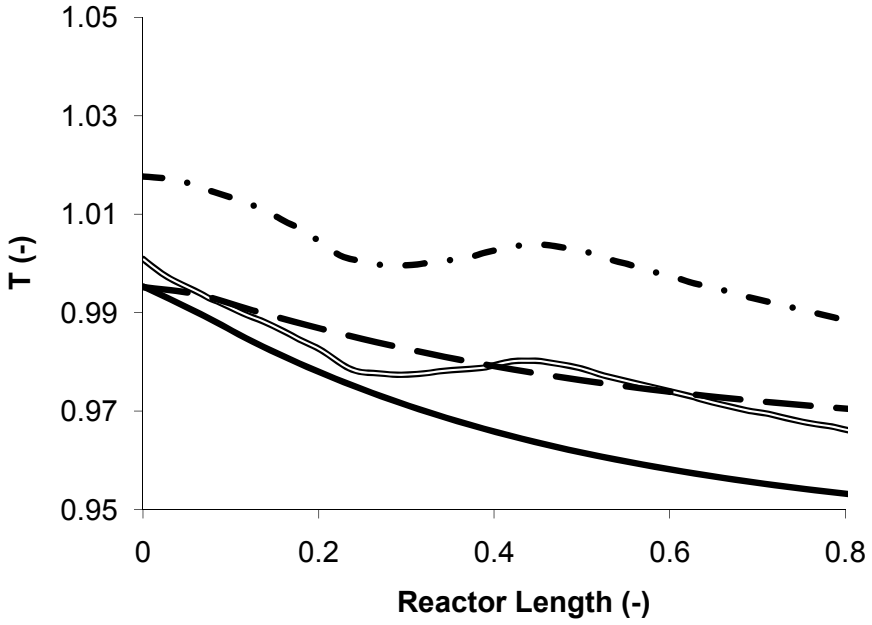

Figure 65: Comparison of measured and simulated temperature profiles for different operating conditions for a complete reactor with layers 1, 2 and 3; T_1 measured (– · –), T_1 simulated (- -), T_2 simulated (—), T_2 measured (=), where $T_1 > T_2$

While the kinetic model of layer 3 shows some weaknesses in the description of reaction temperatures, the representation of selectivity profiles is very good for all components. Considering PA selectivity, the run of the selectivity profile, which is measured at long contact times with layer 3 catalyst, is represented very well by the kinetic model.

The drop of TA and PD selectivities to values of nearly zero selectivity is also reflected in the kinetic model. Considering the o-xylene conversion, the conversion level can be represented very well until conversions of about 99.7%. Above this conversion level, o-xylene conversion is underestimated. As in the layer 2 kinetics, this deviation is caused by the fact that o-xylene goes through several order of magnitude over the reactor length. The kinetic model can describe this very well for two orders of magnitude. Reaching higher accuracies is difficult due to numeric reasons.

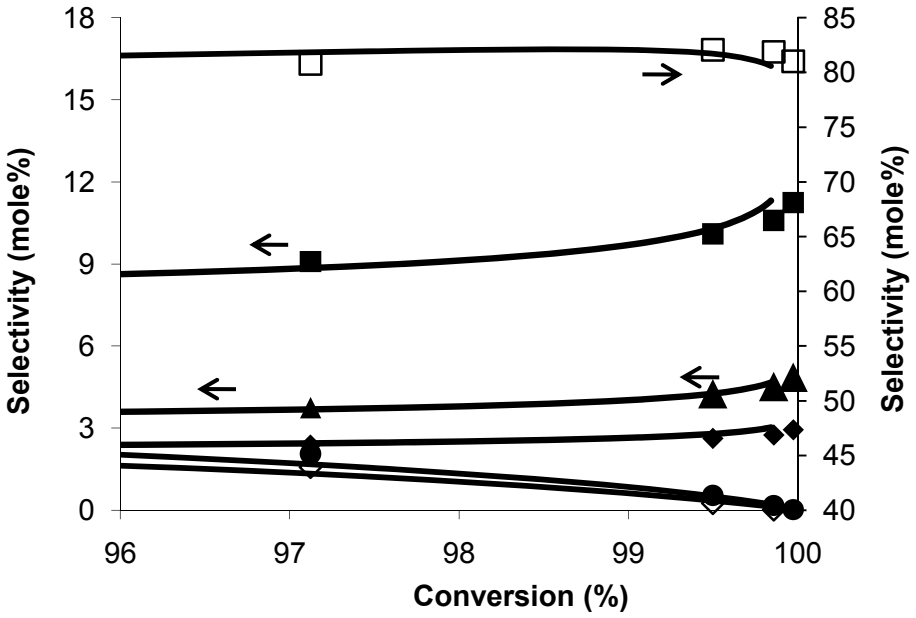

Figure 66: Comparison of measured and simulated selectivity profiles for layer 3 catalyst; complete lines are simulated runs while dots are measured values; TA (◊), MA (♦), CO_2 (■), PA (□), PD (●) and CO (▲)

The very good representation of concentrations CO and CO_2 is shown in figure 67. The simulated values compared to experiments lay within a range of ±5%. Throughout the entire concentration range measured in layer 3, the scattering of simulated data points around the optimal, measured value is random. A clear tendency cannot be derived. Also the broad range of measured concentrations can be seen in these diagrams. At steady state operation of and industrial reactor, this concentration range of different components is far smaller than in the data applied for this kinetic study.

The parity plots of the intermediates TA and PD also show very good representation by the kinetic model (figure 68). For both components, the error span ranges around a maximum of ±10%, which again is excellent for heterogeneous processes. Only the PD concentrations show a slight variation from this range at low concentrations. At these concentration levels, the measurement accuracy of the GC measurement is also less precise.

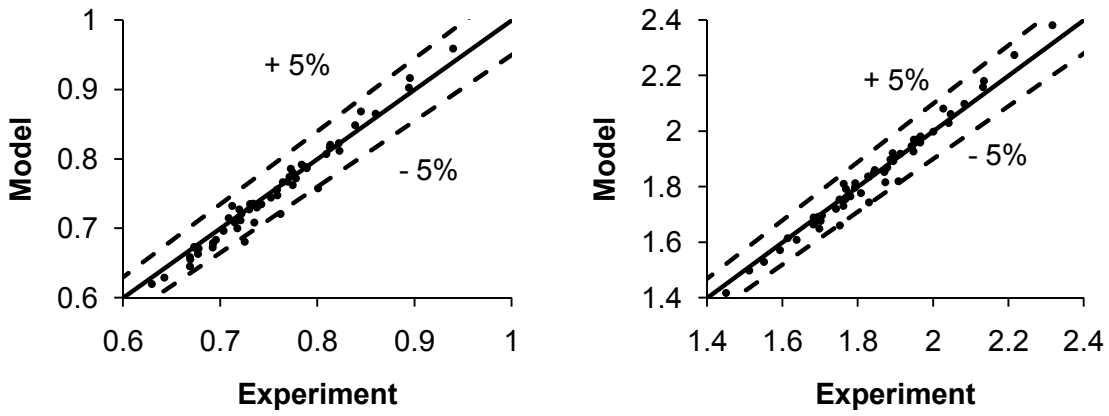

Figure 67: Parity plots of CO (left) and CO_2 (right) for layer 3 catalyst; compared are measured gas phase concentrations of CO and CO_2

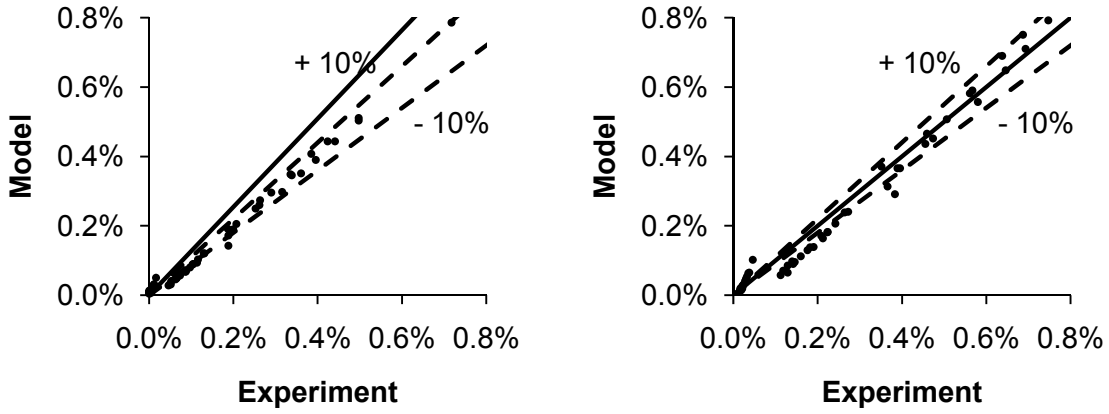

Figure 68: Parity plots of TA (left) and PD (right) for layer 3 catalyst; compared are the raw measured data in terms of composition of the organic compounds as entered to the parameter estimation

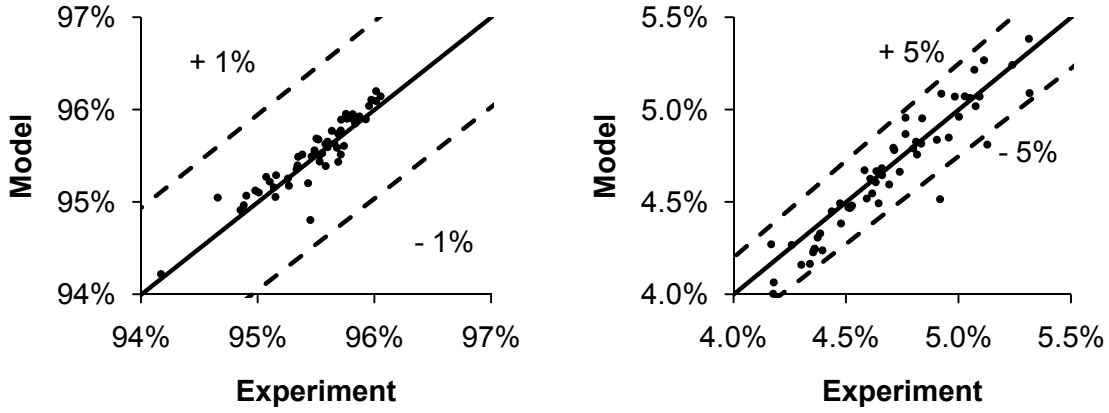

Figure 69: Parity plots of PA (left) and MA (right) of layer 3 catalyst

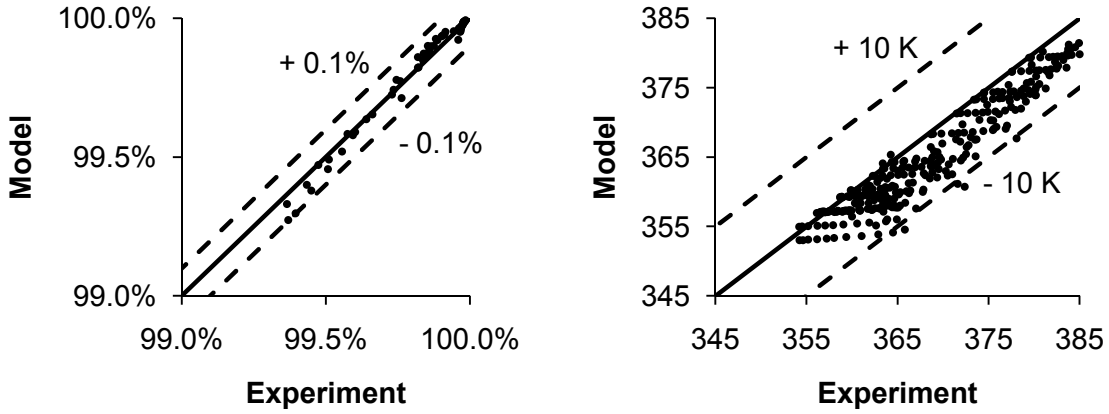

Figure 70: Parity plots comparing experimental and modeled values for o-xylene conversion (left) and reaction temperature (right) for layer 3 catalyst

Particularly PA concentrations are estimated with extremely good accuracy. ±1% represents excellent accuracy for such a heterogeneous process (figure 69). Also the deviation of MA concentrations lies only within very tight borders over a relatively broad range of concentrations.

The discussed underestimation of reaction temperatures becomes apparent also in the parity plot (figure 70) for this value. At higher temperatures, the inlet of layer 3, the deviation is slightly smaller, while at lower temperatures the range reaches up to ± 10K deviation from the measured value. The o-xylene conversion on the other hand is again represented with very good accuracy.

Overall, the representation of experimental data is very good also for layer 3 kinetics. Particularly the concentration measurements at the reactor outlet are represented with excellent accuracy by the kinetic model.

9. Summary and Outlook

This research study was conducted in order to identify potentials in optimizing the performance of industrial catalysts applied in o-xylene oxidation to phthalic anhydride. Particular interest in this respect lays on the improvement of product yields and purities as well as overall performance of industrial reactors.

The reaction scheme of o-xylene oxidation was investigated in this effort in order to identify by which way and through which intermediates significant losses in product selectivity take place. For the first time, a reaction scheme could be presented, which includes numerous experimentally confirmed reaction paths leading to non-selective intermediates and by-products such as MA, CA, BAc, CO and CO_2. Particularly toluene proved to be a key intermediate in the formation paths of many by-products.

Furthermore, in this work, a detailed kinetic model was developed for the first time accounting for each of the different catalysts of a state of the art industrial multilayer catalytic system applied in this process. This task was achieved in application of rigorous mathematical modeling. In the development of this kinetic model, the applied reaction schemes and kinetic formulations for each catalytic layer were systematically reduced to obtain the simplest possible lumped reaction scheme describing the reaction with the lowest possible number of kinetic parameters.

During the development of reaction kinetics, particularly the description of temperature profiles proved a difficult task. It was found that during the start-up procedure of this catalyst, an activity profile develops, dependent only on the axial position. Only with the introduction of an empirical activity profile it was possible to describe the reaction for various cooling temperatures.

In addition, it was aimed to apply the knowledge gained in the investigation of the reaction scheme to the development of the kinetic model. In this effort, it was shown that this reaction is transport limited in terms of selectivity, although the catalyst applied is an eggshell catalyst. Consequently, this needs to be reflected also in the reactor model. In all kinetic models published in literature describing the oxidation of o-xylene to phthalic anhydride, a direct PA formation path is included. In the investigation of the reaction scheme, it was clearly found that such a single step oxidation does not take place on the catalyst surface. By including diffusion within the catalyst pellet in the reactor model, this effect could be considered for the first time in a kinetic model of this reaction.

The development of the reaction scheme has shown that possibly two types of oxidation mechanisms take place on the vanadia catalyst. This includes the nucleophilic oxidative attack of the methyl group and the electrophilic attack of the aromatic ring, the latter leading to the loss in selectivity in this process. Catalyst structures or compositions favoring one or another possible oxidation mechanism could not be clearly identified in this work. Further investigations in this respect would lead to a better understanding of the catalyst and could allow increasing catalyst optimization possibilities.

The different catalyst layers, for which reaction kinetics was developed for have different chemical compositions. It was shown that the differences in selectivity and activity due to modified compositions reflect also in kinetic parameters. However, in this work, separate sets of kinetic parameters were evaluated for the different catalysts. The introduction of the influence of catalyst composition on reactor comportment and product selectivity to the kinetic model is another interesting perspective.

The reactor model applied is based on numerous assumptions considering the heat and mass transfer description. Numerous correlations are documented in literature for each of these transport parameters. It was shown in this work for heat transfer parameters of the catalytic bed that the available correlations may not describe the physical system with sufficient accuracy. Particularly the influence of chemical reactions on the heat transfer comportment of a catalytic bed remains an open question. Consequently, this may also be applicable to predictions for mass transfer parameters.

The developed kinetic model describes this process in an unprecedented manner. However, certain limitations still persist. For instance the description accuracy is not equal for all operating conditions within the described range. Particularly at high conversions certain deviations in terms of concentrations and temperatures are found. Due to relatively small temperature and concentration gradients at these concentrations, the pilot reactor set-up shows its limitations at this point. More detailed investigations of reaction kinetics at high conversions could allow an improved description of the overall process.

The kinetic model presented in this work represents a comparatively detailed reaction scheme. However, this model is an effective kinetic model, which takes into account several lumped reaction steps. In the investigation of the reaction scheme it was shown that numerous intermediate reaction steps take place in the course of this reaction. Further detail in the kinetic reaction scheme including possibly also microkinetic steps offers further perspectives for an improved understanding of the process.

The separation of reaction steps leading to CO and to CO_2 could also not be achieved. For all catalysts, total oxidation reactions were considered to give both CO and CO_2. The relations of stochiometric coefficients of these two components are optimized for each significant reaction but are fixed over the complete temperature and concentration range. The separate consideration of these steps could also lead to a more precise description of the reactor comportment and allow additional conclusions on the catalytic system.

The unprecedented description accuracy of this kinetic model further opens the possibility of optimization of catalyst and reactor operating conditions.

Annex

A1. Experimental Methods

A1.1 Procedures

All experimental procedures were conducted according to the standards documented in the Süd-Chemie integrated management system [188]. In particular this includes the procedures for filling and operation of the pilot reactor, sampling methods and calibration of measuring equipment.

The following system components are calibrated regularly:

- flow measurement of o-xylene an air (every three months or prior to every longterm test),
- concentration measurement with the IR spectrometer (monthly),
- concentration measurement with the GC (every six months),
- temperature measurement for all process temperatures apart from the reaction temperature (annually),
- measurement of reaction temperature (three months or prior to every longterm test) and
- pressure (annually).

Online sampling is conducted as described in the experimental procedure. Offline sampling of organic compounds is conducted according to the Süd-Chemie standard procedure [188] applied also in industrial plants.

A1.2 GC Analysis

The analysis station for online measurement is controlled the MPControl Software supplied by Celpat Ingenieurgesellschaft mbH. Concentration measurement of organic compounds is conducted on a standard GC (HP 6820) in application of the Chemstation software (Version A 10.4). The Method for GC Analysis is shown in table 33

Table 33: GC Method

Column	ZB-5	Zebron
Material	5% Diphenyl, 95% Dimethylpolysiloxane	
Dimensions	60m x 250µm x 0.25µm	
Carrier gas	Helium (4.6)	Linde
Flow rate (ml/min)	1.1	
Column Pressure (bar)	1.64	
Injector Temperature (°C)	270	
Detector	FID	
Detector Temperature (°C)	280	
Make-up gas	Nitrogen	Linde
Air Flow rate (Detector) (ml/min)	450	Linde, 80% N_2 20% O_2
Hydrogen (5.0) Flow rate (Detector) (ml/min)	40	Linde
Temperature Program	Initial Temperature 70 °C 3 K min^{-1} to 90 °C 6 K min^{-1} to 108 °C 10 K min^{-1} to 132 °C 30 K min^{-1} to 230 °C	

The gas chromatograph is calibrated with several calibration solutions with different compositions ranging from high o-xylene, to high intermediate to high PA concentrations. The calibration solutions are mixed by applying pure commercial substances (see chap. A1.6 Components for purities). The organic compounds are dissolved in acetone and response factors are evaluated relative to phthalic anhydride or to o-xylene.

$$RF_{\mathrm{i}} = \frac{{n_i}/{A_i}}{{n_{PA}}/{A_{PA}}} \tag{A1.1}$$

$$RF_{\mathrm{i}} = \frac{{n_i}/{A_i}}{{n_{oX}}/{A_{Ox}}} \tag{A1.2}$$

For measurements close to the reactor entrance (until sample port nr. 10), where significant concentrations of o-xylene are present, o-xylene is applied as internal standard. At the reactor outlet PA is applied as internal standard. With the applied column, p- and m-xylene are not separated. However response factors are very similar. These components are therefore considered as one component, p-xylene. Response factors and measurement errors are shown in table 34.

Table 34: Response factors and measurement errors of components measured in the GC

Component	RF_{PA}	RF_{oX}	Error
Acetic Acid (AAc)	6.9	7.8	± 5%
Toluene (TOL)	1.0	1.1	± 4%
Maleic Anhydride (MA)	3.1	3.5	± 4%
p-Xylene (pX)	0.8	0.9	± 2%
o-Xylene (mX)	0.9	1.0	± 2%
Nonane	0.9	1.0	± 5%
Cumene	0.8	0.9	± 3%
p-Benzoquinone	1.6	1.8	± 4%
Citraconic Anhydride	1.9	2.2	± 3%
Methyl-p-Benzoquinone	1.2	1.4	± 3%
Dimethyl Maleic Anhydride	1.4	1.6	± 3%
Tolualdehyde	0.9	1.1	± 2%
Dimethly-p-Benzoquinone	1.0	1.1	± 5%
Benzoic Acid	1.3	1.4	± 5%
Phthaldialdehyde	0.9	1.1	± 4%
Toluic Acid	1.0	1.1	± 4%
Phthalic Anhydride	1.0	1.1	± 2%
Phthalide	0.9	1.0	± 3%

The response factors are checked every six months with several calibration solutions in different concentrations corresponding to reactor entry composition, reactor outlet composition and several intermediate compositions. For all cases, the evaluated response factors lay within a very narrow range within the measurement error depicted in table 34.

A1.3 GC/MS Method

Table 35: GC/MS Method

Column	CS Supreme 5ms	CS
Material	5% Phenylpolysil-phenylensiloxan 95% Dimethylpolysiloxane	
Dimensions	30m x 250µm x 0.25µm	
Carrier gas	Helium (4.6)	
Flow rate [ml/min]	1.1	
Column Pressure [bar]	1.64	
Injector Temperature (°C)	250	
Detector	MS	
Temperature Program	Initial Temperature 65 °C 10 K min^{-1} to 210 °C hold for 5 mins	

A1.4 IR Measurement

The IR measurement is conducted with an Emerson NGA2000 near infrared analyzer. The measured gas is prepared in a gas cooler and filter system, where it is cooled to 5 °C in a peltier cooler in order to have reproducible water concentrations. The temperature of the IR cell values 60 °C while the pressure is the ambient pressure.

A1.5 Evaluation of Concentration Measurement Results

The measured concentrations of CO and CO_2 are evaluated as percentage of the cold gas stream, without water and all organic compounds. Concentrations of organic compounds are evaluated relative to PA or o-xylene concentrations. The actual concentrations measured in the gas stream are calculated by solving the molar balances over the reactor. In terms of reaction stochiometries it is assumed that one mole of o-xylene is converted to one mole of an organic compound. The carbon, hydrogen and oxygen balances are closed with O_2 CO_2 and H_2O. Impurities within o-xylene are generally considered to totally oxidize to CO_2 and H_2O. In addition, a total oxidation reaction of o-xylene is postulated and o-xylene is oxidized to CO and H_2O.

The following equation results for the carbon balance:

$$\dot{n}_{CO_2} = \dot{n}_{CO_2,0} + 6 \cdot \dot{n}_{AAc} + \dot{n}_{TOL} + 4 \cdot \dot{n}_{MA} + 8 \cdot \left(\dot{n}_{pX,0} - \dot{n}_{pX}\right) + 8 \cdot \left(\dot{n}_{oX,0} - \dot{n}_{org}\right) + 8 \cdot \left(\dot{n}_{CU,0} - \dot{n}_{CU}\right) + 2 \cdot \dot{n}_{BQ} + 3 \cdot \dot{n}_{CA} + \dot{n}_{TQ} + 2 \cdot \dot{n}_{DMMA} + \dot{n}_{BAc} \quad \text{(A1.3)}$$

The oxygen balance reads:

$$\dot{n}_{CO_2} = \dot{n}_{O_2,0} - \Big[8.5 \cdot \dot{n}_{AAc} + 1.5 \cdot \dot{n}_{TOL} + 7.5 \cdot \dot{n}_{MA} + 10.5 \cdot \left(\dot{n}_{pX,0} - \dot{n}_{pX}\right) + 10.5 \cdot \left(\dot{n}_{oX,0} - \dot{n}_{org}\right) + 12 \cdot \left(\dot{n}_{CU,0} - \dot{n}_{CU}\right) + 4.5 \cdot \dot{n}_{BQ} + 6 \cdot \dot{n}_{CA} + 3 \cdot \dot{n}_{TQ} + 4.5 \cdot \dot{n}_{DMMA} + 3 \cdot \dot{n}_{BAc} + \dot{n}_{TA} + 1.5 \cdot \dot{n}_{DMBQ} + 2 \cdot \dot{n}_{PAld} + 1.5 \cdot \dot{n}_{TAc} + 3 \cdot \dot{n}_{PA} + 2 \cdot \dot{n}_{PD} + \frac{8}{11.5} \cdot \dot{n}_{CO}\Big] \quad \text{(A1.4)}$$

The sum of all organic streams and the portion of o-xylene converted to CO is:

$$\dot{n}_{Org} = \dot{n}_{AAc} + \dot{n}_{TOL} + \dot{n}_{MA} + \dot{n}_{BQ} + \dot{n}_{CA} + \dot{n}_{TQ} + \dot{n}_{DMMA} + \dot{n}_{TA} + \dot{n}_{DMBQ} + \dot{n}_{BAc} + \dot{n}_{PAld} + \dot{n}_{TAc} + \dot{n}_{PA} + \dot{n}_{PD} + \dot{n}_{oX} + \frac{1}{8}\dot{n}_{CO} \quad \text{(A1.5)}$$

CO measurement is considered through:

$$\dot{n}_{CO} = x_{CO} \cdot \left(\dot{n}_{N_2} + \dot{n}_{CO_2} + \dot{n}_{CO} + \dot{n}_{O_2}\right) \quad \text{(A1.6)}$$

CO_2 measurement is considered in:

$$\dot{n}_{CO_2} - \dot{n}_{CO_2,0} = x_{CO2} \cdot \left(\dot{n}_{N_2} + \dot{n}_{CO_2} + \dot{n}_{CO} + \dot{n}_{O_2}\right) \quad \text{(A1.7)}$$

Reactor entry conditions are considered the flow rates measured in the mass-flow controllers of air and o-xylene taking into account the composition of o-xylene (98.9% purity) measured offline and the measured entry concentration of CO_2 in air.

The carbon balance is checked regularly by measuring oxygen concentrations in the reactor outlet stream. Significant carbon deposition on the catalyst or in the piping cannot be found. Since the measured oxygen concentration is not explicitly taken into account in the evaluation of results but is a result, the comparison of measured and calculated values indicates whether the carbon balance is closed. Maximum deviations found range around 1%.

A1.6 Components

Table 36: Material Data of all components (1)

Nr	Name	Structure	CAS	Sum	T_{fus} (°C)	T_{boil} (°C)	M (g/mol)	RT (min)	Supplier Purity	Abbr.
1	Carbon monoxide		630-08-0	CO	-	-192	28	-	-	CO_2
2	Carbon dioxide		124-38-9	CO_2	-	-78.5	44	-	-	CO
3	Phthaldialdehyde		643-79-8	$C_8H_6O_2$	55	83	134.13	16.2	Aldrich >97%	PAld
4	Acetic Acid		64-19-7	CH_3COOH	17	116	60.05	5.1	Merck >99%	AAc
5	m-Xylene		108-38-3	C_8H_{10}	-48	137	106.17	8.6	Merck >98%	mX

Table 37: Material Data of all components (2)

Nr	Name	Structure	CAS	Sum	T_{fus} (°C)	T_{boil} (°C)	M (g/mol)	RT (min)	Supplier Purity	Abbr.
6	p-Xylene		106-42-3	C_8H_{10}	13	137	106.17	8.6	Merck >98%	pX
7	o-Xylene		95-47-6	C_8H_{10}	-25	143	106.17	9.8	Merck >98%	oX
8	Nonane	-	111-84-2	C_9H_{20}	-54	151	128.26	10.2	Merck >99%	-
9	Cumol		98-82-8	C_9H_{12}	-96	152	120.19	10.6	Merck >98%	-
10	p-Benzoquinone		106-51-4	$C_6H_4O_2$	112	180	108.1	10.3	Merck >98%	BQ
11	o-Tolualdehyde		529-20-4	C_8H_8O	-35	198	120.15	13.9	Merck >98%	TA

Table 38: Material data of all components (3)

Nr	Name	Structure	CAS	Sum	T_{fus} (°C)	T_{boil} (°C)	M (g/mol)	RT (min)	Supplier Purity	Abbr.
12	Maleic anydride		108-31-6	$C_4H_2O_3$	52	202	98.06	9.1	Fluka >99%	MA
13	Citraconic anhydride	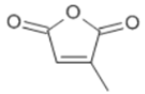	616-02-04	$C_5H_4O_3$	6.00	213	112.08	11	Merck >98%	CA
14	Benzoic acid	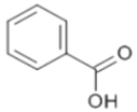	65-85-0	$C_7H_6O_2$	122	250	122.12	15.5	Merck >99.5%	BAc
15	o-Toluic acid	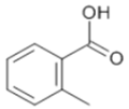	118-90-1	$C_8H_8O_2$	103	260	136.15	16.5	Merck >98%	TAc
16	Benzaldehyde	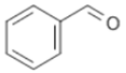	100-52-7	C_7H_6O	-56	179	106.12	13.4	-	BA
17	Benzene		71-43-2	C_6H_6	5	80	78.11	5.6	Merck >99%	BZ

Table 39: Material data of all components (4)

Nr	Name	Structure	CAS	Sum	T_{fus} (°C)	T_{boil} (°C)	M (g/mol)	RT (min)	Supplier Purity	Abbr.
18	Phenol		108-95-2	C_6H_6O	41	182	94.11	-	-	PH
19	Hydroquinone		123-31-9	$C_6H_6O_2$	172	285	110.11	-	-	HQ
20	Dimethyl maleic anhydride		766-39-2	$C_6H_6O_3$		223	126.11	13.2	Merck >98%	DMMA
21	Phthalic anhydride		85-44-9	$C_8H_4O_3$	131	285	148.12	17.2	Merck >98%	PA
22	Phthalic acid		88-99-3	$C_8H_6O_4$	191	289	166.13	17.8	Merck >99.5%	PAc

Table 40: Material data of all components (5)

Nr	Name	Structure	CAS	Sum	T_{fus} (°C)	T_{boil} (°C)	M (g/mol)	RT (min)	Supplier Purity	Abbr.
23	Phthalide		87-41-2	$C_8H_6O_2$	73	290	134.13	17.5	Merck >98%	PD
24	Toluene		108-88-3	C_7H_8	-95	111	92.14	7.1	VWR >99%	TOL
25	2,3 Dimethyl-p-Benzoquinone			$C_8H_8O_2$			136.15	14.7	-	DMBQ
26	2-Methyl-p-Benzoquinone		553-97-9	$C_7H_6O_2$	68		122.12	12.8	Fluka >98%	TQ

A2. Experiments

The following experiments were conducted in the different kinetic runs.

Table 41: Operating conditions of layer 1 kinetic experiments

Nr	$\dot{V}_{air}$ (Nm³/h)	$\dot{m}_{oX}$ (g/h)	SBT (°C)
1	4	320	360
2	3.8	304	360
3	4	340	360
4	3.6	306	360
5	3.8	34.2	360
6	4	360	360
7	4	328	362
8	4	320	360
9	3.5	280	360
10	4	300	364
11	3.8	266	367
12	3.6	252	367
13	4	260	367
14	4	280	365
15	4	280	365
16	3.5	263	363
17	4	320	360
18	4	300	364
19	4	300	355
20	4.2	315	354
21	4.3	318	353
22	4.3	288	351

Table 42: Experimental conditions of layer 2 kinetic experiments

Nr	$\dot{V}_{air}$ (Nm³/h)	$\dot{m}_{ox}$ (g/h)	SBT (°C)
1	4	320	360
2	3.8	304	357
3	4	320	357
4	4	340	356
5	3.8	338	357
6	3.6	324	355
7	3.8	323	352
8	3.8	304	351
9	3.8	304	353
10	3.8	304	355
11	3.8	304	357
12	3.8	304	359
13	3.8	304	362
14	4	320	360
15	3.6	288	362
16	4	300	364
17	3.8	266	366
18	3.5	245	368
19	4	260	370
20	3.6	234	367
21	4	280	363
22	3.5	245	360
23	4	320	360
24	4.3	344	360

Table 43: Experimental conditions of layer 3 kinetic experiments

Nr	$\dot{V}_{air}$ (Nm³/h)	$\dot{m}_{oX}$ (g/h)	SBT (°C)
1	4	320	360
2	3.7	296	358
3	4	320	356
4	3.8	335	355
5	4	356	355
6	4	360	353
7	4	340	353
8	4	320	353
9	4	320	353
10	4	320	353
11	4	320	353
12	4	320	353
13	4	320	351
14	3.9	281	349
15	3.7	281	355
16	3.6	281	358
17	3.5	245	359
18	4	280	360
19	4	260	364
20	4	260	367
21	4	280	369
22	4	280	370
23	4	320	373
24	4	320	375

A3. Estimation of Transport Parameters

A3.1 Axial Dispersion

The estimation of the axial dispersion coefficient D_{ax}, which is necessary to evaluate the Bodenstein number in chap. 6.2 has been conducted according to the suggestions in VDI Wärmeatlas [135]. The following specific correlations were applied:

$$\frac{D_{ax}}{D_{mol}} = \frac{D_{bed}}{D_{mol}} + \frac{Pe_{0,diff}}{K_{ax}} \tag{A3.1}$$

where K_{ax} = 2, $Pe_{0,diff}$ is the molecular Péclet number for diffusivity, D_{mol} is the mean molecular diffusion coefficient. Pe_0 is evaluated by:

$$Pe_{0,diff} = \frac{u_z \cdot d_p}{D_{mol}} \tag{A3.2}$$

The ratio between the mean molecular diffusion coefficient and the bed diffusion coefficient is essentially a function of the bed porosity.

$$\frac{D_{bed}}{D_{mol}} = 1 - \sqrt{1 - \varepsilon} \tag{A3.3}$$

The molecular diffusion coefficient of each component in nitrogen is evaluated by the Fuller equation [189]. The mean molecular diffusion D_{mol} is then:

$$D_{\mathrm{mol}} = \frac{1}{n} \cdot \sum_{i}^{n} \frac{0.00143 \cdot \left(\frac{T}{K}\right)^{1.75} \cdot \sqrt{\left[\frac{M_i}{g/mol} + \frac{M_{N2}}{g/mol}\right]}}{\frac{P}{bar} \cdot \sqrt{2} \cdot \left[{\Delta v_i}^{1/3} + {\Delta v_{N2}}^{1/3}\right]^2} \tag{A3.4}$$

The Bodenstein number of the catalyst bed is then evaluated accordingly.

$$Bo = \frac{u_z \cdot L_{tot}}{D_{ax}} \tag{A3.5}$$

For a realistic bed length ranging between 2.5 and 3.5 m the Bodenstein number in all cases lies in ranges between 2000 and 4000. The critical value for taking into account axial dispersion in the reactor model is 100, where at values above 100 the material transport due to convection prevails while at values below 100 the material transport due to dispersion prevails [55]. Since values obtained generally range above 100, the influence of axial dispersion is neglected in the reactor model.

A3.2 Heat Transfer Parameters

Heat transfer parameters of the catalyst bed are evaluated according to the α_W-model reported in VDI Wärmeatlas [135]. This model assumes a wall heat transfer coefficient dependent on local temperature and flow velocity as well as radial heat conductivity dependent on material data, temperature and fluid flow. This radial heat conductivity is independent not a function of the radial position.

The documented Nusselt correlation for the wall heat transfer coefficient is:

$$Nu_{\mathrm{W}} = \frac{\alpha_W \cdot d_t}{\lambda_f} = \left(1.3 + \frac{5}{d_t/d_p}\right) \cdot \frac{\lambda_{bed}}{\lambda_f} + 0.19 \cdot Re_0^{0.75} \cdot Pr^{1/3} \tag{A3.6}$$

The heat conductivity of the catalyst bed is evaluated by the correlations of Zehner and Schlünder [190]. The Reynolds number applied is:

$$Re_0 = \frac{u_z \cdot d_p \cdot \rho_{\mathrm{f}}}{\eta_f} \tag{A3.7}$$

while the Prandtl number *Pr* is:

$$Pr = \frac{\eta_f \cdot c_{p,f}}{\lambda_f} \tag{A3.8}$$

The radial heat conductivity is evaluated equivalent according to the following equation:

$$\frac{\lambda_r}{\lambda_f} = \frac{\lambda_{bed}}{\lambda_f} + \frac{Pe_{0,th}}{K_r} \tag{A3.9}$$

The factor K_r values 8 while the heat conductivity of the bed is evaluated as described above. The Péclet number for heat transfer is:

$$Pe_{0,th} = \frac{u_z \cdot d_p}{\lambda_f} \tag{A3.10}$$

A4 Supplementary Information to the Kinetic Models

A4.1 Layer 1

Table 44: Reaction enthalpies of in layer 1; stochiometries are according to table 14, denomination of reaction paths according to figure 48

Reaction path	ΔH_R (J/mol)
1	-374074
3	-3781972
4	-285934
5	-544614
6	-2373122
7	-830548
10	-2577350

Table 45: Ranges of measured values which were applied for the estimation of kinetic parameters for layer 1 kinetics

	min	max
p_{oX} (Pa)	11200	266000
p_{TA} (Pa)	0	25000
p_{PD} (Pa)	0	17000
p_{PA} (Pa)	0	210000
p_{MA} (Pa)	0	12000
p_{CO} (Pa)	0	100000
p_{CO2} (Pa)	5600	300000
T(°C)	340	440
$\dot{V}_{air}$ (Nm³/h)	3.5	4.5

A4.2 Layer 2

Table 46: Reaction enthalpies of in layer 2; stochiometries are according to table 27 denomination of reaction paths according to figure 48

Reaction path	ΔH_R (J/mol)
1	-374074
3	-3357502
4	-285934
5	-544614
6	-2373122
10	-2662244

Table 47: Ranges of measured values which were applied for the estimation of kinetic parameters for layer 2 kinetics

	min	max
p_{oX} (Pa)	11200	140000
p_{TA} (Pa)	0	17000
p_{PD} (Pa)	0	10000
p_{PA} (Pa)	35000	210000
p_{MA} (Pa)	1500	15000
p_{CO} (Pa)	21000	100000
p_{CO2} (Pa)	70000	300000
T(°C)	340	440
$\dot{V}_{air}$ (Nm³/h)	3.5	4.5

A4.3 Layer 3

Table 48: Reaction enthalpies of in layer 1; stochiometries are according to table 31 denomination of reaction paths according to figure 63

Reaction path	ΔH_R (J/mol)
1	-374074
4	-285934
5	-544614
10	-2407562
11	-1542574

Table 49: Ranges of measured values which were applied for the estimation of kinetic parameters for layer 3 kinetics

	min	max
p_{oX} (Pa)	11200	14000
p_{TA} (Pa)	0	7000
p_{PD} (Pa)	0	8000
p_{PA} (Pa)	100000	210000
p_{MA} (Pa)	10000	15000
p_{CO} (Pa)	70000	130000
p_{CO2} (Pa)	180000	320000
T(°C)	340	390
$\dot{V}_{air}$ (Nm³/h)	3.5	4.5

A5. Statistical Data

A5.1 Layer 1

Figure 71 shows the distribution of errors for layer 1 parameter estimations. In general a normal distribution of errors can be assumed. No significant second maxima can be seen.

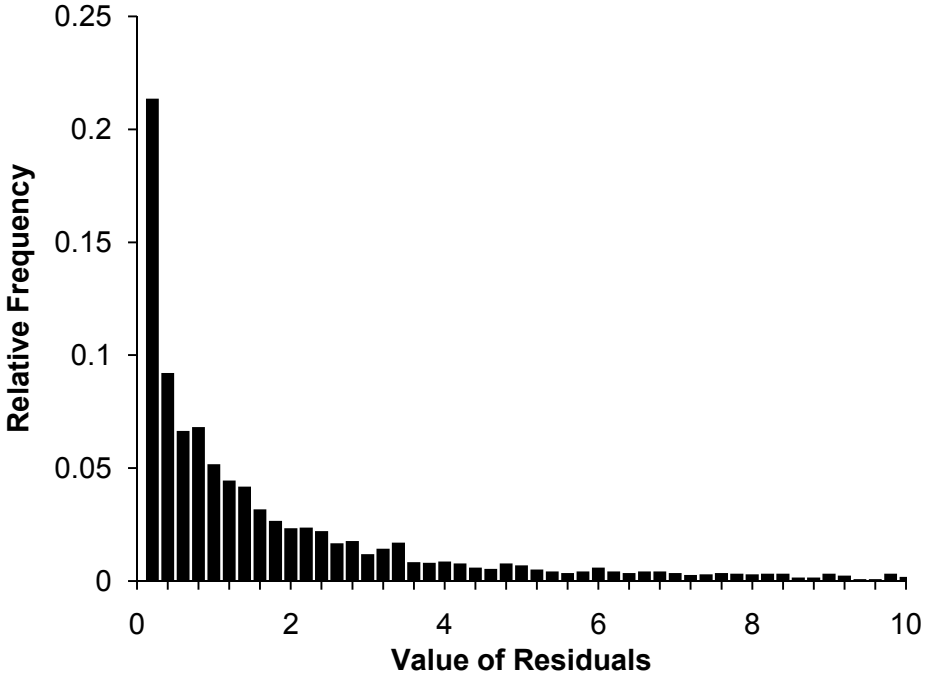

Figure 71: Distribution of weighted errors for layer 1 parameter estimations

Correlations of estimated parameters for layer 1 are shown in table 50. Most parameters show no or only very weak correlations with other parameters. The only strong correlation that can be found is the between the pre-exponential factors of reactions 4 and 5. These are the series reaction from TA to PD (4) and from PD to PA (5). This correlation is somewhat expected. However, expressing these parameters through one single parameter would lead to a simplification which would then not represent the chemical system properly. Therefore it is assumed acceptable

Table 50: Correlations of parameters in layer 1 kinetic parameter estimations

Parameter	No.	1	2	3	4	5	6	7	8	9	10	11	12	13	14	15	16	17	18	19	20	21	22
$f_{\lambda r}$	1	1																					
r	2	0.01	1																				
A_0	3	0.01	-0.4	1																			
C_z	4	-0.2	0.2	-0.7	1																		
ΔH_{oX}	5	-0	-0.1	-0.4	0.24	1																	
$E_{A,1}$	6	0.08	0.7	-0.7	0.4	0.38	1																
$E_{A,3}$	7	0.03	0.58	-0.7	0.42	0.24	0.86	1															
$E_{A,4}$	8	0.01	0.4	-0.3	0.13	0.2	0.31	0.25	1														
$E_{A,5}$	9	0.01	0.09	-0.1	0.1	0.15	0.03	0.02	0.88	1													
$E_{A,6}$	10	0.01	0.5	-0.5	0.18	0.34	0.59	0.51	0.3	0.07	1												
$E_{A,7}$	11	0.01	0.35	-0.5	0.26	0.24	0.62	0.58	-0.4	-0.7	0.37	1											
$E_{A,10}$	12	0.15	0.06	-0.1	0.09	0.17	-0	-0.2	-0.1	-0.1	-0.2	0.05	1										
$K_{0,oX}$	13	-0	-0.2	0.7	-0.5	-0.9	-0.7	-0.6	-0.2	-0.1	-0.5	-0.5	-0	1									
$K_{0,TA}$	14	-0	0.57	-0.7	0.22	0.51	0.87	0.81	0.29	0.03	0.63	0.61	0.02	-0.7	1								
$k_{0,1}$	15	0.08	0.9	-0.7	0.47	0.16	0.84	0.75	0.39	0.1	0.57	0.49	0.11	-0.4	0.75	1							
$k_{0,3}$	16	0.03	0.8	-0.7	0.5	0.13	0.8	0.85	0.36	0.1	0.58	0.48	0.01	-0.4	0.76	0.94	1						
$k_{0,4}$	17	0.01	0.68	-0.4	0.27	0.1	0.48	0.41	0.81	0.67	0.38	-0.2	0.01	-0.2	0.41	0.66	0.61	1					
$k_{0,5}$	18	0	0.58	-0.3	0.21	0.09	0.38	0.32	0.84	0.72	0.32	-0.3	-0	-0.2	0.32	0.54	0.5	0.97	1				
$k_{0,6}$	19	0.03	0.74	-0.7	0.57	0.21	0.79	0.75	0.32	0.08	0.35	0.51	0.17	-0.5	0.72	0.9	0.87	0.57	0.44	1			
$k_{0,7}$	20	0.01	0.29	-0.5	0.42	0.19	0.53	0.52	-0.4	-0.6	0.3	0.88	0.13	-0.4	0.54	0.51	0.52	-0.3	-0.4	0.57	1		
$k_{0,10}$	21	0.14	0.03	-0.2	0.12	0.28	0.18	-0.2	-0	-0.1	0	0.15	0.01	-0.2	0.05	0.07	-0.2	-0	-0	0.03	0.09	1	
n	22	0.18	0.3	0.43	-0.1	-0.1	0.03	0.02	0.08	0.03	0	-0.1	-0.1	0.09	-0.2	0.15	0.12	0.17	0.14	0.08	-0.1	-0.1	1

A5.2 Layer 2

The distribution of errors for layer 2 parameter estimation is shown in figure 72. Generally, the error distribution shows can be considered a normal error distribution. However, a second maximum is shown as residual values just above unity. This represents the systematic model error of temperatures close to the reactor outlet. This has been discussed in chap. 8.5.4.

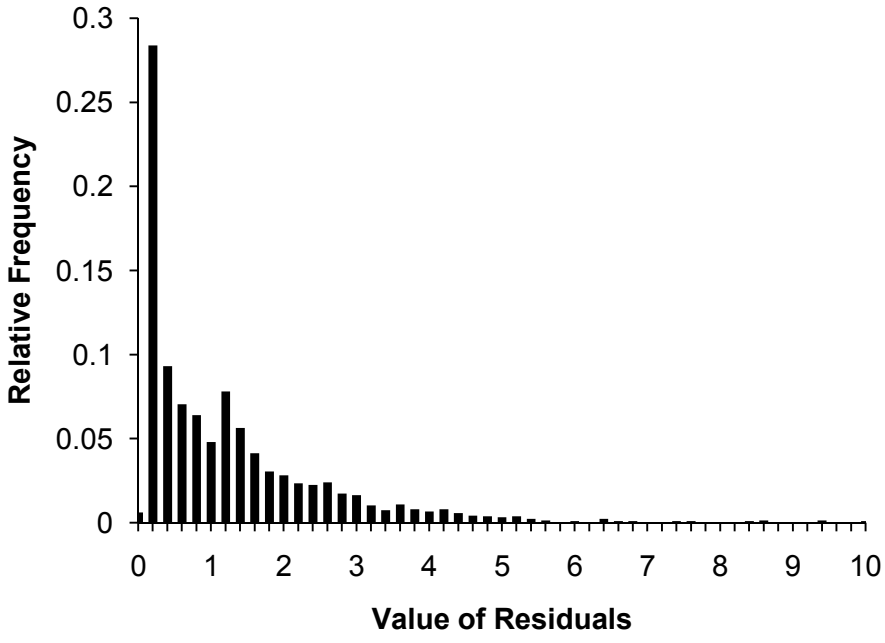

Figure 72: Distribution of weighted errors for layer 2 parameter estimations

The correlations of parameters in layer 2 estimations are shown in table 51. For all parameter sets, these correlations are minimal.

Table 51: Correlations of parameters in layer 2 kinetic parameter estimations

Parameter	No.	1	2	3	4	5	6	7	8	9	10	11	12	13	14
$E_{A,1}$	1	1													
$E_{A,3}$	2	0.1	1												
$E_{A,4}$	3	0.2	-0.2	1											
$E_{A,5}$	4	0.2	-0.2	0.2	1										
$E_{A,6}$	5	-0	-0.2	0.5	0	1									
$E_{A,10}$	6	0.1	-0.1	0.1	0.1	-0	1								
$k_{0,1}$	7	-0.5	0.1	-0	0	0	0	1							
$k_{0,3}$	8	0.2	-0.6	0.2	0.2	0.1	-0.5	-0.2	1						
$k_{0,4}$	9	-0.5	0.2	-0	-0	0.1	0.2	0.6	-0.4	1					
$k_{0,5}$	10	-0.4	0.2	-0.2	0.1	-0	0.2	0.5	-0.5	0.5	1				
$k_{0,6}$	11	-0.2	0	0.1	0.1	-0.3	-0	0.2	-0.1	0.5	0.1	1			
$k_{0,10}$	12	-0.2	0.4	-0.1	-0	-0	0.7	0.3	-0.9	0.5	0.5	0	1		
$v_{CO,3}$	13	0.1	-0	0.1	0.1	0.1	0.4	0.1	-0.2	0.1	0.2	0	0.4	1	
$v_{CO,10}$	14	-0.3	0.3	-0.2	-0.2	-0.1	-0.1	0.2	-0.3	0.2	0.2	0.1	0.2	-0.7	1

A5.3 Layer 3

The error distribution of layer 3 parameter estimations is shown in figure 73. As described in chap. 8.6.4, the description accuracy of temperature profiles in layer 3 is limited and for the final parameter estimations, the temperature profile was not taken into account. The error distribution therefore also shows only the errors of actually fitted measured concentration values. In general, the distribution follows a normal distribution. Additional maxima are not visible. The statistical accuracy of the estimation is consequently very good.

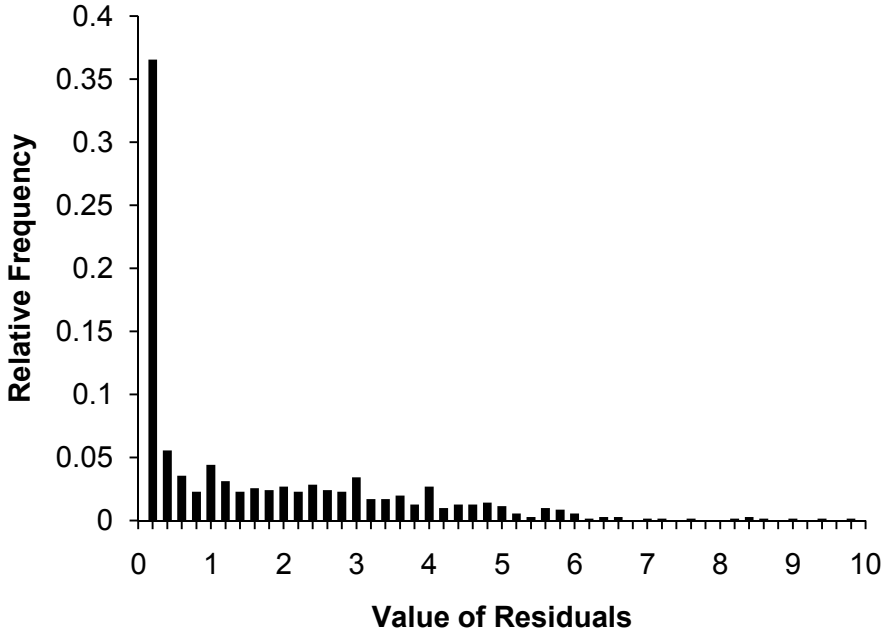

Figure 73: Distribution of weighted errors for layer 3 parameter estimations

The corresponding parameter correlations are shown in table 52. The rather inaccurate description of temperature profiles in layer 3 is reflected also in the correlations of temperature dependencies of the kinetic parameters. Particularly the pre-exponential factors and their activation energies show weak correlations. For all other parameter combinations, correlations are insignificant.

Table 52: Correlations of parameters in layer 2 kinetic parameter estimation

Parameter	No.	1	2	3	4	5	6	7	8	9	10	11
$E_{A,1}$	1	1										
$E_{A,4}$	2	-0.23	1									
$E_{A,5}$	3	-0.07	-0.06	1								
$E_{A,10}$	4	-0.01	0	0	1							
$E_{A,11}$	5	-0	-0.01	-0.01	-0.35	1						
$k_{0,1}$	6	0.94	-0.2	-0.05	-0.01	-0	1					
$k_{0,4}$	7	-0.29	0.93	-0.05	0	-0.01	-0.27	1				
$k_{0,5}$	8	-0.1	-0.06	0.97	0	-0.01	-0.08	-0.06	1			
$k_{0,10}$	9	-0.01	0	0	0.93	-0.32	-0.01	0	0	1		
$k_{0,11}$	10	-0.01	-0.01	-0.01	-0.33	0.94	-0.01	-0.01	-0.01	-0.35	1	
$v_{CO,10}$	11	0	0	0	-0.02	0	0	0	0.01	-0.18	0.04	1

References

[1] http://www.oil-price.net/, 1-5-2011

[2] Cavani, F., *Catalytic selective oxidation: The forefront in the challenge for a more sustainable chemical industry*, Catalysis Today 157, 8-15, 2010

[3] Arpe, H.-J., *Industrial Organic Chemistry,* Wiley-VCH, Weinheim, 2003

[4] Guetlhuber, F., *Reactor for catalytic gas-phase reactions, especially manufacture of phthalic acid anhydride*, WO2003022418 (26-8-2002), assigned to DWE

[5] Takada, M., Uhara, H., and Sato, T., *Method and reactor for vapor phase oxidation*, DE2830765 (13-7-1978), assigned to Nippon Shokubai

[6] Blechschmitt, K., Reuter, P., Wirth, F. and Hornberger, P., *Phthalic anhydride from o-xylene or naphthalene*, DE2546268A1 (16-10-1975), assigned to BASF AG

[7] Gueckel, C., Dialer, H., Estenfelder, M. and Pitschi, W., *Multilayer catalysts for the production of phthalic anhydride*, DE102005009473 (2-3-2005), assigned to Süd-Chemie AG

[8] Gueckel, C., Dialer, H., Estenfelder, M. and Pitschi, W., *Method for producing a multilayer catalyst for obtaining phthalic anhydride*, WO2006092305 (2-3-2006), assigned to Süd-Chemie AG

[9] Hara, T., *Catalyst and process for the manufacture of phthalic anhydride from naphthalene or 1,2-xylene*, EP286448A2 (11-4-1988), assigned to Nippon Steel

[10] Heidemann, T. and Wanjek, H., *Production of phthalic anhydride*, WO9961433A1 (10-5-1999), assigned to BASF AG

[11] Bond, G., *Mechanism of the oxidation of o-xylene to phthalic anhydride*, Journal of Catalysis 116, 531-539, 1989

[12] Bernardini, F. and Ramacci, M., *Oxidation mechanism of o-xylene to phthalic anhydride*, Chimica e Industria 48, 9-17, 1966

[13] Herten, J. and Froment, G., *Kinetics and product distribution in the oxidation of o-xylene on a vanadium pentoxide catalyst*, Industrial and Engineering Chemistry Process Design and Development 7, 516-526, 1968

[14] Vanhove, D. and Blanchard, M., *Catalytic oxidation of o-xylene on catalysts of the vanadium(V) oxide-titanium(IV)oxide series*, Bulletin de la Société Chimique de France, 3291-3295, 1971

[15] Saleh, R. and Wachs, I., *Reaction network and kinetics of o-xylene oxidation to phthalic anhydride over vanadia/titania (anatase) catalysts*, Applied Catalysis 31, 87-98, 1987

[16] Ballarini, N., Brentari, A., Cavani, F., Luciani, S., Cortelli, C., Cruzzolin, F. and Leanza, R., *A revision of the mechanism of o-xylene oxidation to phthalic anhydride with V/Ti/O catalysts, and the role of the promoter Cs*, Catalysis Today 142, 181-184, 2009

[17] Dias, C., Portela, M. and Bond, G., *Oxidation of o-xylene to phthalic anhydride over V_2O_5/TiO_2 catalysts. Part 4. Mathematical modeling study and analysis of the reaction network*, Journal of Catalysis 164, 276-287, 1996

[18] Dias, C., Portela, M. and Bond, G., *Synthesis of phthalic anhydride: catalysts, kinetics, and reaction modeling*, Catalysis Reviews – Science and Engineering 39, 169-207, 1997

[19] Nikolov, V., Klisurski, D. and Anastasov, A., *Phthalic anhydride from o-xylene catalysis: science and engineering*, Catalysis Reviews – Science and Engineering 33, 319-374, 1991

[20] Boag, I., Bacon, D., and Downie, J., *Analysis of the reaction network for the vanadia-catalyzed oxidation of o-xylene*, Journal of Catalysis 38, 375-384, 1975

[21] Yabrov, A. and Ivanov, A., *Response studies of the mechanism of o-xylene oxidation over a vanadium-titanium oxide catalyst*, Reaction Kinetics and Catalysis Letters 14, 347-351, 1980

[22] Boreskov, G., Ivanov, A., Ilyinich, O. and Ponomareva, V., *Influence of alkaline promoters on the selectivity of vanadium catalysts in the oxidation of o-xylene to phthalic anhydride*, Reaction Kinetics and Catalysis Letters 3, 1-8, 1975

[23] Papageorgiou, J., Abello, M. and Froment, G., *Kinetic modeling of the catalytic oxidation of o-xylene over an industrial V_2O_5-TiO_2 (anatase) catalyst*, Applied Catalysis A: General 120, 17-44, 1994

[24] Skrzypek, J., Grzesik, M., Galantowicz, M. and Solinski, J., *Kinetics of the catalytic air oxidation of o-xylene over a commercial vanadium pentoxide-titanium dioxide catalyst*, Chemical Engineering Science 40, 611-620, 1985

[25] Wainwright, M. S. and Hoffman, T. W., *The oxidation of ortho-xylene on vanadium pentoxide catalysts. I. Transient kinetic measurements*, Canadian Journal of Chemical Engineering 55, 552-556, 1977

[26] Li, D., *Partielle Oxidation von o-Xylol zu Phthalsäureanhydrid in einem strukturierten Festbettreaktor*, PhD Thesis, Universität Karlsruhe (TH),1990

[27] Anastasov, A., *An investigation of the kinetic parameters of the o-xylene oxidation process carried out in a fixed bed of high-productive vanadia-titania catalyst*, Chemical Engineering Science 58, 89-98, 2003

[28] Anastasov, A., Elenkov, D. and Nikolov, V., *A model study of a conventional fixed bed tubular reactor with a catalyst layer on the inside tube wall*, Chemical Engineering and Processing 23, 203-211, 1988

[29] Gimeno, M., Gascon, J., Tellez, C., Herguido, J., and Menendez, M., *Selective oxidation of o-xylene to phthalic anhydride over V_2O_5/TiO_2: Kinetic study in a fluidized bed reactor*, Chemical Engineering and Processing 47, 1844-1852, 2008

[30] Lopez-Isunza, F., *Steady State and Dynamic Behaviour of an Industrial Fixed Bed Reactor*, PhD Thesis, University of London, 1983

[31] Mongkhonsi, T., *Dynamic Behaviour of a Fixed-Bed Reactor with Catalyst Deactivation*, PhD Thesis, University of London, 1993

[32] Lorz, P, Towae, F., Enke, W., Jäckh, R. and Bhargava, N., in Ullmann's Encyclopedia of Industrial Chemistry, Wiley-VCH, Weinheim, 2005

[33] Ryder, R., Ryan, R. and Klapproth, W., *Phthalic acid anhydride*, DE2436522A1 (29-7-1974), assigned to Koppers Co., Inc.

[34] Gutermuth, T., Fiebig, B. and Kuchling, T., *Method for manufacturing phthalic acid/phthalic acid solution in acetic acid*, DE 102009036295A1 (10-2-2011), assigned to Lurgi GmbH

[35] Fiebig, B. and Kuchling, T., *Oxidation of o-xylene for manufacture of phthalic anhydride 2. Experimental studies of liquid-phase oxidation*, Chemie Ingenieur Technik 81, 1941-1948, 2009

[36] Fiebig, B. and Kuchling, T., *Oxidation of o-xylene for manufacture of phthalic anhydride. Part 1. Process simulation of heterogeneously catalyzed gas-phase oxidation*, Chemie Ingenieur Technik 81, 1467-1472, 2009

[37] Okuno, M. and Takahashi, T., *Oxidation process and layered catalyst-containing reactors for the manufacture of phthalic anhydride from ortho-xylene and/or naphthalene*, EP1063222A1 (21-6-2000), assigned to Nippon Shokubai

[38] *Vanadium pentoxide catalyst for the gas phase oxidation of naphthalene*, DE1932869 (28-6-1969), assigned to Chemische Fabrik von Heyden

[39] Felice, K., Wiedemann, O., Leitsmann, R., and Gierer, W., *Vanadium pentoxide-titanium dioxide catalysts for the air oxidation of o-xylene to phthalic anhydride*, DE1943759 (28-8-1969), assigned to Chemische Fabrik von Heyden

[40] Estenfelder, M., Kaeding, B., Gueckel, C. and Mestl, G., *Method and apparatus for coating a suspension to a carrier structure for example a catalyst support*, 102007025357 (5-5-2007), assigned to Süd-Chemie AG

[41] Calderbank, P., Chandrasekharan, K. and Fumagalli, C., *The prediction of the performance of packed-bed catalytic reactors in the air-oxidation of o-xylene*, Chemical Engineering Science 32, 1435-1443, 1977

[42] Grabowski, R., Grzybowska, B., Haber, J. and Sloczynski, J., *Catalytic activity of V_2O_5/TiO_2 systems in the oxidation of o-xylene*, Reaction Kinetics and Catalysis Letters 2, 81-87, 1975

[43] Grzybowska-Swierkosz, B., *Active centers on vanadia-based catalysts for selective oxidation of hydrocarbons*, Applied Catalysis A: General 157, 409-420, 1997

[44] Grzybowska-Swierkosz, B., *Vanadia-titania catalysts for oxidation of o-xylene and other hydrocarbons*, Applied Catalysis A: General 157, 263-310, 1997

[45] Knözinger, H. and Mestl, G., *Laser Raman spectroscopy - a powerful tool for in situ studies of catalytic materials71*, Topics in Catalysis 8, 45-55, 1999

[46] Mestl, G., *In situ Raman spectroscopy - a valuable tool to understand operating catalysts*, Journal of Molecular Catalysis A: Chemical 158, 45-65, 2000

[47] Kryukova, G., Zenkovets, G., Mestl, G. and Schlögl, R., *Structural study of titanium doped vanadia and vanadium doped titania catalysts*, Reaction Kinetics and Catalysis Letters 80, 161-9, 2003

[48] Wachs, I., Chan, S. and Saleh, R., *The interaction of V_2O_5 with TiO_2 (anatase): II. Comparison of fresh and used catalysts for o-xylene oxidation to phthalic anhydride*, Journal of Catalysis 91, 366-9, 1985

[49] Saleh, R., Wachs, I., Chan, S. and Chersich, C., *The interaction of V_2O_5 with TiO_2 (anatase): Catalyst evolution with calcination temperature and o-xylene oxidation*, Journal of Catalysis 98, 102-114, 1986

[50] Saleh, R., Wachs, I., Chan, S. and Chersich, C., *Comparison of vanadium pentoxide/titanium dioxide (anatase) and V_2O_5/TiO_2 (rutile): promoting effect of the support*, Preprints of the American Chemical Society – Division of Petroleum Chemistry 31, 272-276, 1986

[51] Wachs, I., Jehng, J., Deo, G., Weckhuysen, B., Guliants, V. and Benziger, J., *In situ Raman spectroscopy studies of bulk and surface metal oxide phases during oxidation reactions*, Catalysis Today 32, 47-55, 1996

[52] Wachs, I. and Weckhuysen, B., *Structure and reactivity of surface vanadium oxide species on oxide supports*, Applied Catalysis A: General 157, 67-90, 1997

[53] Froment, G. and Bischoff, K., *Chemical Reactor Analysis and Design,* Wiley, New York, 1979

[54] Hofmann, H., *Progress in the modeling of fixed bed reactors*, Chemie Ingenieur Technik 51, 257-265, 1979

[55] Baerns, M., Hofmann, H. and Renken, A., *Chemische Reaktionstechnik - Lehrbuch der Technischen Chemie - Band 1,* Georg Thieme Verlag, Stuttgart, 1992

[56] Froment, G., *Fixed-bed catalytic reactors. Current design status*, Industrial and Engineering Chemistry 59, 18-27, 1967

[57] Froment, G., *Fixed bed catalytic reactors. Technological and fundamental design aspects*, Chemie Ingenieur Technik 46, 374-386, 1974

[58] Adler, R., *State of the art of the simulation of heterogeneous gas catalytic reaction processes in fixed bed tubular reactors: Part 1*, Chemie Ingenieur Technik 72, 555-564, 2000

[59] Adler, R., *State of the art of the simulation of heterogeneous gas catalytic reaction processes in fixed bed tubular reactors: Part 2*, Chemie Ingenieur Technik 72, 688-699, 2000

[60] Tsotsas, E. and Schlünder, E.-U., *Wärmeübertragung in Festbetten, durchmischten Schüttgütern und Wirbelschichten,* Georg Thieme Verlag, Stuttgart, 1988

[61] Emig, G. and Dittmeyer, R., in Handbook of Heterogeneous Catalysis; Volume 3 Eds. Ertl, G., Knoezinger, H., Schueth, F., Weitkamp, J., Ch.6.2, p. 1209, Wiley-VCH Verlag, Weinheim, 2008

[62] Vortmeyer, D., *Axial heat dispersion in packed beds*, Chemical Engineering Science 30, 999-1001, 1975

[63] Hinshelwood, C., *The Kinetics of Chemical Change,* Oxford University Press, Oxford, 1940

[64] Rideal, E., *A note on a simple molecular mechanism for heterogeneous catalytic reactions*, Mathematical Proceedings of the Cambridge Philosophical Society 35, 130-2, 1939

[65] Mars, P. and van Krevelen, D., *Oxidations carried out by means of vanadium oxide catalysts*, Chemical Engineering Science 3, 41-59, 1954

[66] Hougen, O. and Watson, K., *Chemical Process Principles. Pt. 3. Kinetics,* John Wiley & Sons, New York,1947

[67] http://webbook.nist.gov/chemistry/name-ser.html, 13-1-2009

[68] Gueckel, C., Mestl, G., and Estenfelder, M., *Production of phthalic acid anhydride using catalyst containing titanium dioxide*, EP1860091 (1-7-2006), assigned to Süd-Chemie AG

[69] Neto, S., Rosowski, F., Storck, S., Zuehlke, J., Allmann, H.-M., Lautensack, T. and Steeg, R., *Method for preparation of oxidation catalysts used in production of aromatic acids, aromatic anhydrides and niacin*, WO2006131480 (31-5-2006), assigned to BASF AG

[70] Neto, S., Rosowski, F., Storck, S., Zuehlke, J., Allmann, H.-M., Lautensack, T. and Steeg, R., *Method to start-up a hydrocarbon oxidation catalyst for production of aromatic acids, anhydrides and niazin*, WO2007003662 (11-1-2007), assigned to BASF AG

[71] Ivanovskaya, F., *Routes of catalytic oxidation of o-xylene to phthalic anhydride*, Reaction Kinetics and Catalysis Letters 45, 107-110, 1991

[72] Bernardini, F., Ramacci, M. and Paolacci, A., *Analysis of products of the vapor phase oxidation of o-xylene*, Chimica e Industria 47, 485-489, 1965

[73] Bernardini, F. and Ramacci, M., *Calculation of conversion yield of o-xylene to phthalic anhydride in an industrial reaction*, Chimica e Industria 48, 37-38, 1966

[74] Blanchard, M. and Vanhove, D., *Vanadium oxide-catalyzed oxidation of methyl carbon-14 labeled o-xylene*, Bulletin de la Société Chimique de France 9, 4134-4137, 1971

[75] Dolgov, B., in *Die Katalyse in der organischen Chemie*, Ch.5 p. 196, Deutscher Verlag der Wissenschaften, Berlin, 1963

[76] Germain, J. and Laugier, R., *Kinetics of the catalytic oxidation of aromatic hydrocarbons. IV. Oxidation of toluene on simple and mixed vanadium and molybdenum oxides*, Bulletin de la Société Chimique de France 2, 650-656, 1971

[77] Bielanski, A. and Najbar, M., *V_2O_5-MoO_3 catalysts for benzene oxidation*, Applied Catalysis A: General 157, 223-261, 1997

[78] Andersson, S., *Reaction networks in the catalytic vapor-phase oxidation of toluene and xylenes*, Journal of Catalysis 98, 138-149, 1986

[79] Parks, W. and Allard, C., *Vapor-phase catalytic oxidation of organic compounds. Production of tolualdehyde and phthalic anhydride from xylene*, Journal of Industrial and Engineering Chemistry 31, 1162-1167, 1939

[80] Riekert, L., *Observation and quantification of activity and selectivity of solid catalysts*, Applied Catalysis 15, 89-102, 1985

[81] Hesse, M., Meier, H. and Zeeh, B., *Spektroskopische Methoden in der organischen Chemie,* Georg Thieme Verlag, Stuttgart, 1987

[82] Brodhagen, A., Roessler, B., Ruehl, T., Wolf, H.-J. and Rosowski, F., *Oxidation of o-xylene into o-toluic acid and other oxidation products by the staggered injection of an oxygen-containing gas*, WO2003078369 (18-3-2003), assigned to BASF

[83] Walch, Andreas, Kammel, Ulrich, and Heidemann, Thomas, *Manufacture of phthalic anhydride*, EP0100303 (7-8-2001), assigned to BASF AG

[84] Bowie, J., Cameron, D., Giles, R. and Williams, D., *Mass spectrometry. Mass spectra of benzoquinones*, Journal of the Chemical Society B, 335-339, 1966

[85] Bowie, J., Cameron, D., Schutz, P., Williams, D. and Bhacca, N., *Solvent effects in N.M.R. spectroscopy. VI. Chemical shifts induced by benzene in quinones*, Tetrahedron 22, 1771-1775, 1966

[86] Zhu, J. and Andersson, S., *Reaction network and kinetics for the catalytic oxidation of toluene over vanadia*, Journal of Catalysis 126, 92-100, 1990

[87] Zhu, J., Rebenstorf, B. and Andersson, S., *Influence of phosphorus on the catalytic properties of vanadium pentoxide/titania catalysts for toluene oxidation*, Journal of the Chemical Society, Faraday Transactions 85, 3645-3662, 1989

[88] Freitag, C., Besselmann, S., Loeffler, E., Gruenert, W., Rosowski, F. and Muhler, M., *On the role of monomeric vanadyl species in toluene oxidation over V_2O_5/TiO_2 catalysts: a kinetic study using the TAP reactor*, Catalysis Today 91-92, 143-147, 2004

[89] Miki, J., Osada, Y., Konoshi, T., Tachibana, Y. and Shikada, T., *Selective oxidation of toluene to benzoic acid catalyzed by modified vanadium oxides*, Applied Catalysis A: General 137, 93-104, 1996

[90] Bulushev, D., Reshetnikov, S., Kiwi-Minsker, L. and Renken, A., *Deactivation kinetics of V/Ti-oxide in toluene partial oxidation*, Applied Catalysis A: General 220, 31-39, 2001

[91] Bulushev, D., Kiwi-Minsker, L. and Renken, A., *Vanadia/titania catalysts for gas phase partial toluene oxidation: Spectroscopic characterisation and transient kinetics study*, Catalysis Today 57, 231-239, 2000

[92] Bulushev, D., Kiwi-Minsker, L. and Renken, A., *Transient kinetics of toluene partial oxidationover V/Ti oxide catalysts*, Catalysis Today 61, 271-277, 2000

[93] Bulushev, D. A., Rainone, F., and Kiwi-Minsker, L., *Partial oxidation of toluene to benzaldehyde and benzoic acid over model vanadia/titania catalysts: role of vanadia species*, Catalysis Today 96, 195-203, 2004

[94] Krylova, E., Luzyanin, B. and Yakubson, A., *Oxygen-containing compounds formed in the oxidation of benzene to maleic anhydride*, Neftekhimiya 23, 255-258, 1983

[95] Volfson, V., Korneichuk, G. P. and Roiter, V., *Peculiarities of the catalytic oxidation of naphthalene. I. Kinetics of the oxidation of phthalic anhydride on vanadium oxide catalysts*, Ukrainski Khimicheskii Zhurnal 26, 305-313, 1960

[96] Plisov, A. and Stepanova, O., *Preparation of benzoic acid by decarboxylation of phthalic anhydride with Odessa green clay*, Trudy Odesskogo Universitata, Seria Khimia 146 (5), 91-93, 1956

[97] Marx, R., Wölk, H.-J., Mestl, G. and Turek, T., *Reaction scheme of o-xylene oxidation on vanadia catalyst*, Applied Catalysis A: General 398 (1-2), 37-43, 2011

[98] Calderbank, P., *Catalytic oxidation of naphthalene*, Industrial Chemist and Chemical Manufacturer 28, 291-295, 1952

[99] Shelstad, K., Downie, J. and Graydon, W., *Kinetics of the vapor-phase oxidation of naphthalene over a vanadium catalyst*, Canadian Journal of Chemical Engineering 38, 102-107, 1960

[100] Volfson, V., Korneichuk, G., Roiter, V. and Zhigailov, Y., *Peculiarities in the catalytic oxidation of naphthalene III. Kinetics of oxidation of naphthalene in long layers of vanadium catalysts*, Ukrainski Khimicheskii Zhurnal 26, 588-593, 1960

[101] Mann, R. and Downie, J., *The vapor-phase oxidation of ortho-xylene over a vanadium oxide catalyst*, Canadian Journal of Chemical Engineering 46, 71-72, 1968

[102] Jaswal, I. , Mann, R., Juusola, J. and Downie, J., *Vapor-phase oxidation of benzene over a vanadium oxide catalyst*, Canadian Journal of Chemical Engineering 47, 284-287, 1969

[103] Juusola, J., Mann, R. and Downie, J., *The kinetics of the vapor-phase oxidation of o-xylene over a vanadium oxide catalyst*, Journal of Catalysis 17, 106-113, 1970

[104] Lyubarskii, A., Gorelik, A., Petoyan, V., Lyapin, E. and Beskov, V., *Kinetics of the catalytic vapor-phase oxidation of o-xylene to phthalic anhydride. II. Kinetics of o-xylene oxidation*, Kinetics and Catalysis 14, 956-961, 1973

[105] Lyubarskii, A., Gorelik, A., Petoyan, V., Lyapin, E. and Beskov, V.*,Kinetics of the catalytic vapor-phase oxidation of o-xylene into phthalic anhydride. I. Kinetics of oxidation of intermediate products*, Kinetics and Catalysis 14(2), 410-417, 1973

[106] Lyubarskii, A., Gorelik, A., Petoyan, V., Lyapin, E. and Beskov, V., *Mathematical modeling of the oxidation process in a fixed catalyst-bed reactor*, Teoreticheskie Osnovy Khimicheskoi Tekhnologii 8, 690-697, 1974

[107] Froment, G., *Model discrimination and parameter estimation in heterogeneous catalysis*, AIChE Journal 21, 1041-1057, 1975

[108] Vanhove, D. and Blanchard, M., *Catalytic oxidation of o-xylene. Kinetic study by competitive reaction*, Journal de Chimie Physique et de Physico-Chimie Biologique 73, 51-56, 1976

[109] Hoffmann, U., *Auslegung und Analyse stationär betriebener Schüttschichtreaktoren für heterogenkatalytische Gas-Feststoffreaktionen mit Hilfe eines Standardrechen-programms*, VDI Fortschrittsbericht 3(49), ISBN 3-18-144903-2, 1977

[110] Chandrasekharan, K. and Calderbank, P., *Kinetics of the catalytic air-oxidation of o-xylene measured in a tube-wall-catalytic reactor*, Chemical Engineering Science 35, 1523-1535, 1980

[111] Kershenbaum, L. and Lopez-Isunza, F., *Measurement and estimation in catalytic reactors for partial oxidation*, Transactions of the Institute of Measurement and Control 8, 137-143, 1986

[112] Lopez-Isunza, F. and Kershenbaum, L., *The role of reversible changes in catalyst activity in the observed multiple steady states during partial oxidation dynamics*, Chemical Engineering Science 47, 2817-2822, 1992

[113] Mongkhonsi, T., Lopez-Isunza, F. and Kershenbaum, L., *The distortion of measured temperature profiles in fixed-bed reactors*, Chemical Engineering Research and Design 70, 255-264, 1992

[114] Cheng, Y., Lopez-Isunza, F., Mongkhonsi, T. and Kershenbaum, L., *Estimation of catalyst activity profiles in fixed-bed reactors with decaying catalysts*, Applied Catalysis A: General 106, 193-199, 1993

[115] Cheng, Y., Abi, C. and Kershenbaum, L., *Online estimation for a fixed-bed reactor with catalyst deactivation using nonlinear programming techniques*, Computers and Chemical Engineering 20, 793-798, 1996

[116] Mongkhonsi, T. and Kershenbaum, L., *The effect of deactivation of a V_2O_5/TiO_2 (anastase) industrial catalyst on reactor behaviour during the partial oxidation of o-xylene to phthalic anhydride*, Applied Catalysis A: General 170, 33-48, 1998

[117] Castillo-Araiza, C. and Lopez-Isunza, F., *Modeling the Partial Oxidation of o-Xylene in an Industrial Packed-Bed Catalytic Reactor: The Role of Hydrodynamics and Catalyst Activity in the Heat Transport*, Industrial & Engineering Chemistry Research 49, 6845-6853, 2010

[118] Skrzypek, J., *Corrigendum*, Chemical Engineering Science 43, 987, 1988

[119] Papageorgiou, J., Abello, M. and Froment, G., *Erratum to: Kinetic modeling of the catalytic oxidation of o-xylene over an industrial V_2O_5-TiO_2 (anatase) catalyst*, Applied Catalysis A: General 124, 165-166, 1995

[120] Ivanov, A., Yabrov, A., Karnatovskaya, L., Petukhova, N. and Chaikovskii, S., *o-Xylene oxidation to phthalic anhydride over unsteady state catalysts*, Reaction Kinetics and Catalysis Letters 61, 75-82, 1997

[121] Yabrov, A., Ismailov, E., Boreskov, G., Ivanov, A. and Anufrienko, V., *ESR studies on the formation and structure of a vanadium-titanium oxide catalyst for o-xylene oxidation under the influence of the reaction medium*, Reaction Kinetics and Catalysis Letters 3, 237-242, 1975

[122] Sadovskaya, E., Pokrovskaya, S., Yabrov, Y. and Ivanov, A., *Relaxation of the rate of o-xylene oxidation to phthalic anhydride on vanadium catalysts*, Reaction Kinetics and Catalysis Letters 39, 431-436, 1989

[123] Nikolov, V. and Anastasov, A., *A study of coolant temperature in an industrial reactor for o-xylene oxidation*, AIChE Journal 35, 511-513, 1989

[124] Nikolov, V., Anastasov, A., Elenkov, D., Ganev, G. and Dimitrov, N., *Oxidation of o-xylene into phthalic anhydride in a reactor with two fixed beds of vanadium-titania catalyst*, Chemical Engineering and Processing 25, 127-131, 1989

[125] Nikolov, V. and Anastasov, A., *Influence of the inlet temperature on the Performance of a fixed-Bed reactor for oxidation of o-xylene into phthalic anhydride*, Chemical Engineering Science 47, 1291-1298, 1992

[126] Anastasov, A., *A study of the influence of the operating parameters on the temperature of the hot spot in a fixed bed reactor*, Chemical Engineering Journal 86, 287-297, 2002

[127] Anastasov, A., *Deactivation of an industrial V_2O_5-TiO_2 catalyst for oxidation of o-xylene into phthalic anhydride*, Chemical Engineering and Processing 42, 449-460, 2003

[128] Anastasov, A., *Corrigendum to "An investigation of the kinetic parameters of the o-xylene oxidation process carried out in a fixed bed of high-productive vanadia-titania catalyst" [Chem. Eng. Sci. 58 (2003) 89-98]*, Chemical Engineering Science 64, 2525, 2009

[129] Guettel, R. and Turek, T., *Assessment of micro-structured fixed-bed reactors for highly exothermic gas-phase reactions*, Chemical Engineering Science 65, 1644-1654, 2010

[130] Anastasov, A. and Nikolov, V., *A catalyst deposited over the external surface of the reactor tubes - a new solution for carrying out heterogeneous catalytic processes*, Canadian Journal of Chemical Engineering 80, 79-87, 2002

[131] Anastasov, A., *Parametric sensitivity of a heterogeneous catalytic process and its connection with the diameter of the contact tube*, Bulgarian Chemical Communications 35, 211-218, 2003

[132] Elshishini, S., Elnashaie, S., *Modelling, Simulation and Optimization of Industrial Fixed Bed Catalytic Reactors,* Gordon and Breach Science Publishers, Singapore, 1993

[133] Ergun, S., *Mass-transfer rate in packed columns. Its analogy to pressure loss*, Chemical Engineering Progress 48, 227-236, 1952

[134] Ergun, S., *Fluid flow through packed columns*, Chemical Engineering Progress 48, 89-94, 1952

[135] Tsotsas, E., chap. Mh in VDI-Wärmeatlas Ed. E. U. Schlünder, Springer Verlag, Berlin Heidelberg New York, 2006

[136] Perry, R., Green, D., Editors, *Perry's Chemical Engineers' Handbook, 7th Edition,* McGraw-Hill, 1997

[137] gPROMS Version 3.3.1, Process Systems Enterprise Ltd., London, 2010

[138] Vatani, A., Mehrpooya, M. and Gharagheizi, F., *Prediction of standard enthalpy of formation by a QSPR model*, International Journal of Molecular Science 8, 407-432, 2007

[139] Orozco, G., Gomez, J., Sanchez, O., Gil, I. and Duran, A., *Effect of kinetic models on hot spot temperature prediction for phthalic anhydride production in a multitubular packed bed reactor*, Canadian Journal of Chemical Engineering 88, 224-231, 2010

[140] Mason, R., Gunst, R. and Hess, J., *Statistical Design and Analysis of Experiments,* Wiley, Hoboken, 2003

[141] Zhao, C. and Wachs, I., *Selective oxidation of propylene over model supported V_2O_5 catalysts: Influence of surface vanadia coverage and oxide support*, Journal of Catalysis 257, 181-189, 2008

[142] van den Bos, A., *Parameter Estimation for Scientists and Engineers,* Wiley, Hoboken, 2007

[143] gPROMS Documentation (Version 3.3), Process Systems Enterprise Ltd., London, 2010

[144] Zander, H.-J., *Dynamische Modellierung reaktionskinetischer Systeme mit Neuronalen Netzen und hybriden Modellen*, PhD Thesis, Friedrich-Alexander Universität Erlangen, 1999

[145] Dittmeyer, R., *Kinetik und Verfahrensaspekte der oxidativen Kopplung von Methan zu höheren Kohlenwasserstoffen*, PhD Thesis, Universität Erlangen, 1994

[146] Hill, T. and Lewicki, P., *Statistics: Methods and Applications,* Statsoft, Tulsa, 2006

[147] Schwaab, M., Silva, F., Queipo, C., Barreto, J., Nele, M. and Pinto, J., *A new approach for sequential experimental design for model discrimination*, Chemical Engineering Science 61, 5791-5806, 2006

[148] Schwaab, M. and Pinto, J., *Optimum reference temperature for reparameterization of the Arrhenius equation. Part 1: Problems involving one kinetic constant*, Chemical Engineering Science 62, 2750-2764, 2007

[149] Schwaab, M., Pinto, J. C., *Optimum reparameterization of power function models*, Chemical Engineering Science 63, 4631-4635, 2008

[150] Schwaab, M., Lemos, L. and Pinto, J., *Optimum reference temperature for reparameterization of the Arrhenius equation. Part 2: Problems involving multiple reparameterizations*, Chemical Engineering Science 63, 2895-2906, 2008

[151] Schwaab, M., Luiz Monteiro, J., Carlos Pinto, J., *Sequential experimental design for model discrimination: Taking into account the posterior covariance matrix of differences between model predictions*, Chemical Engineering Science 63, 2408-2419, 2008

[152] Georgieva, A. and Anastasov, A., *An investigation of the resources of a conventional catalyst O 4-25 calcined under special conditions for oxidation of o-xylene to phthalic anhydride. Part I. Calcination and working characteristics of the catalyst*, Bulgarian Chemical Communications 40, 3-12, 2008

[153] Georgieva, A. and Anastasov, A., *An investigation of the resources of a conventional catalyst O 4-25 calcined under special conditions for oxidation of o-xylene to phthalic anhydride. Part II. Formation of a dual catalyst bed in case of operation with low inlet reagent concentration*, Bulgarian Chemical Communications 40, 13-18, 2008

[154] Georgieva, A. and Anastasov, A., *An investigation of the resources of a conventional catalyst O 4-25 calcined under special conditions for oxidation of o-xylene to phthalic anhydride. Part III. Characteristics of the catalyst bed in the case of operation with high inlet reagent concentrations*, Bulgarian Chemical Communications 40, 19-25, 2008

[155] Georgieva, A. and Anastasov, A., *Activity Profiling in the Oxidation of o-Xylene to Phthalic Anhydride*, Poster Europacat, 2005

[156] Nikolov, V. and Anastasov, A., *Pretreatment of a Vanadia-Titania Catalyst for Partial Oxidation of o-xylene under Industrial Conditions*, Industrial and Engineering Chemistry Research 31, 80-88, 1992

[157] Nikolov, V. and Anastasov, A., *Pretreatment behavior of a fixed-bed vanadia-titania catalyst for partial oxidation of o-xylene. Part II. Experimental verification of the hypothesis for partial catalyst deactivation*, Bulgarian Chemical Communications 25, 471-481, 1992

[158] Georgieva, A., Anastasov, A., and Nikolov, V., *Deactivation properties of a high-productive vanadia-titania catalyst for oxidation of o-xylene to phthalic anhydride*, Brazilian Journal of Chemical Engineering 25, 351-364, 2008

[159] Satterfield, C., *Mass Transfer in Heterogeneous Catalysis,* MIT Press, Cambridge, Massachusetts, 1970

[160] Martin, H. and Nilles, M., *Radial heat transfer in packed tubular reactors*, Chemie Ingenieur Technik 65, 1468-1477, 1993

[161] Bauer, M. and Adler, R., *Heat Transfer in Catalytic Fixed-bed reactors with a gas flow, characterized through low tube/particle diameter ratios*, Chemical Engineering Technology 26, 545-549, 2003

[162] Bauer, M., *Theoretische und experimentelle Untersuchungen zum Wärmetransport in gasdurchströmten Festbettreaktoren*, PhD Thesis, Martin Luther Universität Halle, 2001

[163] Tsotsas, E. and Schlünder, E. U., *Wärmeübertragung in Festbetten, durchmischten Schüttgütern und Wirbelschichten,* Georg Thieme Verlag, Stuttgart, 1988

[164] Tsotsas, E., *Transport phenomena in fixed beds. History, research, and present state*, Chemie Ingenieur Technik 64, 313-322, 1992

[165] Winterberg, M. and Tsotsas, E., *Modelling of heat transport in beds packed with spherical particles for various bed geometries and/or thermal boundary conditions*, International Journal of Thermal Sciences 39, 556-570, 2000

[166] Dixon, A. and van Dongeren, J., *The influence of the tube and particle diameters at constant ratio on heat transfer in packed beds*, Chemical Engineering and Processing 37, 23-32, 1998

[167] Wakao, N. and Vortmeyer, D., *Pressure dependency of effective thermal conductivity of packed beds*, Chemical Engineering Science 26, 1753-1765, 1971

[168] Vortmeyer, D. and Schaefer, R., *Equivalence of one- and two-phase models for heat transfer processes in packed beds: one dimensional theory*, Chemical Engineering Science 29, 485-491, 1974

[169] Vortmeyer, D. and Winter, R., *On the validity limits of packed bed reactor continuum models with respect to tube to particle diameter ratio*, Chemical Engineering Science 39, 1430-1432, 1984

[170] Tsotsas, E., Schluender, E. U., *Heat transfer in packed beds with fluid flow: remarks on the meaning and the calculation of a heat-transfer coefficient at the wall*, Chemical Engineering Science 45, 819-837, 1990

[171] Vortmeyer, D., *Packed bed thermal dispersion models and consistent sets of coefficients*, Chemical Engineering and Processing: Process Intensification 26, 263-268, 1989

[172] Vortmeyer, D. and Haidegger, E., *Discrimination of three approaches to evaluate heat fluxes for wall-cooled fixed bed chemical reactors*, Chemical Engineering Science 46, 2651-2660, 1991

[173] Winterberg, M., Tsotsas, E., Krischke, A. and Vortmeyer, D., *A simple and coherent set of coefficients for modelling of heat and mass transport with and without chemical reaction in tubes filled with spheres*, Chemical Engineering Science 55, 967-979, 2000

[174] Tsotsas, E., *Status and perspectives of modeling transport phenomena in packed beds*, Chemie Ingenieur Technik 72, 313-321, 2000

[175] Daszkowski, T. and Eigenberger, G., *A reevaluation of fluid flow, heat transfer and chemical reaction in catalyst filled tubes*, Chemical Engineering Science 47, 2245-2250, 1992

[176] Bey, O. and Eigenberger, G., *Fluid flow through catalyst filled tubes*, Chemical Engineering Science 52, 1365-1376, 1997

[177] Smirnov, E., Muzykantov, A., Kuzmin, V., Kronberg, A. and Zolotarskii, I., *Radial heat transfer in packed beds of spheres, cylinders and Rashig rings: Verification of model with a linear variation of λ_{er} in the vicinity of the wall*, Chemical Engineering Journal 91, 243-248, 2003

[178] Smirnov, E., Kuzmin, V. and Zolotarskii, I., *Radial Thermal Conductivity in Cylindrical Beds Packed by Shaped Particles*, Chemical Engineering Research and Design 82, 293-296, 2004

[179] Castillo-Araiza, C., Jimenez-Islas, H. and Lopez-Isunza, F., *Heat-Transfer Studies in Packed-Bed Catalytic Reactors of Low Tube/Particle Diameter Ratio*, Industrial & Engineering Chemistry Research 46, 7426-7435, 2007

[180] Bey, O. and Eigenberger, G., *Gas flow and heat transfer through catalyst filled tubes*, International Journal of Thermal Science 40, 152-164, 2001

[181] Papageorgiou, J. and Froment, G., *Simulation models accounting for radial voidage profiles in fixed-bed reactors*, Chemical Engineering Science 50, 3043-3056, 1995

[182] Wijngaarden, R. and Westerterp, K., *Do the effective heat conductivity and the heat transfer coefficient at the wall inside a packed bed depend on a chemical reaction? Weaknesses and applicability of current models*, Chemical Engineering Science 44, 1653-1663, 1989

[183] Wijngaarden, R. and Westerterp, K., *A heterogeneous model for heat transfer in packed beds*, Chemical Engineering Science 48, 1273-1280, 1993

[184] Somorjai, G., *Surface Chemistry and Catalysis,* Wiley, New York, 1994

[185] Redlingshöfer, H., *Reaktionstechnische Untersuchungen zur heterogen katalysierten Gasphasenoxidation von Propen*, PhD Thesis, Universität Erlangen, 2002

[186] Thömmes, T., *Die partielle Oxidation von Propen mit N_2O in der Gasphase*, PhD Thesis, Karlsuhe Institut für Technologie, 2010

[187] Brandstädter, W., *Partial Oxidation of Raffinate II and other Mixtures of n-Butane and n-Butenes to Maleic Anhydride in a Fixed-Bed Reactor*, PhD Thesis, Universität Karlsruhe (TH), 2007

[188] Integrated Management System Handbook, Süd-Chemie AG., 20-9-2009.

[189] Kleiber, M. and Joh, R., chap. Da in VDI-Wärmeatlas Ed. E. U. Schlünder, Springer Verlag, Berlin Heidelberg New York, 2006

[190] Tsotsas, E., chap. Dee in VDI-Wärmeatlas Ed. E. U. Schlünder, Springer Verlag, Berlin Heidelberg New York, 2006

Notation

A	activity (-), area of GC peak (-)
a_v	interfacial area (m²/m³)
a_i	inhibition factor, various units
b_i	inhibition factor, various units
Bo	Bodenstein number (-)
C	concentration (mol/m³)
C_z	dimensionless axial position at which the activity reaches unity
c_p	heat capacity (J/kg)
d	diameter (m)
D	diffusion coefficient (m²/s)
E_A	activation energy (kJ/mol)
f	friction factor (-)
ΔH_R	reaction enthalpy (J/mol)
ΔH_{ads}	adsorption enthalpy (J/mol)
h_f	gas solid heat transfer coefficient (W/m² K)
i	control variable, mostly for components
j	control variable for reactions
k_f	gas solid mass transfer coefficient (m/s)
k	reaction rate constant, various units
K	inhibition rate constant, various units
K_{ax}	constant in the calculation of axial dispersion (-)
K_r	constant in the calculation of the radial heat conductivity (-)
L	length (m)
m	exponent in power law rate equations (-)
$\dot{m}$	o-xylene flowrate (g/h)
$\dot{M}$	mass flux (kg/m² s)
M_W	molecular weight (kg/mol)
N	number of measurements (-)
n	exponent of the activity profile (-), number of moles (mol)

$\dot{N}$	molar flux (mol/m² s)
$\dot{n}$	molar flowrate (mol/s)
N_s	number of oxidized sites (-)
N_p	number of parameters (-)
N_{in}	number of insignificant parameters(-)
N_c	number of correlations (-)
Nu	Nusselt number (-)
OF	objective function
P	total pressure (Pa)
p	partial pressure (Pa)
Pe	Péclet number (-)
Pr	Prandtl number (-)
R	gas constant (J/mol K)
Re	Reynolds number (-)
RF	response factor [-]
r	reaction rate (mol/s g_{cat}), radial variable
r_p	radial variable pellet (-)
T	temperature (K)
U	overall heat transfer coefficient (W/m² K)
u_z	velocity axial (m/s)
Δv	diffusion volume (-)
$\dot{V}$	air flowrate (Nm³/h)
X	conversion (%)
x	molar fraction (-), modeled variable, various units
$\tilde{x}$	measured variable, various units
Y_{PA}	PA yield (%)
z	axial variable (-)

Greek

α_W	wall heat transfer coefficient (W/m² K)
β	stochiometric coefficient of lattice oxygen consumption (-)
ε	porosity (-)
ϕ	objective function value (-)
η	dynamic viscosity (Pa s), efficiency factor (-)
θ	surface coverage (-)
λ_r	radial heat transfer coefficient (W/m K)
λ_s	heat conductivity of the catalyst pellet (W/m K)
ν	stochiometric coefficient (-)
ξ	mass fraction (-)
ρ	density (kg/m^3)
σ	variance (-)
τ	tortuosity

Subscript

ax	axial
bed	catalyst bed
cat	catalyst
diff	diffusion
eff	effective
f	fluid
mol	molecular
org	organics
Ox	oxidation
o	oxidized
p	pellet
r	reduction, radial
ref	reference
s	solid
t	tube

th	thermal
tot	total
W	wall, weight
z	axial

List of Tables

List of Figures

Lebenslauf

Robert Marx

geb. 13.10.1984 in Dernbach

1989 – 1991	St. Anthony of Padua School, Dunmore, PA
1991 – 1993	Jefferson Elementary School, Jefferson, PA
1993 – 1994	Brenschenschule, Witten
1994 – 1996	Ruhr Gymnasium, Witten
1996 – 2003	Gregor-Mendel Gymnasium, Amberg
2003	Abitur am Gregor-Mendel Gymnasium, Amberg
2003 – 2005	Grundstudium der Verfahrenstechnik an der TU Dresden
2005 – 2006	Studium „Génie des Procédés“, Ecole des Mines, St. Etienne, Frankreich
2006 – 2007	Praktikum bei der Süd-Chemie AG, Jinshan, China
2006 – 2008	Hauptstudium, allgemeine Verfahrenstechnik, TU Dresden
2008	Diplomarbeit, Fraunhofer Institut für angewandte Polymerisations-technik / Uni Halle, Halle/Saale
2008	Abschluss Dipl.-Ing. für Verfahrenstechnik, TU Dresden
2008 – 2011	Doktorand bei der Süd-Chemie AG, Heufeld
seit 01.09.2011	Tätigkeit bei der Süd-Chemie AG, München